2

Potential-Energy Surfaces

In this chapter we present a microscopic justification for the potential-energy surface, used in the introduction as an important ingredient in the description of nuclear fission. It will be shown in particular that the liquid-drop model and its shell corrections can be systematically derived from a mean-field approach to the quantal nuclear many-body problem. A number of variants of the liquid-drop model and for the shell corrections have been proposed. Their generic relations will be discussed in the following.

Phenomenological parameters in the liquid-drop energy and in the shell correction are usually fitted to describe empirically known ground-state properties of nuclei, in particular binding energies from the nuclear mass table and fission barrier heights. The same holds for parameters in the effective two-body interactions, used in the selfconsistent mean-field approach. The first sections of this chapter are therefore devoted to the calculation of nuclear ground-state properties. With parameters fitted to these properties, the construction of energy surfaces as functions of shape parameters is presented in the last section with a particular emphasis on secondary minima and saddle points.

2.1 Mean field theories

Many attempts have been made to obtain ground-state binding energies and radii on an a priori basis from empirical nucleon-nucleon potentials by solving the many-body Schrödinger equation in the self-consistent Brueckner-Hartree-Fock approximation. Even with the inclusion of three-body correlations the results were not very encouraging. For a discussion see e.g. Ref. [108] Sec. 5.6.1.1. The success of the local energy-density functional method in correlated many-electron systems [109–112], on the other hand, motivates the more modest approach of using phenomenological nuclear energy-density functionals to obtain nuclear ground-state properties. For historical reasons they are formulated in terms of short-range or zero-range two-body and zero-range

H. J. Krappe and K. Pomorski, *Theory of Nuclear Fission*,
Lecture Notes in Physics 838, DOI: 10.1007/978-3-642-23515-3_2,

three-body potentials to be used in mean-field approximation. A large number of such effective potentials has been proposed and fitted to describe either binding energies of nuclei more or less close to the beta stability line of the mass table or extremely neutron rich nuclei or neutron matter. In addition, certain spectroscopic data, the nuclear level density or fission barriers were used in the fits. In an alternative approach the phenomenological relativistic field theory of Serot and Walecka [113] was used in mean-field approximation to describe a variety of nuclear data. In the following effective potentials and corresponding functionals of relevance in the theory of fission will be described.

We use here the term mean-field theory to include the non-relativistic approach specifically the Hartree-Fock approximation and its semiclassical analogues, the Thomas-Fermi (TF) and extended Thomas-Fermi (ETF) approximations. The term is also used for the Hartree-Fock-Bogolyubov approximation (HFB) when pairing correlations are to be included in the theory. Since these approaches to the many-body problem have been described in many text books (cf. e.g. Ring and Schuck, *The Nuclear Many-Body Problem* [108], Brack and Bhaduri, *Semiclassical Physics* [114], and Petkov and Stoitsov, *Nuclear Density Functional Theory* [112] or the review by Bender, Heenen, and Reinhard [115]), we do not give complete, formal derivations of these theories, but for later references the basic formulae are presented in the following.

2.1.1 The Hartree-Fock theory

The starting point is the Hamiltonian for the A nucleon system

$$H = -\frac{\hbar^2}{2M_{\rm nucl}} \sum_{n=1}^{A} \Delta_n + \sum_{n,n';n<n'}^{A} V(\mathbf{r}_n - \mathbf{r}_{n'}; \sigma_n\sigma_{n'}, \tau_n\tau_{n'}) \,, \tag{2.1}$$

where the two-particle interaction $V(\mathbf{r}_1 - \mathbf{r}_2; \sigma_1\sigma_2, \tau_1\tau_2)$ consists of the long-range Coulomb interaction between the protons and a spin and isospin-dependent, short-range, effective nuclear interaction $V_{\rm eff} = V(\mathbf{r}_1 - \mathbf{r}_2)\hat{A}(\hat{P}_\sigma, \hat{P}_\tau)$, where the operator

$$\hat{A} = W + B\hat{P}_\sigma - H\hat{P}_\tau - M\hat{P}_\sigma\hat{P}_\tau \tag{2.2}$$

represents the standard dependence of the central part of the effective two-body potential on the spin and isospin exchange-operators $\hat{P}_\sigma = \frac{1}{2}(1 + \boldsymbol{\sigma}_1\boldsymbol{\sigma}_2)$ and $\hat{P}_\tau = \frac{1}{2}(1 + \boldsymbol{\tau}_1\boldsymbol{\tau}_2)$ with empirical parameters W, B, H, and M, which are the strength parameters of the Wigner, Bartlett, Heisenberg, and Majorana interactions, respectively.

Let the functions $\chi_i(\mathbf{r}, \sigma, \tau)$ form a complete set of orthonormal single-particle states. They can, for instance, be the eigenstates of a shell-model single-particle Hamiltonian. With respect to this set of states nucleon creation and annihilation operators $\hat{a}_i^+$ and $\hat{a}_i$ are defined in terms of which the Hamiltonian (2.1) may be written in Fock-space representation as

$$\hat{H} = \sum_{l,l'} t_{ll'} \hat{a}_l^+ \hat{a}_{l'} + \frac{1}{2} \sum_{l_1 l_2 l_1' l_2'} V_{l_1 l_2 l_1' l_2'} \hat{a}_{l_1}^+ \hat{a}_{l_2}^+ \hat{a}_{l_2'} \hat{a}_{l_1'} \tag{2.3}$$

with

$$t_{ll'} = -\frac{\hbar^2}{2M_{\text{nucl}}} \int \chi_l^*(\mathbf{r}) \Delta \chi_{l'}(\mathbf{r}) d^3r,$$

and

$$V_{l_1 l_2 l_1' l_2'} = \int d^3r \int d^3r' \;\; \chi_{l_1}^*(\mathbf{r}_1 \sigma_1 \tau_1) \chi_{l_2}^*(\mathbf{r}_2 \sigma_2 \tau_2) \\ V(\mathbf{r}_1 - \mathbf{r}_2) \hat{A}(\hat{P}_\sigma, \hat{P}_\tau)\, \chi_{l_1'}(\mathbf{r}_1 \sigma_1 \tau_1) \chi_{l_2'}(\mathbf{r}_2 \sigma_2 \tau_2) \; .$$

In the Hartree-Fock approximation one seeks an approximate solution of the N-body problem in the set of Slater determinants $\det[\chi_i(\mathbf{r}_j \sigma_j \tau_j)]$, $i, j = 1 \ldots A$ built from A wave functions χ_i. In Fock space these A-particle states are represented by

$$|\text{HF}\rangle = \prod_{i=1}^{A} \hat{a}_i^+ |0\rangle \; .$$

It is the aim of the HF approximation to find the single-particle basis

$$\varphi_i(\mathbf{r}, \sigma, \tau) = \sum_{i'} U_{ii'} \chi_{i'}(\mathbf{r}, \sigma, \tau) \tag{2.4}$$

connected with the original basis of the functions χ_i by a unitary transformation $U_{ii'}$ and with creation and destruction operators

$$\hat{c}_i^+ = \sum_{i'} U_{ii'} \hat{a}_{i'}^+ \quad \text{and} \quad \hat{c}_i = \sum_{i'} U_{ii'} \hat{a}_{i'} \; ,$$

for which the Slater determinant

$$|\text{HF}\rangle^{(0)} = \prod_{k=1}^{A} \hat{c}_k^+ |0\rangle \tag{2.5}$$

minimizes the expectation value $E^{\text{HF}} = \langle \text{HF}|H|\text{HF}\rangle$, while conserving the proton and neutron numbers. The density matrix is given by

$$\rho_{kl} = \langle \text{HF}|\hat{a}_l^+ \hat{a}_k|\text{HF}\rangle$$

with

$$\text{tr}\ \rho = A \; . \tag{2.6}$$

In terms of the density matrix and the antisymmetrized matrix element of the two-particle interaction

$$\overline{V}_{l_1' l_2' l_1 l_2} = V_{l_1' l_2' l_1 l_2} - V_{l_1' l_2' l_2 l_1} \; ,$$

the expectation value $E^{\rm HF}$ is

$$E^{\rm HF} = \langle {\rm HF}|H|{\rm HF}\rangle = \sum_{l_1 l_2} t_{l_1 l_2}\rho_{l_2 l_1} + \frac{1}{2}\sum_{l_1 l_1' l_2 l_2'} \rho_{l_1 l_1'}\overline{V}_{l_1' l_2' l_1 l_2}\rho_{l_2' l_2}\,. \tag{2.7}$$

Effective two-particle nuclear interactions are often density dependent: $V(\mathbf{r}_1 - \mathbf{r}_2; \rho(\mathbf{R}))$ with $\mathbf{R} = (\mathbf{r}_1 + \mathbf{r}_2)/2$. To calculate the variation of such a potential with respect to the density matrix, we consider

$$\rho(\mathbf{R}) = \sum_{ij} \rho_{ij}\chi_i^*(\mathbf{R})\chi_j(\mathbf{R})$$

and get

$$\frac{\partial\overline{V}}{\partial\rho_{ij}} = \frac{\partial\overline{V}}{\partial\rho}\frac{\partial\rho}{\partial\rho_{ij}} = \frac{\partial\overline{V}(\rho(\mathbf{R}))}{\partial\rho}\,\chi_i^*(\mathbf{R})\,\chi_j(\mathbf{R})\,. \tag{2.8}$$

To obtain the minimum of $E^{\rm HF}$ with respect to variations of the density matrix with the constraint of preserving the trace (2.6) we take the derivative

$$\frac{\partial(E^{\rm HF} - \epsilon\ {\rm tr}\ \rho)}{\partial\rho_{kl}} = t_{kl} + \Gamma_{kl} - \epsilon\delta_{kl} = 0\,, \tag{2.9}$$

where ϵ is a Lagrange multiplier and Γ_{kl} is the mean field, defined as

$$\begin{aligned}\Gamma_{kl} &= \frac{\partial\,{\rm tr}[\rho\overline{V}\rho]}{\partial\rho_{kl}} \\ &= \sum_{l_2 l_2'}\overline{V}_{k l_2' l l_2}\rho_{l_2' l_2} + \frac{1}{2}\sum_{l_1 l_2 l_1' l_2'}\rho_{l_1 l_1'}\left[\frac{\partial\overline{V}}{\partial\rho(\mathbf{r})}\chi_k^*\chi_l\right]_{l_1' l_2' l_1 l_2}\rho_{l_2' l_2}\,.\end{aligned} \tag{2.10}$$

The second term on the right-hand-side of the last equation appears when the effective two-particle potential is explicitly density dependent. One sees that the unitary transformation, introduced in Eq. (2.4) diagonalizes the eigenvalue Eqs. (2.9). In space representation the Hartree-Fock equation (2.9) becomes

$$\begin{aligned}&-\frac{\hbar^2}{2M_{\rm nucl}}\Delta\varphi_k(\mathbf{r},\sigma,\tau) + \sum_{j=1}^{A}\sum_{\sigma'\tau'}\int d\mathbf{r}'\varphi_j^*(\mathbf{r}',\sigma',\tau')V(\mathbf{r}-\mathbf{r}')\hat{A}(\hat{P}_\sigma,\hat{P}_\tau) \\ &\times[\varphi_j(\mathbf{r}',\sigma',\tau')\varphi_k(\mathbf{r},\sigma,\tau) - \varphi_j(\mathbf{r},\sigma,\tau)\varphi_k(\mathbf{r}',\sigma',\tau')] = \epsilon_k\varphi_k(\mathbf{r},\sigma,\tau)\,,\end{aligned} \tag{2.11}$$

where the sum is to be extended over the A eigenstates with the smallest eigenvalues ϵ_k.

In the HF basis of the $\varphi_i(\mathbf{r},\sigma,\tau)$ the density matrix is diagonal with eigenvalues 1 for occupied and 0 for unoccupied states $\rho_{ij} = n_i\delta_{ij}$

$$n_i = \begin{cases} 1 & \text{if} \quad i \le i_{\rm Fermi} \\ 0 & \text{if} \quad i > i_{\rm Fermi}\,. \end{cases} \tag{2.12}$$

The HF energy becomes

$$E^{\mathrm{HF}} = \sum_{i=1}^{A} t_{ii} + \frac{1}{2} \sum_{i,j=1}^{A} \overline{V}_{ij,ij} \tag{2.13}$$

and the eigenvalues ϵ_i of Eq. (2.11) are given by

$$\epsilon_i = t_{ii} + \Gamma_{ii} \; ;$$

therefore

$$E^{\mathrm{HF}} = \sum_{i=1}^{A} \left(\epsilon_i - \frac{1}{2} \Gamma_{ii} \right) . \tag{2.14}$$

One can show [108] that

$$[H, \rho] = 0 \tag{2.15}$$

in the HF-basis and admitted variations $\delta\rho_{k'k}$ must be between particle states (i.e. states above the Fermi energy) k' and hole states (i.e. states below the Fermi energy) k or vice versa. Therefore the behavior of the interaction potential in the particle-particle channel does not matter in the HF-approximation.

The HF equation (2.11) is a nonlinear eigenvalue equation. It is solved iteratively, starting e.g. with a Wood-Saxon mean field $\Gamma^{(0)}$. The eigenfunctions $\varphi_i^{(1)}$ obtained from solving the HF equations with this mean field were used to calculate a new mean field $\Gamma^{(1)}$ according to Eq. (2.10) and so forth until selfconsistency is reached. Two points require special care when using this iteration scheme.

First, the HF equation is valid for any stationary point, not only the ground state. It depends on the closeness of the shape of the initial shell-model potential to the final local minimum in the energy surface to which minimum the iteration converges if there are several local minima.

Second, the iteration preserves the symmetry of the initial field. If the desired solution has axial, but not spherical symmetry, the initial field should be given that reduced symmetry. If the solution is expected to be triaxial, the initial field should be triaxial. The same holds for violation of reflection symmetry.

Saddle points cannot be obtained in this way. Instead, one has to add a suitable constraining field qQ_{kl} to Γ_{kl}. Usually $\hat{Q}$ will be the operator of the quadrupole moment and q is a Lagrange parameter. The latter has the meaning of a generalized force, necessary to keep the nucleus in equilibrium at a given value of the quadrupole deformation $Q = \langle \mathrm{HF}|\hat{Q}|\mathrm{HF}\rangle$. Plotting the force parameter $q(Q)$ as function of the external parameter Q, stationary points, including saddle points, correspond to zeros of this function. The sign of the derivative in these points differentiates between minima and saddle points.

2.1.2 The Hartree-Fock-Bogolyubov theory

To include pairing correlations in the mean-field theory, the selfconsistent Hartree-Fock equations were generalized by Baranger [116]. He used the Bogolyubov transformation [117]

$$\begin{aligned} \hat{\alpha}_i &= \sum_{j=1}^{M} (u_{ij}^* \hat{a}_j + v_{ij}^* \hat{a}_j^+) \ , \\ \hat{\alpha}_i^+ &= \sum_{j=1}^{M} (u_{ij} \hat{a}_j^+ + v_{ij} \hat{a}_j) \ , \end{aligned} \tag{2.16}$$

to introduce quasiparticle creation and annihilation operators $\hat{\alpha}_i^+$ and $\hat{\alpha}_i$, where M is the dimension of the single-particle space and u and v are transformation matrices. Introducing the $2M \times 2M$ matrix

$$\hat{B} = \begin{pmatrix} \hat{u} & \hat{v}^* \\ \hat{v} & \hat{u}^* \end{pmatrix} \ , \tag{2.17}$$

the ortho-normalization of quasi-particle states requires that $\hat{B}$ is unitary

$$\hat{B}\,\hat{B}^+ = \hat{B}^+\hat{B} = \hat{I} \ , \tag{2.18}$$

where $\hat{B}^+$ is the hermitian conjugate of the $\hat{B}$ matrix.

The transformation (2.16) and its inverse can now be written as

$$\begin{pmatrix} \hat{\alpha} \\ \hat{\alpha}^+ \end{pmatrix} = \hat{B}^+ \begin{pmatrix} \hat{a} \\ \hat{a}^+ \end{pmatrix} \ ; \qquad \begin{pmatrix} \hat{a} \\ \hat{a}^+ \end{pmatrix} = \hat{B} \begin{pmatrix} \hat{\alpha} \\ \hat{\alpha}^+ \end{pmatrix} \ . \tag{2.19}$$

One assumes that the ground-state wave-function $|\mathrm{HFB}\rangle$ of a nucleus with pairing correlations is a state of independent quasiparticles

$$|\mathrm{HFB}\rangle = \prod_{i=1}^{M} \hat{\alpha}_i |0\rangle \ . \tag{2.20}$$

This shows immediately that the state $|\mathrm{HFB}\rangle$ is the quasiparticle vacuum

$$\hat{\alpha}_i |\mathrm{HFB}\rangle = 0 \ .$$

From the hermitian density matrix

$$\rho_{ij} = \langle \mathrm{HFB}|\hat{a}_j^+ \hat{a}_i|\mathrm{HFB}\rangle = \left[v^* v^T\right]_{ij} \tag{2.21}$$

and the skew-symmetric pairing tensor

$$\kappa_{ij} = \langle \mathrm{HFB}|\hat{a}_j \hat{a}_i|\mathrm{HFB}\rangle = [v^* u^T]_{ij} = -\left[u\, v^+\right]_{ij} \tag{2.22}$$

a generalised hermitian density matrix is formed

$$\hat{R} = \begin{pmatrix} \hat{\rho} & \hat{\kappa} \\ -\hat{\kappa}^* & 1 - \hat{\rho}^* \end{pmatrix} . \tag{2.23}$$

The expectation value of the Hamiltonian $\langle \mathrm{HFB}|\hat{H}|\mathrm{HFB}\rangle$ is given in terms of the matrices ρ_{ij} and κ_{ij} by

$$\begin{aligned} \langle \mathrm{HFB}|\hat{H}|\mathrm{HFB}\rangle = & \sum_{ij} t_{ij}\rho_{ji} + \frac{1}{2}\sum_{ijkl}\langle ij|\overline{V}|kl\rangle \rho_{lj}\,\rho_{ki} \\ & + \frac{1}{4}\sum_{ijkl}\langle ij|\overline{V}|kl\rangle \kappa_{lk}\kappa^*_{ji} \end{aligned} \tag{2.24}$$

and the expectation value of the particle number by

$$\langle \mathrm{HFB}|\hat{N}|\mathrm{HFB}\rangle = \sum_i \rho_{ii} . \tag{2.25}$$

Minimizing the total energy with the constraint that the expectation value of the particle number has the required value, leads to the stationarity condition for the HFB ground state,

$$\delta\left\{\langle \mathrm{HFB}|\hat{H} - \lambda\hat{N}|\mathrm{HFB}\rangle - \mathrm{tr}\left[\Lambda(\hat{R}^2 - \hat{R})\right]\right\} = 0 , \tag{2.26}$$

where $\mathrm{tr}[\Lambda(\hat{R}^2 - \hat{R})]$ is subtracted to take into account the Bogolyubov condition (2.18) expressed here in terms of the generalized density (2.23). The variation is to be done with respect to $\delta\rho$, $\delta\rho^*$, $\delta\kappa$ and $\delta\kappa^*$ and Λ is a hermitian matrix whose elements are Lagrange multipliers.

After performing the variation and eliminating the matrix Λ by using its hermiticity, the condition (2.26) can be expressed by the commutator:

$$[\hat{\mathcal{H}}, \hat{R}] = 0 , \tag{2.27}$$

where $\hat{\mathcal{H}}$ is given by

$$\hat{\mathcal{H}} = \begin{pmatrix} \hat{h} & \hat{\Delta} \\ -\hat{\Delta}^* & -\hat{h}^* \end{pmatrix} , \tag{2.28}$$

with

$$h_{ij} = \frac{\partial}{\partial\rho_{ji}}\langle \mathrm{HFB}|\hat{H} - \lambda\hat{N}|\mathrm{HFB}\rangle \tag{2.29}$$

and

$$\Delta_{ij} = 2\,\frac{\partial}{\partial\,\kappa^*_{ji}}\langle \mathrm{HFB}|\hat{H}|\mathrm{HFB}\rangle . \tag{2.30}$$

Eq. (2.27) is the analogue of Eq. (2.15) in the HF theory. To solve equation (2.27) it is sufficient to choose as Bogolyubov transformation $\hat{B}$ the unitary matrix which diagonalizes $\hat{\mathcal{H}}$. This leads to the HFB equations in their standard form

$$\hat{\mathcal{H}}\hat{B} = \hat{B}\,\hat{\mathscr{E}} \quad \text{with} \quad \mathscr{E}_{ij} = \mathcal{E}_i\,\delta_{ij}\ , \tag{2.31}$$

where $\mathcal{E}_i$ denotes the quasi-particle energy.

With the definition (2.30) the explicit form of the pairing matrix becomes

$$\Delta_{ij} = \frac{1}{2}\sum_{kl}\langle ij|\overline{V}|kl\rangle\kappa_{lk}\,. \tag{2.32}$$

The matrix elements of h (2.29) can be obtained in a similar way. For density-dependent interactions one gets from Eqs. (2.29) and (2.8)

$$h_{ij} = t_{ij} - \lambda\,\delta_{ij} + \Gamma_{ij}\ , \tag{2.33}$$

where

$$\begin{aligned}\Gamma_{ij} &= \sum_{kl}\langle ik|\overline{V}(\rho)|jl\rangle\rho_{lk} \\ &+ \frac{1}{2}\sum_{klmn}\langle mn|\frac{\partial\overline{V}(\rho)}{\partial\rho}\varphi_i^*\,\varphi_j|kl\rangle\left[\rho_{ln}\,\rho_{km} + \frac{1}{2}\,\kappa_{lk}\,\kappa_{nm}^*\right]\end{aligned} \tag{2.34}$$

is the quasiparticle mean-field.

The total binding energy is given by

$$E = \mathrm{tr}\left\{(\hat{t} + \frac{1}{2}\hat{\Gamma})\hat{\rho} + \frac{1}{2}\hat{\Delta}\hat{\kappa}^*\right\} + E_{\mathrm{R}}\ , \tag{2.35}$$

where

$$E_{\mathrm{R}} = -\frac{1}{4}\sum_{ijklmn}\langle mn|\frac{\partial\overline{V}(\rho)}{\partial\rho}\varphi_i^*\,\varphi_j|kl\rangle\left[\rho_{ln}\,\rho_{km} + \frac{1}{2}\,\kappa_{lk}\,\kappa_{nm}^*\right]\rho_{ij}$$

is the rearrangement energy which originates from the dependence of the effective interaction potential on the density [118].

It is seen from Eq. (2.34) that in the case of density-dependent interactions the mean-field depends not only on the density matrix (2.21), but also on the pairing tensor (2.22). The Hartree-Fock equations follow from the HFB equations when the pairing-dependent terms are omitted and in the whole calculation one assumes that the matrices $\kappa = 0$ and $\Delta = 0$. In particular, the selfconsistent HF field depends on the density matrix only. In contrast to the HF theory the results of the HFB theory depend on the particle-hole as well as on the particle-particle channel of the effective interaction potential.

2.1.3 The Bardeen-Cooper-Schrieffer (BCS) theory

In view of the need to solve constrained HFB equations thousands of times to construct potential-energy surfaces, it is desirable to have a numerically less cumbersome alternative to account for pairing effects. Often one therefore uses

the numerically simpler HF+BCS approximation in which one first generates single-particle energies ϵ_i and eigenstates $|i\rangle$ selfconsistently in the Hartree-Fock frame without accounting for the pairing contribution to the mean-field and then one includes the pairing correlations in a BCS step. This approach is in particular necessary when the effective interaction potential, from which the mean field is derived, does not properly describe the particle-particle channel.

In the BCS theory one assumes that the pairing potential acts only between states $|i\rangle$ and their time-reflected counterparts $|\bar{\imath}\rangle = \mathcal{T}|i\rangle$. For spherically symmetric systems $|i\rangle \equiv |nljm\rangle$ and the time-reflected state is given by [83]

$$|\bar{\imath}\rangle = \mathcal{T}|nljm\rangle = (-1)^{j+m}|nlj-m\rangle. \tag{2.36}$$

These pairs of degenerate states are therefore singlets in their relative spin and orbital angular momenta, and must then be isotriplets to satisfy the Pauli principle. In nonaxially symmetric, but time-reflection symmetric systems the single-particle states $|i\rangle$ may be expanded in a spherical basis and the rule Eq. (2.36) extended to such states. We will restrict the discussion in the following to time-reversal invariant systems with pairs of degenerate states (Kramers degeneracy). In particular rotating systems are not time-reversal invariant. For their discussion in the framework of the BCS theory we refer to Section 7.7 of Ref. [108].

The BCS Hamiltonian is

$$\hat{H} = \sum_{i\lesseqgtr 0} \epsilon_i \hat{a}_i^+ \hat{a}_i + \frac{1}{2} \sum_{i,j>0} \overline{V}_{i\bar{\imath},j\bar{\jmath}} \hat{a}_i^+ \hat{a}_{\bar{\imath}}^+ \hat{a}_{\bar{\jmath}} \hat{a}_j. \tag{2.37}$$

(The summation limits $i \lesseqgtr 0$ indicate a summation over all states i and their conjugates $\bar{\imath}$, $i > 0$ means summation over the pairs $(i, \bar{\imath})$ in this order only.) The transformation to quasiparticle operators simplifies in the BCS theory compared to the HFB definition, Eqs. (2.16). One obtains

$$\begin{aligned} \hat{\alpha}_i &= u_i \hat{a}_i - v_i \hat{a}_{\bar{\imath}}^+ \ , & \hat{\alpha}_i^+ &= u_i \hat{a}_i^+ - v_i \hat{a}_{\bar{\imath}} \ , \\ \hat{\alpha}_{\bar{\imath}} &= u_i \hat{a}_{\bar{\imath}} + v_i \hat{a}_i^+ \ , & \hat{\alpha}_{\bar{\imath}}^+ &= u_i \hat{a}_{\bar{\imath}}^+ + v_i \hat{a}_i \end{aligned} \tag{2.38}$$

with real u_i and v_i. With this definition we follow the convention of Ref. [108]. The normalization condition, which guarantees that the quasiparticle operators obey Fermi commutation rules, becomes

$$u_i^2 + v_i^2 = 1 \tag{2.39}$$

instead of Eq. (2.18) in the HFB theory. The ansatz for the BCS ground-state of an even proton-number and even neutron-number state is

$$|\mathrm{BCS}\rangle = \prod_{i>0} (u_i + v_i \hat{a}_i^+ \hat{a}_{\bar{\imath}}^+)|0\rangle \ , \tag{2.40}$$

where $i > 0$ on the product sign indicates that all single-particle states $|i\rangle$, except their time-reversed counterparts should be taken. It is easy to show

that the state $|\mathrm{BCS}\rangle$ is the quasiparticle vacuum, $\hat{\alpha}_k|\mathrm{BCS}\rangle = 0$. The BCS state is not an eigenstate of the particle-number operator. In terms of the u_i and v_i the expectation value of the particle-number operator $\hat{N} = \sum_i \hat{a}_i^+ \hat{a}_i$ is

$$N = \langle \mathrm{BCS}|\hat{N}|\mathrm{BCS}\rangle = 2\sum_{i>0} v_i^2 \tag{2.41}$$

and the expectation value of the Hamiltonian is

$$\begin{aligned} E_{\mathrm{BCS}} = \langle \mathrm{BCS}|\hat{H}|\mathrm{BCS}\rangle = 2\sum_{i>0} \epsilon_i v_i^2 + \sum_{i>0} \overline{V}_{i\bar{i}i\bar{i}} v_i^4 \\ + \frac{1}{2}\sum_{i,j>0} \overline{V}_{i\bar{i}j\bar{j}} u_i v_i u_j v_j \ . \end{aligned} \tag{2.42}$$

Minimization of the expectation value of the Routhian $\hat{H}' = \hat{H} - \lambda\hat{N}$ with respect to variations of the v_i, observing the constraint (2.39), yields the equation

$$\left(\frac{\partial}{\partial v_i} + \frac{\partial u_i}{\partial v_i}\frac{\partial}{\partial u_i}\right)\langle \mathrm{BCS}|\hat{H} - \lambda\hat{N}|\mathrm{BCS}\rangle = 0 \ ,$$

from which the BCS equations

$$2\tilde{\epsilon}_i u_i v_i + \Delta_i(v_i^2 - u_i^2) = 0 \ , \qquad i > 0 \, , \tag{2.43}$$

follow, where the abbreviations

$$\tilde{\epsilon}_i = \epsilon_i - \lambda + \overline{V}_{i\bar{i}i\bar{i}} v_i^2 \tag{2.44}$$

and

$$\Delta_i = -\sum_{j>0} \overline{V}_{i\bar{i}j\bar{j}} u_j v_j \ . \tag{2.45}$$

have been used. From Eqs. (2.39) and (2.43) one obtains

$$\begin{aligned} v_i^2 &= \frac{1}{2}\left(1 - \frac{\tilde{\epsilon}_i}{\sqrt{\tilde{\epsilon}_i^2 + \Delta_i^2}}\right) \\ u_i^2 &= \frac{1}{2}\left(1 + \frac{\tilde{\epsilon}_i}{\sqrt{\tilde{\epsilon}_i^2 + \Delta_i^2}}\right) \ . \end{aligned} \tag{2.46}$$

Inserting Eqs. (2.46) into Eq. (2.45) the gap equation

$$\Delta_i = -\frac{1}{2}\sum_{j>0} \overline{V}_{i\bar{i},j\bar{j}} \frac{\Delta_j}{\sqrt{\tilde{\epsilon}_j^2 + \Delta_j^2}} \tag{2.47}$$

is derived. Together with the constraint (2.41)

$$N = 2\sum_{i>0} v_i^2 \tag{2.48}$$

and Eq. (2.44) the gap equation (2.47) allows to determine the Lagrange multiplier λ and the v_i in terms of the ϵ_i and the matrix elements $\overline{V}_{i\bar{\imath},j\bar{\jmath}}$ by an iterative procedure.

For the pairing potential in Eq. (2.37) sometimes a zero-range interaction is used [119, 120]

$$V^q(\boldsymbol{r}_1,\sigma_1;\boldsymbol{r}_2,\sigma_2) = V_0^q \frac{1-\boldsymbol{\sigma}_1\cdot\boldsymbol{\sigma}_2}{4}\delta(\boldsymbol{r}_1-\boldsymbol{r}_2)\,, \qquad q=n,p\,. \tag{2.49}$$

With this interaction one obtains:

$$V^q_{i\bar{\imath}j\bar{\jmath}} = V_0^q \int d^3r \rho_i^q(\boldsymbol{r})\rho_j^q(\boldsymbol{r})\,,$$

where

$$\rho_i^q(\boldsymbol{r}) = \left|\varphi_i^q(\boldsymbol{r})\right|^2$$

and V_0^q is the pairing strength, adjusted to experimental odd-even mass differences e.g. in Ref. [120].

The term proportional to v_i^2 in Eq. (2.44) leads only to a shift of the energies ϵ_i, i.e. it renormalizes the single-particle potential. Since one assumes that the ϵ_i correspond already to the total mean field, it is reasonable to drop these terms to avoid double-counting. For the calculation of Strutinsky's pairing correction to be discussed in Sec. 2.3, this term does not make any difference.

The states of an odd nucleus with particle number $N+1$ are given in the BCS theory by

$$\hat{\alpha}_k^+|\mathrm{BCS}\rangle = \hat{a}_k^+ \prod_{i>0;i\neq k}(u_i + v_i\hat{a}_i^+\hat{a}_{\bar{\imath}}^+)|0\rangle\,,$$

where $|\mathrm{BCS}\rangle$ is the BCS ground-state of the even nucleus with N particles. The expectation value of the Routhian $\hat{H}' = \hat{H} - \lambda\hat{N}$ of an odd nucleus is

$$E^{(k)}_{\mathrm{BCS}} = \langle\mathrm{BCS}|\hat{\alpha}_k\hat{H}'\alpha_k^+|\mathrm{BCS}\rangle = \langle\mathrm{BCS}|\hat{H}'|\mathrm{BCS}\rangle + \mathcal{E}_k \tag{2.50}$$

with the quasi-particle energy

$$\mathcal{E}_k = \sqrt{\tilde{\epsilon}_k^2 + \Delta_k^2}\,. \tag{2.51}$$

It is assumed that the correlation structure of the paired N particles is not affected by adding an extra odd particle. This is only approximately true if many particles participate in the formation of the correlated state, cf. Sec. 6.3.4 of Ref. [108]. A more accurate treatment of an odd system is given below for the model with a state-independent pairing matrix-element.

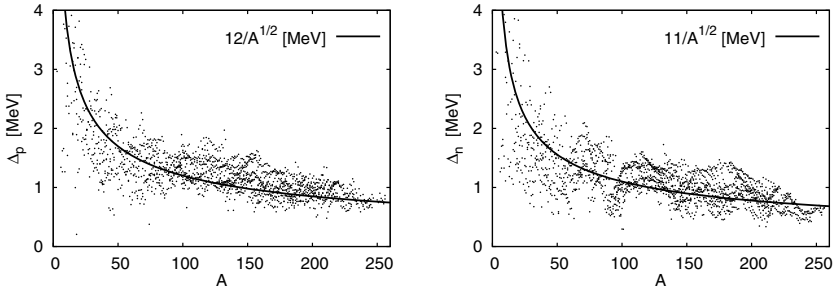

Fig. 2.1. Dependence of the proton and neutron gaps on the mass number, data from the mass table of Ref. [121].

The ground state k_0 corresponds to $\epsilon_{k_0} \approx \lambda$. From Eq. (2.44) follows, neglecting again the v_i^2 terms, $\mathcal{E}_{k_0} = 0$. To obtain the odd-even mass difference, defined usually as second finite difference

$$E_{\rm oe} = -(1/2)\,[\,E^{\rm GS}_{N+2} - E^{\rm GS}_{N+1} - (E^{\rm GS}_{N+1} - E^{\rm GS}_{N})]\,, \quad N \text{ even}, \tag{2.52}$$

one uses the following relations between ground-state energies

$$E^{\rm GS}_{N+2} \approx E^{\rm GS}_{N} + 2\lambda\,, \quad E^{\rm GS}_{N+1} \approx E^{\rm GS}_{N} + \lambda + \mathcal{E}_{k_0}\,,$$

and obtains

$$E_{\rm eo} = \mathcal{E}_{k_0} \approx \Delta_{k_0}. \tag{2.53}$$

Note that there is an odd-even staggering of nuclear binding energies in HF approximation, even without pairing, connected with the breaking of time-reversal symmetry in odd systems. For a discussion of extracting both, the pairing and the mean-field odd-even effects independently from the data we refer to the investigation of Satuła, Dobaczewski, and Nazarewicz [122].

Fig. 2.1 shows that in the average $\Delta_p = 12{\cdot}A^{-1/2}$ MeV and $\Delta_n = 11{\cdot}A^{-1/2}$ MeV describes roughly the data for protons and neutrons, respectively. In Eq. (2.52) the assumption is made that the ground-state binding-energies of the three nuclei on the right-hand-side depend smoothly on N, except for pairing effects. This is not always the case, for example when the ground-state deformation changes rapidly as function of N; see Möller and Nix [123] for a detailed discussion of this problem. Naturally this difficulty occurs even more frequently when forth differences are used instead of the second differences of Eq. (2.52).

To calculate pairing corrections to ground-state binding-energies a rather schematic BCS calculation is mostly used, where the interaction potential in Eq. (2.37) is assumed to have state-independent matrix elements

$$\frac{1}{2}\sum_{i,j>0} \overline{V}_{i\bar{\imath}j\bar{\jmath}}\hat{a}_i^+\hat{a}_{\bar{\imath}}^+\hat{a}_{\bar{\jmath}}\hat{a}_j = -G\sum_{i,j>0}^{(\omega)}\hat{a}_i^+\hat{a}_{\bar{\imath}}^+\hat{a}_{\bar{\jmath}}\hat{a}_j\,. \tag{2.54}$$

The superscript ω on the sum shall indicate that the sum is restricted to states i, j, which lie in a band of width 2ω around the HF Fermi-energy. In this case the gap parameter Δ from Eq. (2.45) becomes also state-independent

$$\Delta = G \sum_{i>0}^{(\omega)} u_i v_i$$

and Eq. (2.44) simplifies to

$$\tilde{\epsilon}_i = \epsilon_i - \lambda - G v_i^2 \ . \tag{2.55}$$

The expectation value of the Routhian $\hat{H}' = \hat{H} - \lambda \hat{N}$ is

$$\langle \mathrm{BCS} | \hat{H}' | \mathrm{BCS} \rangle = 2 \sum_{i>0}^{(\omega)} \tilde{\epsilon}_i v_i^2 + \sum_{i>0}^{(\omega)} G v_i^4 - \Delta^2 / G \tag{2.56}$$

and the gap equation

$$\Delta = \frac{G}{2} \sum_{i>0}^{(\omega)} \frac{\Delta}{\sqrt{\tilde{\epsilon}_i^2 + \Delta^2}} \ . \tag{2.57}$$

Again, the term $G v_i^2$ in Eq. (2.55) and $G v_i^4$ in Eq. (2.56) may be dropped. Inserting

$$v_i^2 = \frac{1}{2} \left(1 - \frac{\tilde{\epsilon}_i}{\sqrt{\tilde{\epsilon}_i^2 + \Delta^2}} \right) \tag{2.58}$$

into Eqs. (2.48) and (2.55), one obtains together with Eq. 2.57 two nonlinear coupled equations for Δ and λ.

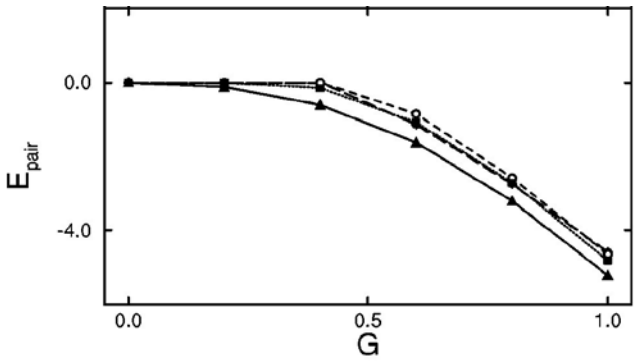

Fig. 2.2. The pairing energy for six particles in a deformed $j = 11/2$ orbital in a pairing-plus-quadrupole model. Results are shown for the HFB approach (full circles •), projection after variation (dashed line ○), the Lipkin-Nogami procedure (full squares, indistinguishable in this figure from the HFB result), and the method of projection before variation (full triangles). Energies in units of G, (from Ref. [124]).

There is always the "trivial", HF solution of these equations

$$\begin{aligned} u_i = 0, \quad v_i = 1 \quad &\text{for} \quad i \leq i_{\text{Fermi}} \\ u_i = 1, \quad v_i = 0 \quad &\text{for} \quad i > i_{\text{Fermi}} \end{aligned}$$

for which $\Delta = 0$. Nontrivial solutions, describing pairing-correlated states, require a large level density around the Fermi energy and also a sufficiently large pairing strength G. It turns out that for realistic parameters no pairing solution exists for magic nuclei, whereas for mid-subshell nuclei there is generally such a solution. Between these extreme situations a sharp transition occurs for fixed level density as a function of G, cf. Fig. 2.2, or for fixed G as function of N (or Z), which in turn determines the level density at the Fermi energy. Particle-number-projected HFB calculations have shown that the sharp phase transition is spurious and connected with the finite particle-number fluctuation in the BCS state (2.40). Various proposals have been made to cope with this problem, in particular, projection of the BCS wave function on to eigenstates of the particle-number operator; see Ref. [108] for a detailed discussion.

In connection with Strutinsky's shell correction, however, the Lipkin-Nogami approach [125–127] is most frequently used. In this approach a constraint on the variance of the particle number is introduced in the Routhian $\hat{H}'$ besides the constraint on the particle number. Calling the Lagrange multiplier for the additional constraint λ_2, Eq. (2.55) is modified to

$$\tilde{\epsilon}_i^{\text{LN}} = \epsilon_i - \lambda + (4\lambda_2 - G)v_i^2 \tag{2.59}$$

and the quasi-particle energy becomes

$$\mathcal{E}_i^{\text{LN}} = \sqrt{\epsilon_i^2 + \Delta^2} + \lambda_2 \tag{2.60}$$

with [127]

$$\lambda_2 = \frac{G}{4} \, \frac{\left(\sum_i^{(\omega)} u_i^3 v_i\right)\left(\sum_i^{(\omega)} u_i v_i^3\right) - \sum_i^{(\omega)} u_i^4 v_i^4}{\left(\sum_i^{(\omega)} u_i^2 v_i^2\right)^2 - \sum_i^{(\omega)} u_i^4 v_i^4} \, . \tag{2.61}$$

The gap and particle-number equations (2.38) and (2.48) have to be solved with the modified definition of $\tilde{\epsilon}_i$. In the light of results obtained for the weak pairing case (i.e. for small G) by Dobaczewski and Nazarewicz [128] and by Sheikh et al. [124], summarized in Fig. 2.2, the improvement gained by the Lipkin-Nogami method compared to plain HFB is only modest. On the other hand there are no systematic investigations on the quality of the Lipkin-Nogami correction in the context of Strutinsky's shell plus pairing correction.

Rather sophisticated procedures have been devised to determine the pairing-strength constant G for a given range ω from empirical mass differences within the BCS and the Lipkin-Nogami schemes [123]. However, all these

efforts cannot hide the fact that the basic assumption of a state-independent pairing matrix element G does not describe the physical situation correctly all along the fission path: Around scission the single particle states separate into those localized in either one of the nascent fragments and those, above the Fermi energy, which are still distributed over the entire nuclear volume. One therefore expects four different characteristic values for G. After scission the states above the Fermi energy will also become localized in one of the fragments, leading, for asymmetric fission, to different pairing strengths in the two fragments and consequently to different chemical potentials and pairing gaps. Therefore there is a phase transition in the pairing degree of freedom around scission [129]: after scission the particle numbers of the two fragments are separately constants of motion whereas for a compact nucleus only the total number of particles is a constant of motion. One should therefore not interpolate G between the ground state of the fissioning nucleus and separated fragments by means of the shape function $B_{\rm surf}$ as proposed in Ref. [130] nor assume a constant G.

For an odd system Eqs.

$$N' = 1 + \sum_{i\neq k_0}^{(\omega)} \left(1 - \frac{\tilde{\epsilon}_i}{\mathcal{E}_i}\right) \qquad \text{and} \qquad \frac{2}{G} = \sum_{i\neq k_0}^{(\omega)} \frac{1}{\mathcal{E}_i} \tag{2.62}$$

have to be solved for Δ and λ, instead of Eqs. (2.48) and (2.57). Here again the notation $\mathcal{E}_i = \sqrt{\tilde{\epsilon}_i^2 + \Delta^2}$ is used and N' is the number of particles occupying states in the 2ω band. The gap parameter Δ is smaller than for the neighboring even systems because the state k_0 is "blocked" and is not available for the set-up of the pairing correlations. Neglecting the v_i^4 term in Eq. 2.56 one finds for the ground-state expectation-value of the Routhian of an odd system

$$\langle \mathrm{BCS}|\hat{H}'|\mathrm{BCS}\rangle = 2\sum_{i\neq k_0}^{(\omega)} \tilde{\epsilon}_i v_i^2 + (\epsilon_k - \lambda) - \Delta^2/G\,.$$

If the pairing gap Δ is large compared to the level spacing, one obtains simple, analytic expressions for the pairing energy and the pairing gap by introducing a continuous, smooth single-particle level-density $g(e)$ (which shall include the time-reflected states) [97]. The gap equation (2.57) then becomes

$$\frac{2}{G} = \int_{\lambda-\omega}^{\lambda+\omega} \frac{\frac{1}{2}g(e)de}{\sqrt{(e-\lambda)^2 + \Delta^2}} \approx \frac{g(\lambda)}{2} \ln \frac{\sqrt{\omega^2+\Delta^2}+\omega}{\sqrt{\omega^2+\Delta^2}-\omega}\,. \tag{2.63}$$

Since the pairing-window half-width ω should be large compared to the pairing gap, $\omega \gg \Delta$, Eq. (2.63) can be simplified to

$$\frac{2}{G} \approx g(\lambda) \ln\left(\frac{2\omega}{\Delta}\right)\,. \tag{2.64}$$

This approximation is sometimes called the "uniform model". The relation (2.64) allows to estimate the pairing strength G when the average pairing gap

is known from experimental data. One can also see that G depends on the width of the window 2ω, i.e. on the number of states included in the sum in Eq. (2.54): G decreases with increasing number of states, included in the pairing Hamiltonian.

The BCS energy-gain with respect to the energy of a system without pairing correlations is

$$\Delta E = \langle \mathrm{BCS}|\hat{H}' + \lambda \hat{N}|\mathrm{BCS}\rangle - 2\sum_{i\le i_{\mathrm{Fermi}}} \epsilon_i = 2\sum_{i>0}^{(\omega)} \epsilon_i v_i^2 - \Delta^2/G - 2\sum_{i\le i_{\mathrm{Fermi}}} \epsilon_i \quad (2.65)$$

for an even particle number, where the Gv^4 term in Eq. (2.56) is neglected and $N = 2\sum_i v_i^2$ is used. The quantity ΔE can be calculated analytically in the uniform model. Using Eqs. (2.55) and (2.58) we obtain

$$\widetilde{\Delta E} = \frac{1}{2}\int_{\lambda-\omega}^{\lambda+\omega} e\left(1 - \frac{e-\lambda}{\sqrt{(e-\lambda)^2+\Delta^2}}\right) g(e)de - \frac{\Delta^2}{G} - \int_{\lambda-\omega}^{\lambda} eg(e)de \ .$$

After evaluation of the integrals and eliminating $1/G$ with Eq. (2.63), the pairing energy becomes

$$\widetilde{\Delta E} = \frac{1}{2} g(\lambda)\omega^2 \left(1 - \sqrt{1 + \left(\frac{\Delta}{\omega}\right)^2}\right) . \quad (2.66)$$

With $\omega \gg \Delta$ the last equation can be approximated by

$$\widetilde{\Delta E} \approx -\frac{1}{4} g(\lambda)\Delta^2 \ . \quad (2.67)$$

The Lipkin-Nogami approach was also reformulated in the uniform model by Möller and Nix [123]. The expression for λ_2, Eq. (2.61), becomes rather lengthy, we refer to Ref. [123] for details.

2.1.4 Thomas-Fermi and extended Thomas-Fermi theories

Of particular importance for the theory of fission is the Thomas-Fermi (TF) approximation because its expression for the binding energy admits a leptodermous expansion, leading to a liquid-drop formula. In TF approximation one assumes that the kinetic energy term in the HF energy, Eq. (2.7), can be approximated by the Fermi-gas expression for neutrons ($q = n$) and protons ($q = p$) [114]

$$T_q = \frac{2}{h^3}\int_{\mathrm{vol}} d^3r \ 4\pi \int dp\, p^2 \frac{p^2}{2M_{\mathrm{nucl}}} = \frac{\hbar^2}{2M_{\mathrm{nucl}}}\,\alpha \int_{\mathrm{vol}} \rho_q^{5/3}(\mathbf{r})\, d^3r \quad (2.68)$$

with $\alpha = (3/5)(3\pi^2)^{2/3}$. The Fermi-gas relation $\rho = (8\pi/3)(p_f/h)^3$ was used in the last equation.

The resulting equation is of little use as long as the exchange term of the potential contains the full density matrix ρ_{ij}. Therefore the Thomas-Fermi scheme has only been used either in connection with zero-range interactions or the Skyrme interactions [32], where the exchange and the direct term contribute with the same radial matrix elements to the potential energy, or momentum-dependent effective interactions, like the Seyler-Blanchard interaction [131], which are supposed to account in the direct term already for exchange effects.

A better approximation of the kinetic energy would take the variation of the potential in the surface into account. The resulting expansion in increasingly higher order derivatives of the potential leads to the extended Thomas-Fermi (ETF) scheme [114,132]. Defining the kinetic energy-density expression by a sum over occupied states

$$\tau_q(\mathbf{r}) = \sum_{i\sigma} |\nabla\varphi_i(\mathbf{r},\sigma,q)|^2 \tag{2.69}$$

in analogy to the density

$$\rho_q(\mathbf{r}) = \sum_{i\sigma} |\varphi_i(\mathbf{r},\sigma,q)|^2 \,, \tag{2.70}$$

one derives an expansion

$$\tau_q(\rho,\boldsymbol{\nabla}\rho) = \tau_q^{(\mathrm{TF})}(\rho) + \tau_q^{(2)}(\rho,\boldsymbol{\nabla}\rho) + \tau_q^{(4)}(\rho,\boldsymbol{\nabla}\rho)\,, \tag{2.71}$$

where $\tau_q^{(\mathrm{TF})}(\rho)$ is the Thomas-Fermi term

$$\tau_q^{(\mathrm{TF})}(\rho_q) = \alpha\rho_q^{5/3}(\mathbf{r})\,. \tag{2.72}$$

It yields the approximation (2.68) for the kinetic energy. The next term contains second order derivatives of the density (or squares of first order derivatives). If the effective potential does not depend on spin and momentum, the result is

$$\tau_q^{(2)}(\rho,\boldsymbol{\nabla}\rho) = \frac{1}{36}\frac{(\boldsymbol{\nabla}\rho_q)^2}{\rho_q} + \frac{1}{3}\Delta\rho_q \,. \tag{2.73}$$

The frequently used Skyrme and Gogny effective potentials (to be presented in Section 2.1.7) are momentum and spin dependent, which yields additional contributions to $\tau_q^{(2)}$

$$\begin{aligned}\tau_q^{(2)}[\rho_q] = {} & \frac{1}{36}\frac{(\boldsymbol{\nabla}\rho_q)^2}{\rho_q} + \frac{1}{3}\Delta\rho_q + \frac{1}{6}\frac{\boldsymbol{\nabla}\rho_q\cdot\boldsymbol{\nabla}f_q}{f_q} + \frac{1}{6}\rho_q\frac{\Delta f_q}{f_q} \\ & -\frac{1}{12}\rho_q\left(\frac{\boldsymbol{\nabla}f_q}{f_q}\right)^2 + \frac{1}{2}\left(\frac{2m}{\hbar^2}\right)^2\rho_q\left(\frac{\boldsymbol{W}_q}{f_q}\right)^2 ,\end{aligned} \tag{2.74}$$

where $f_q(\boldsymbol{r}) = M_{\mathrm{nucl}}/M^*_{\mathrm{nucl}}(\boldsymbol{r})$ is the effective mass form-factor, defined in Eq. (2.112), and $\boldsymbol{W}_q(\boldsymbol{r})$ is the spin-orbit form-factor given in Eq. (2.113) in

terms of the parameters of the effective interaction potential. The next term in the ETF expansion of the kinetic energy $\tau_q^{(4)}(\rho, \boldsymbol{\nabla}\rho)$ is a rather lengthy expression containing fourth order derivatives of ρ, cf. Ref. [133, 134].

Using a zero-range interaction like the Skyrme potential, the result (2.74) allows to express the total energy as a functional of the densities $\rho_n(r)$, $\rho_p(r)$, and their derivatives. Minimization of the energy involves then a variation of densities, rather than wave functions as in the Hartree-Fock approach. The variation is subject to the constraint that the volume integrals over the densities should be equal to the neutron and proton numbers.

It is instructive to calculate some basic liquid-drop parameters with a Skyrme energy-functional of the general form (cf. Eq. (2.105))

$$\mathcal{E}(\rho, \tau) = \epsilon\tau + C\rho^2 + F\rho^\nu + B(\nabla\rho)^2 + G\rho\tau \tag{2.75}$$

with $\epsilon = \hbar^2/(2M_{\rm nucl})$ and using the second order ETF approximation of the general structure [135]

$$\tau \approx \alpha\rho^{5/3} + \beta(\nabla\rho)^2/\rho + \gamma\nabla^2\rho \ .$$

In terms of the parameters C, F, and G one obtains for the volume energy

$$c_1 = \frac{\mathcal{E}(\rho_0)}{\rho_0} = \epsilon\alpha\rho_0^{2/3} + C\rho_0 + F\rho_0^{\nu-1} + G\alpha\rho_0^{5/3} \ ,$$

where the saturation density ρ_0 is the solution of the equation

$$d\mathcal{E}/d\rho|_{\rho_0} = (5/3)\epsilon\alpha\rho_0^{2/3} + 2C\rho_0 + \nu F\rho_0^{\nu-1} + (8/3)G\alpha\rho_0^{5/3} = 0.$$

The nuclear incompressibility constant

$$K = 9\rho_0^2 \left.\frac{\partial^2(\mathcal{E}(\rho)/\rho)}{\partial\rho^2}\right|_{\rho=\rho_0}$$

is given in terms of ρ_0 by

$$K = 10\epsilon\alpha\rho_0^{5/3} + 18C\rho_0^2 + 9\nu(\nu-1)F\rho_0^\nu + 40G\alpha\rho_0^{8/3}$$

and the effective mass $M^*_{\rm nucl}$ by

$$\frac{M_{\rm nucl}}{M^*_{\rm nucl}} = \frac{1}{\epsilon}\frac{\partial\mathcal{E}}{\partial\tau} = 1 + \rho_0\frac{G}{\epsilon}$$

and therefore the volume part of the level-density parameter (cf. Chapter 3, Eq. (3.93)).

$$\frac{a_{\rm vol}}{A} = \frac{2\pi}{9}(9\pi)^{1/3}\frac{M_{\rm nucl}\, r_0^2}{\hbar^2}\frac{\epsilon}{\epsilon + G\rho_0} \ .$$

The four parameters C, F, ν, and G, relevant for homogeneous nuclear matter, correspond to the four quantities c_1, ρ_0, K, and $a_{\rm vol}/A$. To the extend that

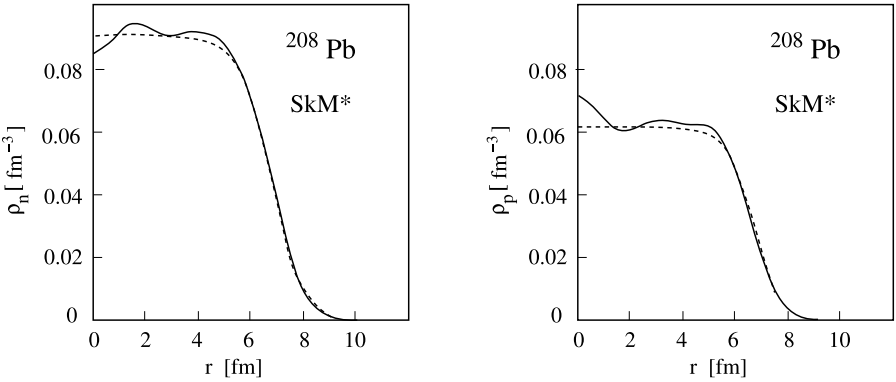

Fig. 2.3. Selfconsistent ETF neutron and proton densities (dashed lines) obtained with the Skyrme interaction SkM* for the nucleus ^{208}Pb compared with the corresponding Hartree-Fock densities (solid lines) (after Ref. [134]).

the latter are empirically known, the parameters in the Skyrme functional, except B, can be fitted.

For a plane infinite surface one obtains the surface-energy coefficient [136]

$$c_2 = 2(36\pi)^{1/3} c_1 \int_0^1 dx\, x\{[k_E + (1-k_E)x^2][b + c(1-x)]\}^{1/2} \qquad (2.76)$$

with

$$k_E = K/(18c_1), \qquad b = \epsilon\beta\rho_0^{2/3}/c_1, \qquad c = [\,B + G(\beta-\gamma)]\rho_0^{5/3}/c_1\ .$$

The equation can be used to determine also the parameter B for given ETF parameters β and γ. To derive Eq. (2.76) the simplified equation of state for homogeneous matter

$$\mathcal{E}_{\rm hom} = c_1 \frac{\rho}{\rho_0}\left[-1 + k_E\left(\frac{\rho-\rho_0}{\rho_0}\right)^2 + (1-k_E)\left(\frac{\rho-\rho_0}{\rho_0}\right)^4\right]$$

was used, which yields the same equilibrium values for ρ_0, c_1, and K as Eq. (2.75).

In general the density profile and the surface energy has to be determined numerically from minimizing the ETF energy with respect to the density $\rho(\mathbf{r})$. One expects densities of leptodermous type, i.e. without shell oscillations. In fact, the Euler-Lagrange equations of the variational procedure were solved numerically and it was shown [132, 137] that the resulting densities are very close to modified Fermi functions of the form

$$\rho(r) = \frac{\rho_c}{\left(1 + \exp\left([r - R^{(\rho)}]/d^{(\rho)}\right)^\gamma\right.}\,, \qquad (2.77)$$

where the parameter γ allows for an asymmetry of the density profile in the nuclear surface. When one performs the much simpler variational calculation in the restricted subspace of these modified Fermi functions, the variational parameters are the coefficients ρ_c, $R^{(\rho)}$, $d^{(\rho)}$ and γ for both, protons and neutrons.

An example of the ETF variational calculation is shown in Fig. 2.3 taken from Ref. [134], where the selfconsistent semiclassical neutron and proton densities obtained with the Skyrme interaction SkM* [138] for the nucleus ^{208}Pb are compared with the corresponding Hartree-Fock densities.

2.1.5 Relativistic mean field theory

Calculations of the lifetime of superheavy nuclei are very sensitive to the shell corrections to the liquid-drop background. These corrections depend crucially on the strength of the spin-orbit coupling in these nuclei. In nonrelativistic mean-field theories the spin-orbit potential depends on certain terms in the effective two-particle interaction which are fitted to properties of known nuclei. Their extrapolation to exotic nuclei is not quite unambiguous. It is therefore interesting to treat fission, in particular of superheavy nuclei, in a relativistic field theory were the spin-orbit coupling comes out naturally, without being added ad hoc from outside. In the following we discuss the relativistic, classical field theory of Walecka [139].

In this field-theoretical approach to the nuclear many-body problem the nucleus is treated as a set of nucleons described by Dirac spinors, which interact by the exchange of mesons. The attraction of the nucleons is caused by an effective scalar meson field σ ($I^\pi = 0^+, T = 0$), which is to simulate the effect of the real scalar mesons. The short-ranged, repulsive interaction is connected with the exchange of a vector meson ω ($I^\pi = 1^-, T = 0$) and an isovector meson denoted here by $\boldsymbol{\rho}$ ($I^\pi = 0^-, T = 1$). The electromagnetic interaction is carried by photons with the vector field A. The Walecka model is derived from the phenomenological, Lorentz-invariant, renormalizable Lagrangian [113,140]

$$\begin{aligned}\mathcal{L} = \bar{\psi}_i\{i\,\gamma^\mu\,\partial_\mu - M_{\rm nucl}\}\psi_i \\ +\frac{1}{2}\partial^\mu\sigma\,\partial_\mu\sigma - \frac{1}{2}m_\sigma\sigma^2 - g_\sigma\,\bar{\psi}_i\psi_i\,\sigma \\ -\frac{1}{4}\Omega^{\mu\nu}\,\Omega_{\mu\nu} + \frac{1}{2}m_\omega^2\,\omega^\mu\omega_\mu - g_\omega\,\bar{\psi}_i\,\gamma^\mu\,\psi_i\,\omega_\mu \\ -\frac{1}{4}\boldsymbol{R}^{\mu\nu}\,\boldsymbol{R}_{\mu\nu} + \frac{1}{2}m_\rho^2\,\boldsymbol{\rho}^{\,\mu}\boldsymbol{\rho}_\mu - g_\rho\bar{\psi}_i\,\gamma^\mu\boldsymbol{\tau}\,\psi_i\,\boldsymbol{\rho}_\mu \\ -\frac{1}{4}F^{\mu\nu}F_{\mu\nu} - e\bar{\psi}_i\,\gamma^\mu\,\frac{(1-\tau_3)}{2}\,\psi_i\,A_\mu\ ,\end{aligned} \tag{2.78}$$

where $M_{\rm nucl}$ is the nucleon mass, $m_\sigma, m_\omega, m_\rho$ are meson masses, and $g_\sigma, g_\omega, g_\rho$ are meson coupling constants. The isovector quantities are indicated by bold symbols. Following the usual practice we use in this subsection units such that $\hbar = c = 1$ and the four 4×4 matrices γ^μ, $\mu = 0 \ldots 3$, are defined by

$$\gamma^0 = \beta = \begin{pmatrix} I & 0 \\ 0 & -I \end{pmatrix}, \qquad \gamma^i = \begin{pmatrix} 0 & \boldsymbol{\sigma}^i \\ -\boldsymbol{\sigma}^i & 0 \end{pmatrix}, \quad i = 1, 2, 3 \,,$$

where I is the 2×2 unit matrix and $\boldsymbol{\sigma}^i$, $i = x, y, z$, are the standard 2×2 Pauli matrices. The notation $\bar{\psi} = \psi^+ \gamma^0$ is used. The field tensors of the vector bosons are given by

$$\begin{aligned} \Omega^{\mu\nu} &= \partial^\mu \omega^\nu - \partial^\nu \omega^\mu, \\ \mathbf{R}^{\mu\nu} &= \partial^\mu \boldsymbol{\rho}^\nu - \partial^\nu \boldsymbol{\rho}^\mu - g_\rho (\boldsymbol{\rho}^\mu \times \boldsymbol{\rho}^\nu) \\ F^{\mu\nu} &= \partial^\mu A^\nu - \partial^\nu A^\mu \,. \end{aligned} \tag{2.79}$$

In the non-linear σ-ω-ρ model of Boguta and Bodmer [141] realistic compression and surface properties of nuclei could be obtained by replacing the mass term of the σ field by a nonlinear, self-interaction potential of the σ-field

$$\frac{1}{2} m_\sigma^2 \sigma^2 \to U(\sigma) = \frac{1}{2} m_\sigma^2 \sigma^2 + \frac{1}{3} g_2 \sigma^3 + \frac{1}{4} g_3 \sigma^4 \tag{2.80}$$

with additional phenomenological parameters g_2 and g_3.

So far the field variables in Eq. (2.78) are creation and destruction operators in Fock space. In the Walecka model one introduces a mean-field approximation by treating all fields as classical fields

$$\psi \to \langle \psi \rangle, \quad \sigma \to \langle \sigma \rangle, \quad \omega_\mu \to \langle \omega_\mu \rangle, \quad \boldsymbol{\rho}_\mu \to \langle \boldsymbol{\rho}_\mu \rangle, \quad A_\mu \to \langle A_\mu \rangle$$

and assuming that the meson and the electric fields are time-independent in the rest frame of the nucleus and that the time-dependence of the spinor can be split off as a phase factor $\exp(i\epsilon t)$. This allows us to omit all boson currents in the Euler-Lagrange equations of $\mathcal{L}$. Note that the term "mean field" is used here not with the same meaning as in the previously considered nonrelativistic theories.

With these approximations the Euler-Lagrange equations of the Lagrangian (2.78) yield a stationary Dirac equation for the spinor field ψ

$$\{-i\alpha\nabla + \beta M^*_{\text{nucl}}(\boldsymbol{r}) + V(\boldsymbol{r})\}\psi_i(\boldsymbol{r}) = \varepsilon_i \psi_i(\boldsymbol{r}) \,, \tag{2.81}$$

stationary Klein-Gordon equations for the meson fields,

$$\begin{aligned} (-\Delta + m_\sigma^2)\, \sigma(\boldsymbol{r}) &= -g_\sigma \rho_s(\boldsymbol{r}) - g_2 \sigma^2 - g_3 \sigma^3 \,, \\ (-\Delta + m_\omega^2)\, \omega^0(\boldsymbol{r}) &= g_\omega j^0(\mathbf{r}) \,, \\ (-\Delta + m_\rho^2)\, \boldsymbol{\rho}^0(\boldsymbol{r}) &= g_\rho \boldsymbol{j}^0(\boldsymbol{r}) \,, \end{aligned} \tag{2.82}$$

and the Poisson equation for the photon field

$$-\Delta\, A^0 = e j_p^0(\boldsymbol{r}) \,, \tag{2.83}$$

where the source terms of the last four equations are the scalar density

$$\rho_s = \sum_{i=1}^{A} \bar{\psi}_i \psi_i \tag{2.84}$$

and the time-like components of the current, the isovector current, and the charge current of the nuclear field. They are defined by

$$j^0 = \sum_{i=1}^{A} \psi_i^+ \psi_i \,, \quad \boldsymbol{j}^0 = \sum_{i=1}^{A} \psi_i^+ \boldsymbol{\tau}\, \psi_i \,, \quad j_p^0 = \sum_{i=1}^{A} \psi_i^+ \frac{(1-\tau_3)}{2} \psi_i \,. \tag{2.85}$$

The space-like components of these currents were assumed to vanish in the Walecka model. In the Dirac equation (2.81) β and $\alpha^i = \beta\gamma^i$ $(i = 1, 2, 3)$ are the Dirac matrices. The mass in Eq. (2.81) is renormalized by the σ field and becomes an effective mass

$$M^*_{\rm nucl}(\boldsymbol{r}) = M_{\rm nucl} + g_\sigma\, \sigma(\boldsymbol{r}) \,, \tag{2.86}$$

and the so-called vector potential

$$V(\boldsymbol{r}) = g_\omega\, \omega^0(\boldsymbol{r}) + g_\rho \tau_3\, \rho^0(\boldsymbol{r}) + \frac{e(1-\tau_3)}{2} A^0(\boldsymbol{r}) \tag{2.87}$$

is the time-like component of a Lorentz vector. The eigenvalues ϵ_i of the Dirac equation (2.81) are labeled by quantum numbers i. For a spherical system $i = \{njm_j\kappa t_z\}$, where n is the radial quantum number, j and m_j are the total angular momentum and its z component, $\kappa = \pm(j + 1/2)$, and t_z is an isospin quantum-number. It is assumed that in the ground state the nucleons occupy the lowest A eigenstates of Eq. (2.81). Eqs. (2.81)-(2.85) have to be solved selfconsistently by an iterative procedure [142, 143]

Treating the spinor field as a classical field implies the neglect of exchange contributions to the total energy

$$E = \sum_{i=1}^{A} \epsilon_i - \frac{1}{2} \int d^3r \left(g_\sigma \rho_s(\mathbf{r}) \sigma(\mathbf{r}) + \frac{1}{3} g_2 \sigma^3(\mathbf{r}) \right.$$
$$\left. + \frac{1}{2} g_3 \sigma^4(\mathbf{r}) + g_\omega j^0(\mathbf{r}) \omega^0(\mathbf{r}) + g_\rho \boldsymbol{j}^0(\mathbf{r}) \boldsymbol{\rho}^0(\mathbf{r}) + e j_p^0(\mathbf{r}) A^0(\mathbf{r}) \right) . \tag{2.88}$$

This approximation is therefore called Hartree approximation in field theory. For a treatment of the quantized nucleon field and inclusion of exchange terms in the energy we refer to the work of Brockmann [144] and numerical calculations also for spherical nuclei by Bouyssy et al. [145].

The cheapest way to account for pairing correlations in this context is the use of the BCS scheme of subsection 2.1.3 with a constant pairing matrix-element G, fitted to odd-even mass differences, using the ϵ_i as single-particle energies. From Eq. (2.46) occupation numbers v_i^2 are obtained and all sums over i in Eqs. (2.84), (2.85), and (2.88) are replaced by sums weighted with

v_i^2: $\sum_{i=1}^{A} \rightarrow \sum_i^{(\omega)} v_i^2$. The system consisting of the BCS equations and Eqs. (2.81)-(2.85) is solved selfconsistently [146]. Considerably more involved is an attempt to obtain pairing correlations from the coupling of the meson fields to the nucleons since it requires to treat all fields in their quantized form [140].

There are several parameter sets of the RMF theory and frequently used ones are the NL1, NL-Sh, and NL-3 sets [147] and the NL-Z2 parameters [148]. The latter set is

$$\begin{array}{ll} M_{\rm nucl} = 939.0 \text{ MeV} & g_\sigma = 10.217 \\ m_\sigma = 508.194 \text{ MeV} & g_2 = \text{-}10.431 \\ m_\omega = 782.501 \text{ MeV} & g_3 = \text{-}28.885 \\ m_\rho = 763.000 \text{ MeV} & g_\omega = 12.868 \\ & g_\rho = 4.474 \end{array}$$

and was fitted to ground-state masses and electric formfactors of a selection of spherical nuclei between ^{16}O and ^{208}Pb, where a correction for the spurious center-of-mass motion was included.

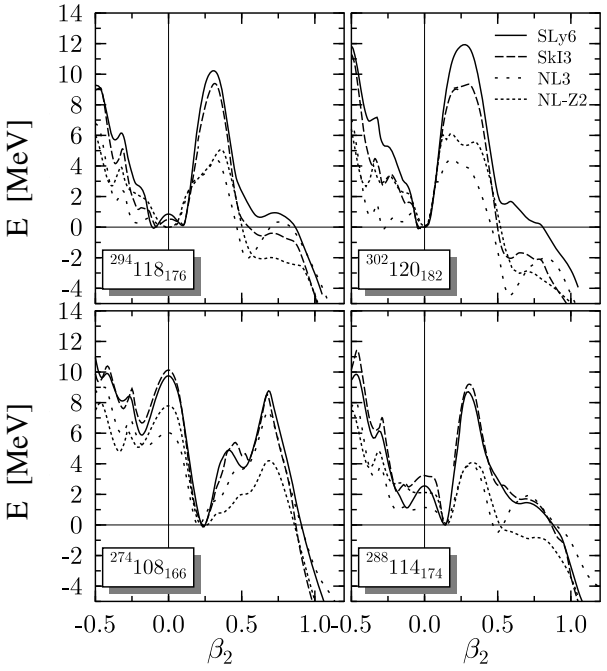

Fig. 2.4. The energetically favored fission barriers of four superheavy nuclei normalized to the ground-state energy. They were evaluated in Ref. [149] for two Skyrme interactions (SLy6, SkI3) and for the RMF theory with parameter sets NL-3 and NL-Z2 (from Ref [149]).

The RMF theory provides a reasonably good description of many features of nuclei, but it yields rather poor fission barrier heights and widths. In Fig. 2.4, taken from Ref. [149], the lowest selfconsistent fission barriers of four different superheavy nuclei are shown. Results obtained with two sets of RMF parameters (NL-3 and NL-Z2) are compared with estimates obtained with the Skyrme forces SLy6 and SkI3. It is seen that the barrier heights evaluated in these four models differ significantly from each other. Generally, the present parametrizations of the RMF theory yield too low barriers.

2.1.6 Spontaneous symmetry breaking

In all mean-field approaches the ground-state wave function violates fundamental symmetries of the Hamiltonian. A Slater determinant of bound states violates translational and Galilean invariances and for deformed ground states it also violates rotational symmetry. It is worth noting that in the iterative solution procedure of the HF equations the initial state should already contain the symmetry-breaking property of the ground state. If one starts, for example, with a spherically symmetric density, all iterations remain spherically symmetric since the Hamiltonian is rotationally invariant, even when the actual ground state is nonspherical. Alternatively, the desired symmetry violation may be induced by adding an appropriate constraint to the Hamiltonian H. Octupole-deformed local minima also violate space-reflection symmetry and non-spin-saturated systems violate in addition time-reflection symmetry.

Ground states in the HFB theory are not eigenstates of the particle-number operator and therefore violate the gauge symmetry of the Hamiltonian. A simple, approximate way to account for these deficiencies is to require that the mean-field solution shall at least in the average have the required values for the proton and neutron numbers, the total angular momentum, and the square of the linear momentum. Average conservation of the particle number is achieved in the HFB scheme by the $\lambda\hat{N}$-term in the variational principle Eq. (2.26). Spurious zero-point center-of-mass motion can be accounted for by subtracting the center-of-mass kinetic energy operator $\hat{E}_{\mathrm{c.m.}}$ from the kinetic energy term in the Hamiltonian

$$\begin{aligned}\hat{E}_{\mathrm{kin}} - \hat{E}_{\mathrm{c.m.}} &= \sum_{i=1}^{A} \frac{\hat{\mathbf{p}}_i^2}{2M_{\mathrm{nucl}}} - \frac{(\sum_{i=1}^{A} \hat{\mathbf{p}}_i)^2}{2M_{\mathrm{nucl}}A} \\ &= \frac{1}{2M_{\mathrm{nucl}}}\left(1 - \frac{1}{A}\right)\sum_{i=1}^{A} \hat{\mathbf{p}}_i^2 - \frac{1}{2M_{\mathrm{nucl}}A}\sum_{i>j} \hat{\mathbf{p}}_i\hat{\mathbf{p}}_j \ . \quad (2.89)\end{aligned}$$

The second term in the above equation is numerically involved as it includes double integrals and is neglected in most applications. A more detailed discussion of this problem is given e.g. in Ref. [150].

Similarly, to approximate the effect of the angular momentum projection on the energy of a deformed nucleus, one subtracts the zero-point rotational

energy $E^0_{\rm rot}$ from the total HFB energy (2.35)

$$E^0_{\rm rot} = \frac{1}{2\mathcal{J}} \langle 0| \sum_i \hat{\mathbf{j}}_i^2 |0\rangle \ , \tag{2.90}$$

where $\mathcal{J}$ is the moment of inertia of the nucleus. For its choice see for example Refs. [151, 152].

Within the framework of the mean-field theory this is the best one can do. However, the wave function of the ground state is still not an eigenstate of the symmetry operators, which is very undesirable when discussing spectroscopic observables. Let us consider the special case of rotational bands, either over a deformed ground state, or over secondary minima or fission saddle-points. The HF or HFB states in space representation $\Phi(\mathbf{x}_1, \mathbf{x}_2, \ldots \mathbf{x}_A)$ depend on the coordinates $\mathbf{x}_i$ in space, spin and isospin spaces of all A nucleons. They refer to an arbitrary space-fixed coordinate system. A wave function $\mathcal{D}(\theta_1, \theta_2, \theta_3)\Phi$ referring to a coordinate system, rotated by Euler angles $\theta_1, \theta_2, \theta_3$, would also be a solution of the HF or HFB equations to the same energy. Peierls and Yoccoz [153] therefore extended the mean-field scheme by considering test wave functions of the form

$$\Psi = \frac{1}{8\pi^2} \int_0^{2\pi} d\theta_1 \int_0^{\pi} \sin\theta_2 d\theta_2 \int_0^{2\pi} d\theta_3 \, g(\theta_1, \theta_2, \theta_3) \mathcal{D}(\theta_1, \theta_2, \theta_3) \Phi \tag{2.91}$$

in the variational principle (2.26), where $g(\theta_1, \theta_2, \theta_3)$ is a weight function to be determined from the variational principle

$$\delta \frac{\langle \Psi | \hat{H} | \Psi \rangle}{\langle \Psi | \Psi \rangle} = 0. \tag{2.92}$$

It turns out that the function g becomes a representation of the rotational group (Zeh's theorem [154]) thus making Ψ an eigenfunction of the angular momentum operator.

One may either vary the weight function g and the single-particle states in the HF state or the quasiparticle states in the HFB state at the same time, which is called "variation after projection" (VAP), or the single-particle or quasiparticle states are first determined by the variational principle (2.26) and only the function g is determined from Eq. (2.92). This is the "variation before projection". The latter approach is numerically less demanding, but leads to higher, i.e. less satisfactory, ground-state energies [155]. It can be shown that the difference between the binding energies in the two approaches becomes smaller when the symmetry breaking gets larger, that is, when the deviation from sphericity of the HF or HFB state increases. For a more detailed discussion of symmetry restoration by projection techniques we refer to Chap. 11 of Ref. [108]. For approximation schemes to VAP see the review by Flocard and Onishi [156]. Their relation to the generator-coordinate method in connection with the Gaussian overlap approximation (see Ref. [108], Chap. 10) has

been studied in the work of Góźdź, Pomorski, Brack, and Werner [157–159], in particular in cases of simultaneous symmetry violation in several degrees of freedom.

To obtain states with well-defined particle number from the BCS wave function, the definition (2.40) is generalized by introducing a phase angle ϕ

$$|\mathrm{BCS}(\phi)\rangle = \prod_{i>0}(u_i + e^{i\phi} v_i \hat{a}_i^+ \hat{a}_{\bar{i}}^+ |0\rangle \; .$$

One can convince oneself that expectation values like $\langle \mathrm{BCS}(\phi)|\hat{N}|\mathrm{BCS}(\phi)\rangle$ and $\langle \mathrm{BCS}(\phi)|\hat{H}|\mathrm{BCS}(\phi)\rangle$ or Δ are independent of ϕ and are still given by Eqs. (2.41), (2.42), and (2.47), respectively. Putting $e^{i\phi} = \zeta$ the state

$$|\Psi(p)\rangle = \frac{1}{2\pi i} \oint \frac{d\zeta}{\zeta^{p+1}} \prod_{i>0}(u_i + \zeta v_i \hat{a}_i^+ \hat{a}_{\bar{i}}^+ |0\rangle \tag{2.93}$$

consists of exactly p pairs, i.e. is an eigenstate of the particle number $N = 2p$, because, due to the residue theorem, the integral picks out just the term with p factors $\zeta v_i \hat{a}_i^+ \hat{a}_{\bar{i}}^+$ in the numerator of the integrand [160, 161]. Using Wick's theorem [108] one can show that in terms of the operator of the number of pairs $\hat{N}/2$

$$|\mathrm{BCS}(\phi)\rangle = e^{i\phi\hat{N}/2}|\mathrm{BCS}\rangle \, .$$

Therefore Eq. (2.93) can also be written

$$|\Psi(p)\rangle = \int_0^{2\pi} d\phi \, e^{i\phi(\hat{N}/2-p)}|\mathrm{BCS}\rangle \; . \tag{2.94}$$

One should note the analogy with Eq. (2.91) when the latter is restricted to rotations by an angle θ_3 around a symmetry axis: The expression $\mathcal{D}(\theta_3)\Phi = \Phi(\theta_3)$ corresponds to the transition from $|\mathrm{BCS}\rangle$ to $|\mathrm{BCS}(\phi)\rangle$. Since the degeneracy with respect to ϕ is due to a one-dimensional Abelian group, its representations are the phase functions $e^{-ip\phi}$ with integer p. Identifying the weight function $g(\theta_3)$ in Eq. (2.91) according to Zeh's theorem with this phase function, one obtains the integral (2.94).

2.1.7 Effective interactions

It is assumed, somewhat arbitrarily, that the central part of the nuclear effective two-body interaction is hermitian and – in space representation – short-ranged, compared to a typical inverse wave number $1/k_f$ of bound-state nuclear wave functions. It is further assumed to be rotational invariant in space, spin space, and isospin space and translational invariant. A prototype of such potential, local in the space variables $\mathbf{r}_1$ and $\mathbf{r}_2$ and in the spin and isospin variables, has the general form

$$V(\mathbf{r}_1, \mathbf{r}_2, \boldsymbol{\sigma}_1, \boldsymbol{\sigma}_2, \boldsymbol{\tau}_1, \boldsymbol{\tau}_2) = f(|\mathbf{r}_1 - \mathbf{r}_2|/\beta)\hat{A}(\hat{P}_\sigma, \hat{P}_\tau) \tag{2.95}$$

with a short-range function $f(x)$, for example $f = \exp(-x^2)$, $x = |\mathbf{r}_1 - \mathbf{r}_2|/\beta$ and a range parameter $\beta \ll 1/k_f$. The dependence on spin and isospin variables is given by the operator $\hat{A}$ of Eq. (2.2).

Skyrme interactions

The fast variation of the effective two-body interaction potential on the scale of the nuclear radius suggests a moment expansion of the matrix element $\langle l'm'|f(\mathbf{r}_1 - \mathbf{r}_2)|lm\rangle$ [162]. Introducing coordinates $\mathbf{r} = \mathbf{r}_1 - \mathbf{r}_2$ and $\mathbf{R} = \frac{1}{2}(\mathbf{r}_1 + \mathbf{r}_2)$ one expands the integrand in the spatial integral up to second order in $\mathbf{r}$

$$\begin{aligned}\langle l'm'|f(r)|lm\rangle &= \int \varphi^*_{l'}(\mathbf{r}_1)\varphi^*_{m'}(\mathbf{r}_2) f(r)\varphi_l(\mathbf{r}_1)\varphi_m(\mathbf{r}_2) d^3r\, d^3R \\ &\approx \int f(r)\left[1 + (\mathbf{r}\boldsymbol{\nabla}_\mathbf{r}) + \frac{1}{2}(\mathbf{r}\boldsymbol{\nabla}_\mathbf{r})^2\right][\varphi^*_{l'}(\mathbf{r}_1)\varphi^*_{m'}(\mathbf{r}_2)]_{\mathbf{r}=0} \\ &\times \left[1 + (\mathbf{r}\boldsymbol{\nabla}_\mathbf{r}) + \frac{1}{2}(\mathbf{r}\boldsymbol{\nabla}_\mathbf{r})^2\right][\varphi_l(\mathbf{r}_1)\varphi_m(\mathbf{r}_2)]_{\mathbf{r}=0}\, d^3r\, d^3R\,. \end{aligned} \tag{2.96}$$

Since for fixed $\mathbf{R}$

$$\begin{aligned}\boldsymbol{\nabla}_\mathbf{r}[\varphi_l(\mathbf{r}_1)\varphi_m(\mathbf{r}_2)] &= \frac{\partial\varphi_l(\mathbf{r}_1)\varphi_m(\mathbf{r}_2)}{\partial\mathbf{r}_1}\frac{\partial\mathbf{r}_1}{\partial\mathbf{r}} + \frac{\partial\varphi_l(\mathbf{r}_1)\varphi_m(\mathbf{r}_2)}{\partial\mathbf{r}_2}\frac{\partial\mathbf{r}_2}{\partial\mathbf{r}} \\ &= \frac{1}{2}[\partial_{\mathbf{r}_1} - \partial_{\mathbf{r}_2}][\varphi_l(\mathbf{r}_1)\varphi_m(\mathbf{r}_2)]\ ,\end{aligned}$$

one defines operators $\overleftarrow{\boldsymbol{\nabla}}_{12} = \boldsymbol{\nabla}_1 - \boldsymbol{\nabla}_2$ and $\overrightarrow{\boldsymbol{\nabla}}_{12} = \boldsymbol{\nabla}_1 - \boldsymbol{\nabla}_2$ acting on the bra-states $\varphi^*_{l'}(\mathbf{r}_1)\varphi^*_{m'}(\mathbf{r}_2)$ and on the ket-states $\varphi_l(\mathbf{r}_1)\varphi_m(\mathbf{r}_2)$, respectively. Performing the integration with respect to $\mathbf{r}$ first and calling the first nonvanishing moments of the function $f(r)$

$$V_0 = \int f(r)d^3r, \qquad \text{and} \qquad 2V_2 = \int r^2 f(r)d^3r$$

the integral of Eq. (2.96) can be rewritten as

$$\begin{aligned}&\int d^3R\,[\varphi^*_{l'}(\mathbf{r}_1)\varphi^*_{m'}(\mathbf{r}_2)]_{\mathbf{r}=0}\left[V_0 + \frac{V_2}{4}(\overleftarrow{\boldsymbol{\nabla}}^2 + \overrightarrow{\boldsymbol{\nabla}}^2 + 2\,\overleftarrow{\boldsymbol{\nabla}}\overrightarrow{\boldsymbol{\nabla}})\right][\varphi_l(\mathbf{r}_1)\varphi_m(\mathbf{r}_2)]_{\mathbf{r}=0} \\ &= \int d^3r_1 d^3r_2 \delta(\mathbf{r}_1 - \mathbf{r}_2)\,[\varphi^*_{l'}(\mathbf{r}_1)\varphi^*_{m'}(\mathbf{r}_2)]\left[V_0 + \frac{V_2}{4}(\overleftarrow{\boldsymbol{\nabla}}^2 + \overrightarrow{\boldsymbol{\nabla}}^2 + 2\,\overleftarrow{\boldsymbol{\nabla}}\overrightarrow{\boldsymbol{\nabla}})\right] \\ &\qquad\qquad \times [\varphi_l(\mathbf{r}_1)\varphi_m(\mathbf{r}_2)]\ .\end{aligned} \tag{2.97}$$

Note that all odd moments of $f(r)$ vanish. The exchange operator $\hat{A}$ simplifies considerably for zero-range potential-functions f. Introducing the operator of spatial exchange $\hat{P}_r$, we have

$$\hat{P}_r^2 = \hat{P}_\sigma^2 = \hat{P}_\tau^2 = 1 \,.$$

When applied to an antisymmetrized two-nucleon state,

$$\hat{P}_r \hat{P}_\sigma \hat{P}_\tau = -1 \,.$$

From these relations follows

$$\begin{aligned}
&\hat{P}_r \delta(\mathbf{r}_1 - \mathbf{r}_2) = \delta(\mathbf{r}_1 - \mathbf{r}_2), && \hat{P}_r \overleftarrow{\boldsymbol{\nabla}}^2 \delta(\mathbf{r}_1 - \mathbf{r}_2) = \overleftarrow{\boldsymbol{\nabla}}^2 \delta(\mathbf{r}_1 - \mathbf{r}_2), \\
&\hat{P}_r \overleftarrow{\boldsymbol{\nabla}} \delta(\mathbf{r}_1 - \mathbf{r}_2) = -\overleftarrow{\boldsymbol{\nabla}} \delta(\mathbf{r}_1 - \mathbf{r}_2), && \hat{P}_\tau \overleftarrow{\boldsymbol{\nabla}} \delta(\mathbf{r}_1 - \mathbf{r}_2) = \hat{P}_\sigma \overleftarrow{\boldsymbol{\nabla}} \delta(\mathbf{r}_1 - \mathbf{r}_2), \\
&\hat{P}_\tau \delta(\mathbf{r}_1 - \mathbf{r}_2) = -\hat{P}_\sigma \delta(\mathbf{r}_1 - \mathbf{r}_2), && \hat{P}_\tau \overleftarrow{\boldsymbol{\nabla}}^2 \delta(\mathbf{r}_1 - \mathbf{r}_2) = -\hat{P}_\sigma \overleftarrow{\boldsymbol{\nabla}}^2 \delta(\mathbf{r}_1 - \mathbf{r}_2)
\end{aligned}$$

and the same equations with $\overrightarrow{\boldsymbol{\nabla}}$. From these results, together with Eq. (2.97), the general form of the two-particle effective potential becomes, in the approximation of very short range,

$$\begin{aligned}
V_{12} = {} & t_0(1 + x_0\hat{P}_\sigma)\,\delta(\boldsymbol{r}_1 - \boldsymbol{r}_2) \\
& - \frac{1}{8} t_1 (1 + x_1 \hat{P}_\sigma) \left[\overleftarrow{\boldsymbol{\nabla}}_{12}^2 \; \delta(\boldsymbol{r}_1 - \boldsymbol{r}_2) + \delta(\boldsymbol{r}_1 - \boldsymbol{r}_2) \; \overrightarrow{\boldsymbol{\nabla}}_{12}^2 \right] \\
& + \frac{1}{4} t_2 \,(1 + x_2 \hat{P}_\sigma) \; \overleftarrow{\boldsymbol{\nabla}}_{12} \; \delta(\boldsymbol{r}_1 - \boldsymbol{r}_2) \; \overrightarrow{\boldsymbol{\nabla}}_{12}
\end{aligned} \tag{2.98}$$

with

$$\begin{aligned}
t_0 &= (W + M)V_0, & t_0 x_0 &= (B + H)V_0 \\
-t_1 &= 2(W + M)V_2, & -t_1 x_1 &= 2(B + H)V_2 \\
t_2 &= 2(W - M)V_2, & t_2 x_2 &= 2(B - H)V_2 \,.
\end{aligned}$$

To control the size of the spin-orbit splitting in the HF single-particle potential, derived from the two-body interaction (2.98), Bell and Skyrme [163] added a spin-orbit term

$$V_{LS} = i(1/4) W_{LS} \big[\overleftarrow{\boldsymbol{\nabla}}_{12} \times \delta(\boldsymbol{r}_1 - \boldsymbol{r}_2) \; \overrightarrow{\boldsymbol{\nabla}}_{12} \big] \cdot (\boldsymbol{\sigma}_1 + \boldsymbol{\sigma}_2) \tag{2.99}$$

to the central potential (2.98), where $\boldsymbol{\sigma}_i$ is twice the spin operator of nucleon i. To enforce proper saturation density and energy density in bulk nuclear matter, Skyrme added also a repulsive three-body force of zero range $V_{123} = t_3 \delta(\mathbf{r}_1 - \mathbf{r}_2)\delta(\mathbf{r}_2 - \mathbf{r}_3)$ to the two-body interaction [164]. For spin-saturated systems this term was shown by Bäckmann, Jackson, and Speth [165] to be equivalent to a density-dependent two-particle potential

$$V_{123} = \frac{t_3}{6}(1 + x_3 \hat{P}_\sigma)\rho(\mathbf{R})\delta(\mathbf{r}_1 - \mathbf{r}_2) \,,$$

where $\rho(\mathbf{R})$ is the sum of proton and neutron densities. To obtain more flexibility to reproduce the position of giant monopole resonance-energies, one uses generally the slightly more general form

$$V_{123} = \frac{t_3}{6}(1 + x_3\hat{P}_\sigma)[\rho(\mathbf{R})]^\gamma \delta(\mathbf{r}_1 - \mathbf{r}_2) \tag{2.100}$$

with additional parameters x_3 and γ. Finally, the Coulomb two-body potential between protons is given by

$$V_{\rm Coul} = \frac{e^2}{|\mathbf{r}_1 - \mathbf{r}_2|} \ . \tag{2.101}$$

The total effective interaction is the sum of the potentials (2.98)-(2.101)

$$V_{\rm Skyrme} = V_{12} + V_{LS} + V_{123} + V_{\rm Coul} \, . \tag{2.102}$$

The parameters of the Skyrme interaction are: $t_0, t_1, t_2, t_3, x_0, x_1, x_2, x_3, W_{LS}$ and γ. There are several sets of these parameters adjusted to binding energies of various mass regions and additional observables, in particular RPA-type excitations of monopole, dipole or quadrupole character. Frequently used sets are, e.g., SkIII [166] (fairly good binding energies, less perfect radii), SkM* [138] (good binding energies, including fission barriers, good radii), SkP [167] (gives realistic pairing with Skyrme interactions), SLy6 [168] (fitted to describe neutron-rich nuclei and neutron stars), SkI3 [169] (gives isovector spin-orbit splitting and electromagnetic form factors), or BSk1 [170] (based on an astrophysically biased, large-scale mass-fit); see Fig. 2.4 for fission-barrier heights of superheavy nuclei, calculated with Skyrme interactions SLy6 and SkI3.

For fission studies the SkM* potential has often been used. Its set of parameters

$$\begin{array}{ll} t_0 = \text{-2645 MeV fm}^3 & x_0 = 0.09 \\ t_1 = 410 \text{ MeV fm}^5 & x_1 = 0 \\ t_2 = \text{-135 MeV fm}^5 & x_2 = 0 \\ t_3 = 15595 \text{ MeV fm}^{(3+3\gamma)} & x_3 = 0 \\ W_{LS} = 130 \text{ MeV fm}^5 & \gamma = 1/6 \end{array}$$

was chosen to reproduce in particular experimental fission barrier heights.

Using Slater determinants to calculate the expectation value of the Hamiltonian with Skyrme interactions, leads to the energy functional

$$E = \int \mathcal{E}(\rho(\mathbf{r}), \boldsymbol{\nabla}\rho(\mathbf{r}), \tau(\mathbf{r}), \mathbf{J}) \, d^3r \ , \tag{2.103}$$

where the energy density $\mathcal{E}$ is a function of the nucleon densities ρ_q, Eq. (2.70), the kinetic energy densities τ_q, Eq. (2.69), and spin-orbit densities

$$\mathbf{J}_q = -i \sum_{i,\sigma,\sigma'} \varphi_i(\mathbf{r}, \sigma, q)[\boldsymbol{\nabla}\varphi_i(\mathbf{r}, \sigma', q) \times \langle\sigma|\boldsymbol{\sigma}|\sigma'\rangle] \ . \tag{2.104}$$

Assuming that there is no isospin mixing in the HF basis and that the ground state is time-reversal invariant, the explicit form of $\mathcal{E}$ was derived by Vautherin and Brink [171]

$$
\begin{aligned}
&\mathcal{E}[\rho_q(\boldsymbol{r}),\tau_q(\boldsymbol{r}),\boldsymbol{J}_q(\boldsymbol{r})] = \\
&\frac{\hbar^2}{2M_{\rm nucl}}\tau + \frac{1}{2}t_0\left[\left(1+\frac{x_0}{2}\right)\rho^2 - \left(x_0+\frac{1}{2}\right)(\rho_n^2+\rho_p^2)\right] \\
&+\frac{1}{12}t_3\rho^\gamma\left[\left(1+\frac{x_3}{2}\right)\rho^2 - \left(x_3+\frac{1}{2}\right)(\rho_n^2+\rho_p^2)\right] \\
&+\frac{1}{4}\left[t_1\left(1+\frac{x_1}{2}\right)+t_2\left(1+\frac{x_2}{2}\right)\right]\tau\rho \\
&-\frac{1}{4}\left[t_1\left(x_1+\frac{1}{2}\right)-t_2\left(x_2+\frac{1}{2}\right)\right](\tau_n\rho_n+\tau_p\rho_p) \\
&+\frac{1}{16}\left[3t_1\left(1+\frac{x_1}{2}\right)-t_2\left(1+\frac{x_2}{2}\right)\right](\boldsymbol{\nabla}\rho)^2 \\
&-\frac{1}{16}\left[3t_1\left(x_1+\frac{1}{2}\right)+t_2\left(x_2+\frac{1}{2}\right)\right][(\boldsymbol{\nabla}\rho_n)^2+(\boldsymbol{\nabla}\rho_p)^2] \\
&+\frac{W_{LS}}{2}[\boldsymbol{J}\cdot\boldsymbol{\nabla}\rho+\boldsymbol{J}_n\cdot\boldsymbol{\nabla}\rho_n+\boldsymbol{J}_p\cdot\boldsymbol{\nabla}\rho_p]+\mathcal{E}_{\rm Coul}\ ,
\end{aligned}
\tag{2.105}
$$

where $\rho=\rho_p+\rho_n$, $\tau=\tau_p+\tau_n$, and $\mathcal{E}_{\rm Coul}$ is the Coulomb energy-density. The latter can be written as sum of a direct and an exchange contribution. The exchange contribution is usually approximated by the Slater form [162, 172] (cf. Eq. (2.142) below)

$$
\mathcal{E}_{\rm Coul}(\boldsymbol{r}) = \frac{e^2}{2}\rho_p(\boldsymbol{r})\int d^3r'\,\frac{\rho_p(\boldsymbol{r}\,')}{|\,\boldsymbol{r}-\boldsymbol{r}\,'|} - \frac{3}{4}e^2\left(\frac{3}{\pi}\right)^{1/3}\rho_p^{4/3}(\boldsymbol{r})\ . \tag{2.106}
$$

For systems whose ground-state wave-function is not time-reversal invariant, for example, for odd systems, the energy density has additional terms [115, 173]. The terms in the first two lines on the left-hand-side of Eq. (2.105) determine essentially properties of bulk nuclear matter, the saturation density ρ_0, the volume-energy coefficient of the liquid-drop formula c_1, and the incompressibility parameter K. The terms in the third and fourth line control the effective mass $M^*_{\rm nucl}$ and those in the fifth and sixth line contribute to the surface energy.

Minimizing the total energy of Eq. (2.103) with respect to variations of the single-particle wavefunctions $\varphi_j^{(q)}$, one obtains the Skyrme HF-equation

$$
\hat{h}_q\varphi_j^{(q)} = \varepsilon_j^{(q)}\varphi_j^{(q)}\ . \tag{2.107}
$$

for the mean-field single-particle Hamiltonian

$$
\hat{h}_q = -\boldsymbol{\nabla}\frac{\hbar^2}{2M^{(q)*}_{\rm nucl}(\boldsymbol{r})}\boldsymbol{\nabla} + V_q(\boldsymbol{r}) - i\boldsymbol{W}_q(\boldsymbol{r})\cdot(\boldsymbol{\nabla}\times\boldsymbol{\sigma})\ . \tag{2.108}
$$

The central nuclear potential $V_q(\mathbf{r})$ is obtained as functional derivative of the energy (2.103) with respect to the density

$$V_q(\boldsymbol{r}) = \frac{\delta E}{\delta \rho_q(\boldsymbol{r})} = \frac{\partial \mathcal{E}}{\partial \rho_q} - \boldsymbol{\nabla}\left(\frac{\partial \mathcal{E}}{\partial(\boldsymbol{\nabla}\rho_q)}\right) . \tag{2.109}$$

For Skyrme potentials this yields

$$\begin{aligned} V_q(\boldsymbol{r}) &= t_0\left(1+\frac{x_0}{2}\right)\rho - t_0\left(x_0+\frac{1}{2}\right)\rho_q \\ &+ \frac{t_3}{12}\gamma\rho^{\gamma-1}\left[\left(1+\frac{x_3}{2}\right)\rho^2 - \left(x_3+\frac{1}{2}\right)(\rho_n^2+\rho_p^2)\right] \\ &+ \frac{t_3}{6}\rho^{\gamma}\left[\left(1+\frac{x_3}{2}\right)\rho - \left(x_3+\frac{1}{2}\right)\rho_q\right] \\ &+ \frac{1}{4}\left[t_1\left(1+\frac{x_1}{2}\right)+t_2\left(1+\frac{x_2}{2}\right)\right]\tau \\ &- \frac{1}{4}\left[t_1\left(x_1-\frac{1}{2}\right)+t_2\left(x_2+\frac{1}{2}\right)\right]\tau_q \\ &- \frac{1}{8}\left[3t_1\left(1+\frac{x_1}{2}\right)-t_2\left(1+\frac{x_2}{2}\right)\right](\boldsymbol{\nabla}^2\rho) \\ &+ \frac{1}{8}\left[3t_1\left(x_1+\frac{1}{2}\right)+t_2\left(x_2+\frac{1}{2}\right)\right](\boldsymbol{\nabla}^2\rho_q) \\ &- \frac{W_{LS}}{2}[\boldsymbol{\nabla}\cdot\boldsymbol{J}+\boldsymbol{\nabla}\cdot\boldsymbol{J}_q] + V_{\rm Coul} , \end{aligned} \tag{2.110}$$

where the Coulomb potential is given by

$$V_{\rm Coul}(\boldsymbol{r}) = e^2\int\frac{\rho_p(\boldsymbol{r}')}{|\,\boldsymbol{r}-\boldsymbol{r}'\,|}d^3r' - e^2\left(\frac{3}{\pi}\right)^{1/3}\rho_p^{1/3}(\boldsymbol{r}) . \tag{2.111}$$

The effective-mass form-factor is defined as

$$\begin{aligned} f_q(\boldsymbol{r}) &= \frac{M^{(q)}_{\rm nucl}}{M^{(q)*}_{\rm nucl}(\boldsymbol{r})} = \frac{2M^{(q)}_{\rm nucl}}{\hbar^2}\frac{\delta E}{\delta\tau_q(\boldsymbol{r})} \\ &= 1+\frac{2M^{(q)}_{\rm nucl}}{\hbar^2}\left\{\frac{1}{4}\left[t_1(1+\frac{x_1}{2})+t_2(1+\frac{x_2}{2})\right]\rho(\boldsymbol{r})\right. \\ &\quad \left.-\frac{1}{4}\left[t_1(x_1+\frac{1}{2})-t_2(x_2+\frac{1}{2})\right]\rho_q(\boldsymbol{r})\right\} \end{aligned} \tag{2.112}$$

and the spin-orbit potential as

$$\boldsymbol{W}_q(\boldsymbol{r}) = \frac{\delta E}{\delta \boldsymbol{J}_q(\boldsymbol{r})} = \frac{1}{2}W_{LS}\,\boldsymbol{\nabla}(\rho+\rho_q) . \tag{2.113}$$

With the exception of the potential SkP, Skyrme potentials are unrealistic in the particle-particle channel and therefore cannot be used alone in the HFB theory. Pairing correlations have to be accounted for e.g. in the framework of the HF+BCS scheme with specially fitted pairing matrix elements. An

example for a global fit of the ground-state binding energies of the 1995 mass table [174] is the work of Goriely, Tondeur, and Pearson [152]. They use the Skyrme potential MSk7 for the HF part (the particle-hole channel) and the δ potential of Eq. (2.49) for the BCS part (the particle-particle channel) with slightly different parameters V_0^q for even and odd systems. Later these authors used the full HFB equations with specially fitted Skyrme potentials plus a delta potential (2.49) and a phenomenological Wigner term (cf. Eq. (2.156)) for a comprehensive mass fit [170, 175].

Gogny interaction

Gogny proposed an effective interaction, suitable for HFB calculations, which could be fitted to ground-state binding-energies, single-particle levels in light nuclei and RPA-type modes [118, 176]. He combined the pair of Gauss functions from the Brink-Bocker interaction potential [177] with the three-body and the spin-orbit terms of the Skyrme interaction. The resulting potential is

$$\begin{aligned} V_{12} = \sum_{i=1}^{2} \exp\left[-\frac{|\boldsymbol{r}_1-\boldsymbol{r}_2|^2}{\mu_i^2}\right] \cdot (W_i + B_i\hat{P}_\sigma - H_i\hat{P}_\tau - M_i\hat{P}_\sigma\hat{P}_\tau) \\ +t_3(1+x_0\hat{P}_\sigma)\,\delta(\boldsymbol{r}_1-\boldsymbol{r}_2)\left[\rho\left(\frac{\boldsymbol{r}_1+\boldsymbol{r}_2}{2}\right)\right]^\gamma \\ +iW_{\mathrm{LS}}(\boldsymbol{\sigma}_1+\boldsymbol{\sigma}_2)\cdot \overleftarrow{\boldsymbol{\nabla}}_{12} \times\delta(\boldsymbol{r}_1-\boldsymbol{r}_2)\,\overrightarrow{\boldsymbol{\nabla}}_{12} + V_{\mathrm{Coul}}\,. \end{aligned}$$

In the first line are two finite range potentials ($i = 1, 2$), one attractive and the other repulsive, with the usual superposition of Wigner, Bartlett, Heisenberg and Majorana spin-isospin contributions. $\hat{P}_\sigma$ and $\hat{P}_\tau$ are the exchange operators of spin and isospin variables, respectively. The remaining terms are taken over from the standard Skyrme interaction.

Dechargé and Gogny adopted the following set of parameters in 1980 [178] and called it D1S

$\mu_1 = 0.7$ fm	$\mu_2 = 1.2$ fm
W_1 = -1720.3 MeV	W_2 = 103.639 MeV
B_1 = 1300 MeV	B_2 = -163.483 MeV
H_1 = -1813.53 MeV	H_2 = 162.812 MeV
M_1 = 1397.60 MeV	M_2 = -223.934 MeV
t_3 = 1390.60 MeV fm$^{3(1+\gamma)}$	$x_0 = 1$
$\gamma = 1/3$	W_{LS} = 130 MeV fm^5

This parameter set describes binding energies and pairing properties of nuclei across the periodic table. Its predictive power is remarkable: Over the past 25 years, since the force was fitted, the number of accurately measured nuclear binding energies has increased considerably. These new data are still well described by the parameter set D1S.

Seyler-Blanchard interactions

Seyler and Blanchard [131] proposed a momentum-dependent, finite-range interaction

$$V_\nu(r,p) = -C_\nu \frac{e^{-r/\beta)}}{r/\beta}\left[1-\left(\frac{p}{p_D}\right)^2\right], \tag{2.114}$$

to be used in the Thomas-Fermi approximation. It is supposed to include already the effect of the exchange term in the potential energy. In this definition $r = |\mathbf{r}_1 - \mathbf{r}_2|$, $p = |\mathbf{p}_1 - \mathbf{p}_2|$, which means that the interaction is translational and rotational invariant in ordinary and, independently, in momentum space. The strength parameter C_ν has one value for proton-proton and for neutron-neutron interaction, $\nu =$ like, and another value for proton-neutron interaction, $\nu =$ unlike. The interaction becomes repulsive for large relative momenta, which corresponds in TF-theory to large density. The parameter p_D therefore controls the saturation density of nuclear matter. To obtain the potential U_q, seen by a proton ($q = 1$) or a neutron ($q = 2$), the interaction (2.114) has to be folded into the proton and neutron densities in phase space, which are $2/h^3$ in TF approximation

$$U_q(\mathbf{r},\mathbf{p}) = \frac{2}{h^3}\sum_{\nu=1,2}\int_{\text{vol}} d^3r'\left[\int_{(p_f^\mu)} d^3p' V_\nu(|\mathbf{r}-\mathbf{r}'|,|\mathbf{p}-\mathbf{p}'|)\right] + \delta_{q1}V_{\text{Coul}}\,,$$

where $\mu = (\nu q \bmod 3)$ and the p-integration is over the Fermi sphere of the protons for $\mu = 1$ or the neutrons for $\mu = 2$. The total nuclear energy is given again as a phase-space integral in terms of U_q by

$$\begin{aligned} E &= \frac{2}{h^3}\sum_{q=1,2}\int_{\text{vol}} d^3r \int_{(p_f^{(q)})} d^3p \left\{\frac{p^2}{2M_{\text{nucl}}^{(q)}} + \frac{1}{2}U_q(\mathbf{r},\mathbf{p})\right\} \\ &= \frac{2}{h^3}\sum_{q=1,2}\int d^3r \left\{\frac{4\pi}{10}\frac{(p_f^{(q)}(\mathbf{r}))^5}{M_{\text{nucl}}^{(q)}} + \frac{C_q}{h^3}\int d^3r' \frac{e^{|\mathbf{r}-\mathbf{r}'|/\beta}}{|\mathbf{r}-\mathbf{r}'|/\beta}\sum_{\mu=1,2} I_{q\mu}\right\} \\ &\quad + \frac{2e^2}{h^6}\left(\frac{4\pi}{3}\right)^2 \int d^3r \int d^3r' \frac{[p_f^{(1)}(\mathbf{r})p_f^{(1)}(\mathbf{r}')]^3}{|\mathbf{r}-\mathbf{r}'|} + E_{\text{Coulex}}\,, \end{aligned} \tag{2.115}$$

where the Coulomb exchange-energy E_{Coulex} is treated in the Slater approximation (2.141). The two integrations in momentum space

$$I_{q\mu}(\mathbf{r},\mathbf{r}') = \int_{(p_f^{(q)})} d^3p \int_{(p_f^{(\mu)})} d^3p' \left[1 - \frac{(\mathbf{p}-\mathbf{p}')^2}{p_D^2}\right]$$

can be done in an elementary way:

$$I_{q\mu} = \left(\frac{4\pi}{3}\right)^2 \left(p_f^{(q)}p_f^{(\mu)}\right)^3 \left\{1 - \frac{3}{5}\left[\left(\frac{p_f^{(q)}(\mathbf{r})}{p_D}\right)^2 + \left(\frac{p_f^{(\mu)}(\mathbf{r})}{p_D}\right)^2\right]\right\}.$$

In the last equations $p_f^{(q)}$ is the Fermi momentum of nucleons of type q.

The proton and neutron numbers Z and N can be written as functionals of $p_f^{(q)}(\mathbf{r})$

$$n_q = \frac{2}{h^3}\int_{\text{vol}} d^3r \int_{p_f^{(q)}} d^3p = \frac{8\pi}{3h^3}\int_{\text{vol}} d^3r (p_f^{(q)})^3\,, \qquad q = 1,2\,.$$

The energy has to be minimized with respect to $p_f^{(1)}$ and $p_f^{(2)}$ with the constraint that $n_1 = Z$ and $n_2 = N$

$$\frac{\delta(E\{p_f(\mathbf{r})\} - \lambda_f^{(1)} n_1\{p_f(\mathbf{r})\} - \lambda_f^{(2)} n_2\{p_f(\mathbf{r})\})}{\delta p_f^{(q)}(\mathbf{r})} = 0, \qquad q = 1,2\,.$$

The resulting two coupled, nonlinear integral equations for the functions $p_f^{(1)}(\mathbf{r})$ and $p_f^{(2)}(\mathbf{r})$ have to be solved numerically. In general the integrals are three-dimensional with integral kernels

$$\frac{\exp(|\mathbf{r}-\mathbf{r}'|/\beta)}{(|\mathbf{r}-\mathbf{r}'|/\beta}$$

from the Seyler-Blanchard interaction and $|\mathbf{r}-\mathbf{r}'|^{-1}$ from the Coulomb potential. For spherical shapes these integrals can be reduced to one-dimensional integrals [179]. The Lagrange multipliers $\lambda_f^{(1)}$ and $\lambda_f^{(2)}$ are the separation energies for protons and neutrons, respectively.

The Seyler-Blanchard interaction (2.114) was used in Myers and Swiatecki's droplet model [180], where the parameter set

$$\begin{array}{lll} C_{\text{like}} = 367.56 \text{ MeV} & & C_{\text{unlike}} = 289.66 \text{ MeV} \\ p_D^2/(2M_{\text{nucl}}) = 82.030 \text{ MeV} & & \beta = 0.62567 \text{ fm} \end{array}$$

was fitted to the liquid-drop mass-formula of Ref. [37].

Myers and Swiatecki later extended the Seyler-Blanchard interaction (2.114) to have seven, instead of the four original adjustable parameters

$$V(r,p) = -C\frac{e^{-r/\beta}}{r/\beta} \times \left\{(1 \mp \xi) - (1 \mp \zeta)\left[\left(\frac{p}{p_D}\right)^2 - \frac{c_\gamma}{p} + c_\sigma(\rho(\mathbf{r}_1)^{2/3} + \rho(\mathbf{r}_2)^{2/3})\right]\right\},$$

where the upper sign refers to like nucleons and the lower sign to unlike nucleons. A set of fit parameters given in Ref. [181] is

$$\begin{array}{lll} C = 86.98 \text{ MeV} & p_D/\hbar = 4.8067 \text{ fm}^{-1} & c_\gamma/\hbar = 68.459 \text{ MeV fm}^{-1} \\ c_\sigma = 155.7 \text{ MeV fm}^2 & \xi = 0.27976 & \zeta = 0.55665 \\ \beta = 0.5929 \text{ fm}. & & \end{array}$$

2.1.8 Mean-field potential and other leptodermous distributions

One of the most remarkable properties of nuclei is their very large incompressibility. As a consequence, the density in the nuclear interior is in Thomas-Fermi approximation constant and nearly independent of the size and shape of the nucleus and it falls off to zero in a surface layer with a thickness of the order of one femtometer. Distributions in space which are constant in the interior and decrease monotonically to zero in a thin surface layer have been called leptodermous by Myers and Swiatecki [180, 182]. For a spherical nucleus the equivalent sharp radius is defined as the radius of a density distribution with a sharp surface, the same saturation density in the interior and the same volume integral as the actual nucleus. Because of the large nuclear incompressibility it is this radius rather than the half-density radius which is proportional to $A^{1/3}$ [183] and in fact, not only in Thomas-Fermi, but also in Hartree-Fock approximation. Experimentally this is well confirmed for the charge distribution by elastic electron scattering data [184]. There is an obvious generalization of the equivalent sharp-surface sphere of spherical nuclei to the equivalent sharp surface of deformed nuclei as a general reference surface defining the nuclear shape.

The representation of a leptodermous distribution ρ most frequently used is the Fermi function. For spherical nuclei

$$\rho(r) = \frac{\rho_0}{1 + \exp\left([r - R_0]/d\right)} \tag{2.116}$$

with the saturation density ρ_0, half-density radius R_0 and diffuseness parameter d. The equivalent sharp radius is $R_{\mathrm{eq}} = R_0\{[1 + (\pi d/R_0)^2]\}^{1/3} + \mathcal{O}(\exp[-R_0/d])$ [183,185]. For non-spherical, but axially symmetric nuclei the equivalent sharp surface may be defined in cylindrical coordinates r, z by a function $\pi(r, z; \beta_i) = 0$, where the β_i are deformation parameters. The difference $r - R_0$ in the spherical Fermi function (2.116) is then replaced by $l = \pi(r, z)/|\nabla\pi(r, z)|$ [186]. This ansatz guaranties that the surface thickness, measured in the direction of the surface normal, remains constant over the surface. In addition, an overall deformation-dependent scaling of r and z in $\pi(r, z)$ is needed to account for the fact that $l = 0$ refers to the half-density surface in the Fermi function rather than the equivalent sharp surface [132].

In connection with a leptodermous ansatz for a variational density in ETF calculations the generalized Fermi function

$$\rho(r) = \frac{\rho_0}{\{1 + \exp\left([r - R_0]/d\right)\}^{\gamma}} \tag{2.117}$$

with variational parameters ρ_0, d, and γ was found to be useful [132,137]. To account also for a central density depression because of Coulomb repulsion effects, Chu, Jennings, and Brack [187] employed the five-parameter ansatz

$$\rho(r) = \frac{\rho_0}{1 + \rho_1} \, \frac{1 + \rho_1 e^{-r^2/\beta^2}}{\{1 + \exp\left([r - R_0]/d\right)\}^{\gamma}} \, , \tag{2.118}$$

where ρ_0 is the central density.

An alternative method to construct a leptodermous function is to fold a step function Θ, which is constant inside the equivalent sharp surface and zero outside, into a short-range function S, normalized so that its volume integral is one and to multiply the folding product by the central depression factor $(1 + wr^2)$ [188]

$$\rho(r) = \rho_0(1 + wr^2) \int \Theta(\mathbf{r}')S(|\mathbf{r} - \mathbf{r}'|)d^3r' \; . \tag{2.119}$$

Friedrich, Voegler, and Reinhard [189] obtained a very convenient representation of the scattering form factor $F(q)$ by taking the Fourier transform of this expression

$$F(q) = \mathcal{F}_{r\to q}\{\rho(r)\} = \rho_0\mathcal{F}_{r\to q}\{S\}(1 - w\Delta_q)\mathcal{F}_{r\to q}\{\Theta\} \; ,$$

directly comparable with the elastic cross section of electron-scattering experiments.

Another example for a leptodermous distribution is the Woods-Saxon shell-model potential [190], approximating the selfconsistent mean field. It consists of a central part $V_{\rm cent}$, the spin-orbit term $V_{\rm so}$, and the Coulomb potential $V_{\rm Coul}$ for protons:

$$V^{WS}(\boldsymbol{r}, \boldsymbol{p}, \boldsymbol{s}; \beta_i) = V_{\rm cent}(\boldsymbol{r}; \beta_i) + V_{\rm so}(\boldsymbol{r}, \boldsymbol{p}, \boldsymbol{s}; \beta_i) + V_{\rm Coul}(\boldsymbol{r}; \beta_i) \, . \tag{2.120}$$

The central part is defined by

$$V_{\rm cent}(\boldsymbol{r}; \beta_i) = \frac{V_0[1 \pm \kappa \, I]}{[1 + \exp(l(\boldsymbol{r}; \beta_i)/d)]} \; , \tag{2.121}$$

where $I = (N - Z)/A$ is the relative neutron excess. The plus sign in this formula holds for protons, the minus sign for neutrons. There are three empirical parameters. V_0, κ, and d. The function $l(\boldsymbol{r}, \beta_i)$ has to be determined numerically.

The spin-orbit potential is taken in the form

$$V_{\rm so}(\boldsymbol{r}, \boldsymbol{p}, \boldsymbol{s}; \beta_i) = i\lambda^q \left(\frac{\hbar}{2M_{\rm nucl}c}\right)^2 (\boldsymbol{\nabla} V_{\rm cent} \times \boldsymbol{\nabla}) \cdot \boldsymbol{\sigma}, \quad q = p, n \; , \tag{2.122}$$

where the linear momentum is $\mathbf{p} = -i\hbar\boldsymbol{\nabla}$ and the spin vector is $\mathbf{s} = (1/2)\hbar\boldsymbol{\sigma}$. For spherical mean fields Eq. (2.122) can be written

$$V_{\rm so}(\mathbf{r}, \mathbf{l}, \boldsymbol{\sigma}) = -\lambda^q \left(\frac{\hbar}{2M_{\rm nucl}c}\right)^2 \frac{\partial V_{\rm cent}}{r\partial r} \, (\mathbf{l} \cdot \boldsymbol{\sigma}) \; ,$$

where $\mathbf{l} = \mathbf{r} \times \mathbf{p}/\hbar$. The Coulomb potential for protons is assumed to be that of a uniform charge distribution with a sharp surface and radius $R_{\rm Coul} = r_p A^{1/3}$ in the spherical case.

Table 2.1. Frequently used sets of Woods-Saxon potential parameters. The radii R_0 in the definition of the function $l(r, z; \beta_i)$ in Eq. (2.121) are related to the r_q parameters in the table by $R_0^{(q)} = r_q A^{1/3}$, q =p,n. The diffuseness parameters of the Woods-Saxon potential d_V and $d^{\rm so}$ refer to the central and spin-orbit potentials, respectively.

Parameter	units	Universal [191]	Blomqvist [192]	Rost [193]	Chepurnov [194]	Myers/Pauli [195, 196]
V_0	MeV	49.6	51.0	49.65	53.3	51.4
κ	-	0.86	0.649	0.86	0.63	$0.829\ \overline{\delta}/I$
d_V	fm	0.70	0.67	0.70	0.63	0.66
$d^{\rm so}$	fm	0.70	0.67	0.70	0.63	0.55
r_n	fm	1.347	1.27	1.347	1.24	$1.16\,\alpha\beta_n\gamma_n$
λ^n	-	35.0	32.0	31.5	23.8·(1+2I)	$1087/(51.4 - 42.6\overline{\delta})$
$r_n^{\rm so}$	fm	1.31	1.27	1.28	1.24	$1.16\,\alpha(1 - 0.98/R_0^2)$
r_p	fm	1.275	1.27	1.275	1.24	$1.16\,\alpha\beta_p\gamma_p$
λ^p	-	36.0	32.0	17.8	23.8·(1+2I)	$1087/(51.4 + 42.6\overline{\delta})$
$r_p^{\rm so}$	fm	1.20	1.27	0.932	1.24	$1.16\,\alpha(1 - 0.98/R_0^2)$

A few commonly used parameter sets for the Woods-Saxon potential are listed in Table 2.1. The parameter sets reported by Blomqvist and Wahlborn [192] and by Rost [193] were fitted to single-particle and single-hole energies of odd nuclei in the vicinity of ^{208}Pb, corrected for some couplings of these states to collective excitations, whereas the set "universal" of Ref. [191] was adjusted to the single-particle levels of all odd-A nuclei with $A \geq 40$. The latter was quite successful in generating single-particle spectra of nuclei across the periodic table. The potential depth and the spin-orbit strength of the parameter set used by Pauli [196] were fitted to single-particle levels in the lead region. The radius parameters were taken from the droplet-model potential of Myers [195]. For a detailed discussion of the various effects incorporated in the droplet model we refer to Sec. 2.2.3 of this chapter. The small quantities

$$\overline{\delta} = \frac{(N-Z)/A + 0.0112Z^2/A^{5/3}}{1 + 3.15/A^{1/3}}$$
$$\overline{\epsilon} = -0.147A^{-1/3} + 0.33\,\overline{\delta}^2 + 0.00248Z^2A^{-4/3}\ .$$

have the same form as in Eqs. (2.173) and (2.174) (except for the shape dependent functions which are dropped here). The parameter $\overline{\delta}$ plays the role of the relative neutron excess $I = (N-Z)/A$ in the droplet model and $\overline{\epsilon}$ accounts for an average density compression, due to the opposing effects of surface tension and Coulomb repulsion. The basic quantity of the droplet model is the equivalent sharp radius $R_0 = 1.16\alpha A^{1/3}$ of the density with $\alpha = (1-\overline{\epsilon})$. The equivalent sharp radius of the shell-model potential is $R_V^q = R_0\beta_q$ with $\beta_q = 1 + \Delta R/R_0 \pm 0.22\overline{\delta}/R_0$. Here $\Delta R = 0.82 - 0.56R_0^{-1}$ accounts for the fact that the radius of the potential is by ΔR larger than the density radius because of nonlinear saturation effects of the effective two-body interaction. The term $\pm 0.22\overline{\delta}$ accounts for the difference in the radius between neutron (upper sign) and proton (lower sign) nuclear potentials. The factor $\gamma_q = 1 - (\pi^2/3)(d_V/R_0^q)^2$ converts the equivalent sharp radius into the slightly smaller half-value radius of the Woods-Saxon potential.

Alternatively Bolsterli, Fiset, Nix, and Norton [96] used a folding product of the step function Θ, introduced in Eq. (2.119) and a Yukawa function as short-range function S

$$Y(r) = \frac{e^{-|r|/a}}{4\pi a^2|r|} \tag{2.123}$$

to generate the central part of a leptodermous shell-model potential by a folding product

$$V_{\rm cent}(\mathbf{r}) = V_0 \int \Theta(\mathbf{r}')Y(|\mathbf{r}-\mathbf{r}'|)d^3r'\,, \tag{2.124}$$

for which we shall use in the following the short-hand notation

$$V(\mathbf{r}) = V_0 \int \Theta(\mathbf{r}')S(|\mathbf{r}-\mathbf{r}'|)d^3r' \stackrel{\rm def}{=} V_0\,\Theta(\mathbf{r}) * S(r)\,.$$

The central depth is denoted by V_0. The volume enclosed in the equivalent sharp surface is not changed by folding

$$\int \Theta(\mathbf{r})d^3r = \int \Theta(\mathbf{r}) * S(r)d^3r, \tag{2.125}$$

independent of the shape of the equivalent sharp surface for any folding function S, normalized to unit volume. To prove this theorem we define three-dimensional Fourier transforms

$$\mathcal{F}_{\mathbf{r}\to\mathbf{k}}\{\Theta\} = \int \Theta(\mathbf{r})e^{i\mathbf{r}\mathbf{k}}d^3r$$

and notice that for $\mathbf{k} \to 0$ one obtains the volume integral of Θ. Using the folding theorem for the Fourier transformation

$$\mathcal{F}_{\mathbf{r}\to\mathbf{k}}\{\Theta * S\} = \mathcal{F}_{\mathbf{r}\to\mathbf{k}}\{\Theta\}\mathcal{F}_{\mathbf{r}\to\mathbf{k}}\{S\},$$

in the limit $\mathbf{k} \to 0$, Eq. (2.125) follows immediately.

As in Eq. (2.120) the complete shell-model potential consists of central $V_{\rm cent}$, spin-orbit $V_{\rm so}$ and Coulomb $V_{\rm Coul}$ parts. The central part is written by Möller et al. [197]

$$V_{\rm cent}(\mathbf{r}) = (V_s \pm V_a\overline{\delta}) \int_{\rm vol} Y(|\mathbf{r} - \mathbf{r}'|) d^3r' \,,$$

where the Yukawa function Y has the range $a_{\rm pot} = 0.8$ fm and the integration is extended over the volume enclosed by the equivalent sharp potential surface. The radius of the latter is $R_{\rm eq} = (1 - \overline{\epsilon})(R_0 + 0.82 - 0.56/R_0 \pm 0.22\overline{\delta})$, where the upper and lower sign refers to protons and neutrons, respectively and the parameters $\overline{\epsilon}$ and $\overline{\delta}$ are taken from the droplet model [195]. They are the same as in the Pauli-Myers potential [196], discussed above. The strength parameters of the central potential are

$$V_s = 52.5 \text{ MeV}, \quad V_a = 48.7 \text{ MeV}.$$

The spin-orbit term is obtained in the same way from the central potential as in Eq. (2.122). The strength parameters, given in Ref. [197], are (in MeV)

$$\lambda^p = 6.0 \left(\frac{A}{240}\right) + 28.0 \,,$$

$$\lambda^n = 4.5 \left(\frac{A}{240}\right) + 31.5 \,.$$

The Coulomb potential is evaluated assuming a uniform density distribution inside the equivalent sharp surface

$$V_{\rm Coul}(\boldsymbol{r}_1) = \frac{Ze^2}{(4\pi/3)Ar_0^3} \int_{\rm vol} \frac{d^3r_2}{|\boldsymbol{r}_1 - \boldsymbol{r}_2|} \,. \tag{2.126}$$

It is a disadvantage of folding products that one has to calculate the folding integral. For some important shapes closed-form expressions exist [188]. For example, for the sphere with the choice $S = Y$ [96] the integration in $\mathbf{r}$-space in Eq. (2.124) is elementary and yields

$$V_{\rm cent}(r) = V_0 \begin{cases} 1 - \left(1 + \dfrac{R_{\rm eq}}{a}\right) e^{-R_{\rm eq}/a} \sinh\left(\dfrac{r}{a}\right) \Big/ (r/a) & r \le R_{\rm eq} \,, \\ \left\{ \dfrac{R_{\rm eq}}{a} \cosh\left(\dfrac{R_{\rm eq}}{a}\right) - \sinh\left(\dfrac{R_{\rm eq}}{a}\right) \right\} \dfrac{e^{(-r/a)}}{(r/a)} & r > R_{\rm eq} \,. \end{cases} \tag{2.127}$$

In general, using the divergence theorem, the three-dimensional folding integral can be reduced to a surface integral [188, 198] which has to be evaluated numerically. Use of the Yukawa function (2.123) leads to leptodermous

distributions with a discontinuous second normal derivative at the equivalent sharp surface as seen explicitly in formula (2.127). For some applications this is undesirable, e.g. when one wants to use analytic continuation techniques. Homomorphic folding distributions are obtained with the choice $S = (\pi^{1/2}a)^{-1} \exp(-r^2/a^2)$. Unfortunately, most applications require distributions with an exponential, rather than a Gaussian tail [184]. See Ref. [199] how to overcome this deficiency approximately. For an extensive presentation of other forms of leptodermous functions we refer to the book by Hasse and Myers [200].

2.2 Macroscopic mass formulae

2.2.1 Leptodermous expansions

In Thomas-Fermi approximation a local nuclear energy density $\mathcal{E}(\mathbf{r})$ is defined. Because of the saturation property of nuclear matter the quantity $g(\mathbf{r}) = \mathcal{E}(\mathbf{r}) - c_1\rho(\mathbf{r})$ vanishes in the bulk of a nucleus when c_1 is the volume-energy parameter of the liquid-drop formula. Outside the surface $\mathcal{E}(\mathbf{r})$ and the particle density $\rho(\mathbf{r})$ vanish individually so that $g(\mathbf{r})$ is different from zero only in a surface layer. It turns out that the shape of the profile of g in the direction of the surface normal is rather independent of the size and shape of the nucleus for which it is calculated. Writing now the nuclear binding energy in Thomas-Fermi approximation as $E = c_1 A + \int g(\mathbf{r}) d^3r$, the volume integral over g gives rise to the surface energy in the liquid-drop formula.

To show this more explicitly we introduce surface coordinates u and v on the equivalent sharp surface Σ, leading to a surface-integration element $d\sigma$. In addition, we define a coordinate z in the direction of the surface normal. Starting from Σ we may construct a sequence of surfaces $\Sigma', \Sigma'', \ldots$ by shifting each point P on Σ by the amount $dz, 2dz, \ldots$ in the direction of the surface normal in P. The surface element $d\sigma$ may be mapped by this construction on to surface elements $d\sigma(dz), d\sigma(2dz), \ldots$ on the surfaces $\Sigma', \Sigma'', \ldots$. The same construction can be made to both sides of the reference surface Σ. The volume element d^3r may now be expanded in the form

$$d^3r = d\sigma(z)dz = (1 + \kappa z + \mathcal{K}z^2 \ldots)d\sigma(0)dz, \tag{2.128}$$

with coefficients

$$\kappa = \left.\frac{\partial[d\sigma(z)/d\sigma(0)]}{\partial z}\right|_{z=0} \quad \text{and} \quad \mathcal{K} = \left.\frac{\partial^2[d\sigma(z)/d\sigma(0)]}{\partial z^2}\right|_{z=0}.$$

Keeping in mind that $g(\mathbf{r})$ depends only on the z coordinate in the direction of the surface normal, the volume integral of the surface energy may be expanded in moments of g

$$E_{\rm surf} = \int g(\mathbf{r}) d^3\mathbf{r} = \int g(z)dz \int d\sigma + \int g(z)zdz \int \kappa d\sigma + \int g(z)z^2 dz \int \mathcal{K} d\sigma + \ldots . \qquad (2.129)$$

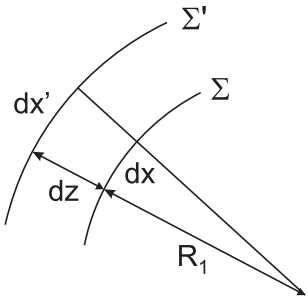

Fig. 2.5. Cut through the surfaces Σ and Σ' along the main curvature line in the x direction.

To exhibit the geometrical meaning of the coefficients κ and $\mathcal{K}$ we use the fact that in an infinitesimal neighborhood of a point P on Σ one can introduce orthogonal coordinates x, y instead of u, v such that the metric becomes Euclidean in x, y in this neighborhood. These coordinates point in the direction of the main curvature lines on Σ [201]. When R_1 is the curvature radius corresponding to the main curvature direction x, the line element dx on Σ is mapped onto $dx' = (1 + dz/R_1)dx$ on the surface Σ' as shown in Fig.2.5. Similarly dy is mapped onto $dy' = (1 + dz/R_2)dy$ and therefore

$$dx'dy' = dxdy\,[1 + (R_1^{-1} + R_2^{-1})dz + (R_1R_2)^{-1}(dz)^2$$

$$+ \text{ additional terms of order } (dz)^2].$$

From this equation we see by comparison with Eq. (2.128) that $\kappa = R_1^{-1} + R_2^{-1}$ is twice the mean curvature and $\mathcal{K} = (R_1R_2)^{-1}$ is the Gaussian curvature, where we have dropped other terms of quadratic order in the main curvatures proportional to κ^2 [41]. We can now interpret the first term on the right-hand-side of Eq. (2.129) as the surface-energy constant $c_2 = \int g(z)dz$ times the surface area $\int d\sigma$, the second term is the curvature-energy constant $c_3 = \int g(z)zdz$ times twice the mean curvature, integrated over the surface Σ, and the last term kept is proportional to the Gaussian curvature, integrated over Σ. According to the Gauß-Bonnet theorem [201] this integral is 4π for a smooth, simply connected surface Σ, independent of its shape, and it jumps to 8π beyond scission.

For spherical nuclei the first term of the expansion (2.129) is proportional to R^2, the second to R, and the third to R^0. Formula (2.129) is therefore

often seen as the beginning of an asymptotic expansion in decreasing powers of $R_{\rm eq}$ or $A^{1/3}$. Therefore, the coefficient c_2 is obtained from a Thomas-Fermi treatment of an infinite, plane surface [132], c_3 follows by subtracting the volume and the surface term from the Thomas-Fermi binding energy of a spherical nucleus in the limit $R_{\rm eq} \to \infty$, and so on, recursively (see e.g. Erdelyi [202] for this expansion technique). For any finite $R_{\rm eq}$ (or finite $A^{1/3}$) the asymptotic series has to be truncated to achieve an optimal representation of the generalized surface energy. It has to be truncated the earlier, the smaller $R_{\rm eq}$ is. In practice one does however not really consider the asymptotic series, but truncates the expansion (2.129) with the first or the second term and determines the coefficients c_i by a least-squares fit to a finite set of nuclei. Note that the c_i from this fit must not be identical with the coefficients of the asymptotic series.

There is a clear indication that the asymptotic series should be terminated before the term with the Gaussian curvature: The jump of this term at scission does certainly not reflect the behavior of the Thomas-Fermi model which the liquid-drop expansion is supposed to represent.

It is convenient to introduce the ratio of the surface energy to the surface energy of the sphere with the same volume $B_{\rm surf} = (\text{surface area})/(4\pi R^2)$ and similarly for the curvature energy $B_{\rm curv} = \int \kappa \, dS/(8\pi R)$. Both quantities are independent of the nuclear size and depend only on the shape of the equivalent sharp surface.

The liquid-drop expansion (2.129) does not account for the contribution of proximity forces to the total binding energy in strongly necked-in configurations ("crevices") and between fragments beyond scission ("gaps"). Therefore an extra term must be added to the liquid-drop expansion for the proximity energy. In Ref. [41] such term is derived as a generalization of Eq. (1.8) for arbitrarily shaped, but smooth juxtaposed surfaces.

There is an alternative approach to a parameterization of the surface-energy integral on the left-hand-side of Eq. (2.129): One can try a simple, two-parameter ansatz for the function $g(\mathbf{r})$ [188]: Since the gradient of the folding product $\Theta * Y$ is surface-peaked, one can construct a surface-peaked scalar by taking the square of it. One is therefore lead to the ansatz $g(\mathbf{r}) = 4a\sigma[\nabla(\Theta * Y)]^2$ with the range parameter a in the Yukawa function and a strength parameter σ. (In the limit of a sharp surface, $a \to 0$, the expression $4a \int [\nabla(\Theta * Y)]^2 d^3r \to$ surface area [188]. Therefore the parameter σ has the meaning of the surface tension in this limit.) The generalized surface energy $E_{\rm surf} = E - E_{\rm vol} = \int g(\mathbf{r}) d^3r$ may therefore be written in short-hand notation as

$$E_{\rm surf} = \int g(\mathbf{r}) d^3r = 4a\sigma \nabla(\Theta * Y) \cdot \nabla(Y * \Theta), \tag{2.130}$$

where the dot shall indicate integration over the spatial coordinates as well as vector multiplication of the gradients. The multiple integrations in this expression can be simplified somewhat. Partial integration yields $E_{\rm surf} = -4a\sigma\Theta * Y * \Delta Y \cdot \Theta$, where use has been made of the fact that differentiation

of a folding product can be done by differentiating either factor and that the multiple product in Eq. (2.130) is associative as well as commutative, which is easily verified by writing the implied integrations explicitly. We now use the identity[1] $Y * \Delta Y = [1/(2a)]\partial_a Y$, which can be proved by taking the Fourier transforms of both sides of the identity and using $\mathcal{F}_{\mathbf{r}\to\mathbf{k}}\{Y\} = (1 + a^2k^2)^{-1}$. With this identity one obtains

$$E_{\text{surf}} = -2\sigma\partial_a\Theta * Y \cdot \Theta, \tag{2.131}$$

which is the representation of the nuclear surface energy proposed by Krappe, Nix, and Sierk [203] with $\sigma = c_2/(4\pi r_0^2)$ in terms of the constant c_2, used in Eq. (1.1). Performing the differentiation with respect to a, one gets a linear combination of a Yukawa and an exponential function, folded into $\Theta(\mathbf{r})$

$$\begin{aligned} E_{\text{surf}} &= -\frac{4\sigma}{a}\Theta * (E_{\text{nor}} - Y) \cdot \Theta \\ &\equiv -\frac{4\sigma}{a}\int d^3r\, d^3r' [E_{\text{nor}}(\mathbf{r}-\mathbf{r}') - Y(\mathbf{r}-\mathbf{r}')], \end{aligned} \tag{2.132}$$

where the integration is in $\mathbf{r}$ and $\mathbf{r}'$ over the volume enclosed by the equivalent sharp surface and E_{nor} denotes the normalized exponential function $\exp(-r/a)/(8\pi a^3)$. The representation (2.131) for the surface energy has therefore been referred to as "Yukawa-plus-exponential". The derivation of this expression is based on the assumption that the local curvature radius is always larger than the surface-thickness parameter a. For high-order multipole vibrations this assumption is not satisfied and the ansatz (2.131) cannot be used (if such modes make sense for a drop with a diffuse surface in the first place). If the condition is satisfied, all shape information is contained in the function $\Theta(\mathbf{r})$ and the profile of g in the direction of the surface normal is given by Y.

An advantage of this representation over the liquid-drop expansion is that it automatically includes proximity effects. For instance, for two nuclei with a center-of-mass distance $\mathbf{D}$, whose shapes are given by the shape functions $\Theta_1(\mathbf{r})$ and $\Theta_2(\mathbf{r}-\mathbf{D})$ and which do not overlap, insertion of $\Theta = \Theta_1 + \Theta_2$ into Eq. (2.131) yields the proximity energy as a double folding product

$$E_{\text{prox}}(\mathbf{D}) = -\frac{c_2}{2\pi r_0^2}\,\partial_a\,\Theta_1 * Y * \Theta_2. \tag{2.133}$$

Multiple folding products as in Eq. (2.133) are often conveniently calculated by taking the Fourier transforms of the folding factors and transforming their product back into ordinary space [204]. For two spheres with radii R_1 and R_2 and $R_i \gg a$ it is shown in Ref. [203] that their interaction potential becomes

[1] We use the short-hand notation $\partial_a \equiv \partial/\partial a$

$$E_{\rm prox}(D) = -\frac{a(R_1-a)(R_2-a)\,c_2}{r_0^2\,D(2+s/a)}\left(4-\frac{R_1}{R_1-a}-\frac{R_2}{R_2-a}+\frac{s}{a}\right)e^{-s/a}\,,$$

where the exponentially small terms $\exp(-R_1/a)$ and $\exp(-R_2/a)$ are neglected compared to unity. Neglecting also a/R_1, a/R_2, and $s/(R_1+R_2)$ compared to 1, one obtains

$$E_{\rm prox}(D) \approx -\frac{a\overline{R}c_2}{r_0^2}e^{-s/a} \tag{2.134}$$

with $s = D - R_1 - R_2$. This expression is compatible with Eq. (1.8) for the proximity potential, except that the reduced radius $\overline{R} = R_1R_2/(R_1+R_2)$ refers there to the half-density radii and in this case to the equivalent sharp radii.

Note that the interaction energy (2.133) is based on a "frozen-density" assumption, which is often called " sudden approximation" in scattering theory. Another advantage of the folding ansatz is a lesser sensitivity of the deformation energy to high multipole wiggles on the surface compared to sharp-surface formulae, which is somewhat unphysical. In a radial moment expansion of the folding expression for g all odd moments vanish. One may compensate this deficiency by adding at least a curvature energy term to the expression (2.131). However, liquid-drop model fits show that this term is rather small [41].

A disadvantage of the Yukawa-plus-exponential ansatz is the need to calculate the six-dimensional integral in Eq. (2.132). Although closed expressions for the integral exist for some important shape classes, like a sphere or two spheres at a given distance [203] and expansions of the interaction of deformed nuclei in terms of their multipole moments [188], in general the double volume integral can be reduced only to a double surface integral which must then be evaluated numerically [203]. To see how the reduction is achieved, use is made of the possibility to represent the folding kernel $K(|\mathbf{r}-\mathbf{r}'|)$ in Eq. (2.132) by a double divergence [188]

$$K(|\mathbf{r}-\mathbf{r}'|) = \sum_{i,j}^{1\ldots3}\frac{\partial}{\partial x_i}\frac{\partial}{\partial x'_j}(x_i-x'_i)(x_j-x'_j)F(|\mathbf{r}-\mathbf{r}'|)\,,$$

so that the application of Gauss' theorem to the $\mathbf{r}$-integration as well as to the $\mathbf{r}'$-integration yields

$$\Theta * K\cdot\Theta = \int\int\{d\mathbf{S}(\mathbf{r}-\mathbf{r}')\}\,\{d\mathbf{S}'(\mathbf{r}-\mathbf{r}')\}F(|\mathbf{r}-\mathbf{r}'|). \tag{2.135}$$

The function $F(r)$ satisfies the differential equation

$$r^2F''(r)+8rF'(r)+12F(r) = -K(r)$$

with boundary conditions $\lim\limits_{r\to0} r^4F(r) = 0$ and $\lim\limits_{r\to\infty} F(r) = 0$. Simple closed-form solutions of the differential equation exist e.g. for the Yukawa function $K(r) \equiv Y(r) = (4\pi a^3)^{-1}e^{-x}/x$ with $x = r/a$:

$$F(r) = -(4\pi a^3 x^4)^{-1}[x - 2 + (x+2)e^{-x}] \tag{2.136}$$

and for $K(r) = 1/r$:

$$F(r) = -1/(6r).$$

One defines the shape function $B_{\rm surf}$ for the Yukawa-plus-exponential model as the ratio of $E_{\rm surf}$ to the surface energy of a sphere with the same volume and a sharp surface. Using Eqs. (2.131), (2.135), and (2.136) we write $B_{\rm surf}$ as a double surface integral to be extended in both variables over the equivalent sharp surface [205]

$$B_{\rm surf} = \frac{1}{8\pi^2 r_0^2 A^{2/3}} \int\int \left\{ 2 - \left[\frac{(\mathbf{r}-\mathbf{r}')^2}{a^2} + 2\frac{|\mathbf{r}-\mathbf{r}'|}{a} + 2 \right] e^{-|\mathbf{r}-\mathbf{r}'|/a} \right\}$$
$$\times \frac{\{(\mathbf{r}-\mathbf{r}')\cdot d\mathbf{S}\}\,\{(\mathbf{r}-\mathbf{r}')\cdot d\mathbf{S}'\}}{|\mathbf{r}-\mathbf{r}'|^4}\,. \tag{2.137}$$

The quantity $B_{\rm surf}$ does now depend on the size of the system and it is not unity for a sphere as in the case of a sharp surface.

We have so far discussed only the nuclear part of the liquid-drop formula. The Coulomb part consists of a direct and an exchange contribution. In the direct part $E_{\rm Coul} = (1/2)\rho_p * (e^2/r)\cdot\rho_p$ the Thomas-Fermi proton-number density ρ_p is conveniently represented by a folding product $\rho_p^{(0)}\,\Theta(\mathbf{r}) * Y$ with the charge density constant $\rho_p^{(0)}$ and a charge-diffuseness parameter $a_{\rm den}$ in the Yukawa function. The Fourier transform of the resulting double folding product $Y*(1/r)*Y$ is, according to the folding theorem, given by the ordinary product of the Fourier transforms of the three folding factors Y, $1/r$, and Y

$$\frac{4\pi}{k^2}\frac{1}{(1+a_{\rm den}^2k^2)^2} = 4\pi\left[\frac{1}{k^2} - \frac{a_{\rm den}^2}{1+a_{\rm den}^2k^2} - \frac{a_{\rm den}^2}{(1+a_{\rm den}^2k^2)^2}\right],$$

where a partial fraction expansion with respect to k^2 has been made on the right-hand-side. The bracket may also be written $k^{-2} - a_{\rm den}^2[(a_{\rm den}/2)\partial_{a_{\rm den}} + 2](1+a_{\rm den}^2k^2)^{-1}$. Transforming back into ordinary space, one obtains

$$E_{\rm Coul} = \frac{[\rho_p^{(0)}e]^2}{2}\left\{\Theta * \frac{1}{r}\cdot\Theta - 4\pi a_{\rm den}^2\left[\frac{a_{\rm den}}{2}\partial_{a_{\rm den}} + 2\right]\Theta * Y\cdot\Theta\right\}$$
$$= \frac{[\rho_p^{(0)}e]^2}{2}\,\Theta * \left\{\frac{1}{r} - \left(\frac{1}{r} + \frac{1}{2a_{\rm den}}\right)\exp(-r/a_{\rm den})\right\}\cdot\Theta. \tag{2.138}$$

The direct part of the Coulomb energy is seen to consist of a sum of the Coulomb energy of a sharp-surface charge distribution and a surface-diffuseness correction in the form of some Yukawa-plus-exponential expression. The double volume integration implied in these formulae can again be converted into a double surface integration by writing $1/r$ and Y as double divergence. Using this transformation the ratio of the direct Coulomb energy

to the Coulomb energy of the sphere with equal volume and sharp surface is given in terms of the ratio $\xi = |\mathbf{r} - \mathbf{r}'|/a_{\rm den}$ by

$$B_{\rm Coul} = -\frac{15}{32\pi^2 R^5 a_{\rm den}} \int\int \left[\frac{1}{6\xi} - \frac{2\xi - 5 + (5 + 3\xi + \xi^2/2)\exp(-\xi)}{\xi^4}\right] \times\{(\mathbf{r} - \mathbf{r}') \cdot d\mathbf{S}\}\,\{(\mathbf{r} - \mathbf{r}') \cdot d\mathbf{S}'\}\,. \tag{2.139}$$

To calculate the volume contribution to the Coulomb exchange energy

$$E_{\rm Coulex} = -\frac{1}{2}\int \frac{e^2}{|\mathbf{r} - \mathbf{r}'|}|\rho_p(\mathbf{r}, \mathbf{r}')|^2 d^3r d^3r'$$

one needs the mixed proton density for a homogeneous, infinite fermion system,

$$\rho_p(\mathbf{r}, \mathbf{r}') = \frac{2}{(2\pi)^3}\int_{|k|<k_f} \exp i[\mathbf{k}(\mathbf{r} - \mathbf{r}')] d^3k\,,$$

where $\hbar k_f$ is the Fermi momentum of the protons [206]. Introducing the Fourier transform of the Coulomb potential

$$\frac{e^2}{|\mathbf{r} - \mathbf{r}'|} = 4\pi e^2 \int \frac{d^3q}{(2\pi)^3}\frac{e^{i\mathbf{q}(\mathbf{r}-\mathbf{r}')}}{q^2}\,,$$

the Coulomb exchange energy becomes

$$E_{\rm Coulex} = -\frac{8\pi e^2}{(2\pi)^9}\int d^3(\mathbf{r}-\mathbf{r}')\int d^3R \int \frac{d^3q}{q^2}\int_{|k'|<k_f} d^3k \int_{|k|<k_f} d^3k' e^{i(\mathbf{q}+\mathbf{k}-\mathbf{k}')(\mathbf{r}-\mathbf{r}')}\,,$$

where the change of variables $\int d^3r \int d^3r' = \int d^3R \int d^3(\mathbf{r} - \mathbf{r}')$ was made. The spatial integrals can be easily performed. With the normalization volume $v = \int d^3R$ one obtains

$$\begin{aligned} E_{\rm Coulex} &= -\frac{8\pi e^2 v}{(2\pi)^6}\int_{|k|<k_f} d^3k \int_{|k'|<k_f} d^3k' \frac{1}{(\mathbf{k} - \mathbf{k}')^2} \\ &= -\frac{16\pi e^2 v p_f^4}{h^4}\int_0^1 x dx \int_0^1 x' \ln\frac{x + x'}{x - x'} dx' \\ &= -4\pi e^2 p_f^4 h^{-4} v, \end{aligned} \tag{2.140}$$

where $x = k/k_f$. Using the relation $p_f^3 = 3\pi^2\hbar^3 Z/v$ for the Fermi momentum p_f of the protons in Thomas-Fermi approximation, the volume contribution of the Coulomb exchange energy becomes

$$E_{\rm Coulex} = -3e^2 p_f Z/(4\pi\hbar) = -(3/4)(3/2\pi)^{2/3}(e^2/r_0)Z^{4/3}A^{-1/3}\,. \tag{2.141}$$

In the mass formula it is referred to as Slater term [172], though it was first derived by Felix Bloch [207]. In empirical fits of the liquid-drop formula this term

is sometimes absorbed in the nuclear volume energy. The Coulomb exchange energy-density used in Eq. (2.106) follows immediately from Eq. (2.140)

$$E_{\text{Coulex}}/v = \mathcal{E}_{\text{Coulex}}(\boldsymbol{r}) = -(3/4)e^2(3/\pi)^{1/3}\rho_p^{4/3}(\boldsymbol{r}) \tag{2.142}$$

with $(p_f(\mathbf{r})/\hbar)^3 = 3\pi^2\rho_p(\mathbf{r})$.

To obtain the surface contribution to the Coulomb exchange energy we consider the local Fermi momentum $p_f(\mathbf{r})$ in Thomas-Fermi approximation in terms of the single-particle potential $V(\mathbf{r})$ and the Fermi energy ϵ_f

$$p_f^2(\mathbf{r}) = 2M_{\text{nucl}}\left[\epsilon_f - V(\mathbf{r})\right]\Theta(\epsilon_f - V(\mathbf{r})),$$

the volume v in terms of the saturation density $\rho_p^{(0)}$ of the protons

$$v = \int \rho_p(\mathbf{r})/\rho_p^{(0)}\; d^3r = \int \left(\frac{\epsilon_f - V(\mathbf{r})}{\epsilon_f - V(0)}\right)^{3/2} \Theta(\epsilon_f - V(\mathbf{r}))\, d^3r,$$

and the quantity $q_2 = \int g_{\text{Coulex}}(\mathbf{r})d^3r$ with the surface-peaked integrand

$$\begin{aligned} g_{\text{Coulex}}(\mathbf{r}) &= p_f^4(\mathbf{r})/p_f^4(0) - \rho(\mathbf{r})/\rho(0) \\ &= \left[\left(\frac{\epsilon_f - V(\mathbf{r})}{\epsilon_f - V(0)}\right)^2 - \left(\frac{\epsilon_f - V(\mathbf{r})}{\epsilon_f - V(0)}\right)^{3/2}\right] \Theta(\epsilon_f - V(\mathbf{r}))\ . \end{aligned}$$

Inserting these definitions into Eq. (2.140) yields

$$E_{\text{Coulex}} = -4\pi e^2 h^{-4} \int p_{\text{f}}^4(\mathbf{r})\, d^3r = -4\pi e^2 h^{-4} p_{\text{f}}^4(\mathbf{r}=0)\ (v + q_2). \tag{2.143}$$

An expansion of q_2 in moments of $g_{\text{Coulex}}(r)$ analogous to Eq. (2.129) leads to the surface (and curvature) contributions of the Coulomb exchange energy.

For some representations of a spherical, leptodermous charge distribution other than in terms of a folding product, the Coulomb energy was evaluated as a power series in the ratio between the surface diffuseness and the radius, see Hasse and Myers, Ref. [200] Chap. 4.2.

2.2.2 Liquid-drop mass-formulae

From the leptodermous expansion of the nuclear binding energy in Thomas-Fermi approximation follows the classical three-term mass formula [14, 29] discussed in the second section of the introduction

$$E = E_{\text{vol}} + E_{\text{surf}} + E_{\text{Coul}} \tag{2.144}$$

with the volume energy

$$E_{\text{vol}} = a_V(1 - \kappa_V I^2)A\,, \tag{2.145}$$

the surface energy

$$E_{\rm surf} = a_S(1-\kappa_S I^2)A^{2/3}B_{\rm surf}\,, \tag{2.146}$$

and the direct Coulomb energy

$$E_{\rm Coul} = \frac{1}{2}\left(\frac{3Ze}{4\pi R_0^3}\right)^2 \int_{\rm vol} d^3r \int_{\rm vol} d^3r' \frac{1}{|\mathbf{r}-\mathbf{r}'|} = \frac{3}{5}\frac{e^2}{r_0}Z^2A^{-1/3}B_{\rm Coul}\,, \tag{2.147}$$

where the dependence of the nuclear binding energy on the relative neutron excess $I=(N-Z)/A$ is to be seen as a power-series expansion, which should contain only even powers of I because of the charge symmetry of the nuclear forces. Empirically it appears to be sufficient to retain only the quadratic term in this expansion. The shape-dependence is contained in the shape functions $B_{\rm surf}$ and $B_{\rm Coul}$. In the liquid-drop model $B_{\rm surf}$ is the ratio of the surface area of the nucleus and the surface of a sphere of equal volume. In cylindrical coordinates one has for axially symmetric shapes

$$B_{\rm surf} = \frac{1}{2R_0^2}\int_{z_{\rm min}}^{z_{\rm max}} \rho\sqrt{1+\rho'^2}\,dz\,. \tag{2.148}$$

In the finite-range liquid-drop model it is given by Eq. (2.137). The Coulomb shape-function is represented by the double-surface integral

$$B_{\rm Coul} = -\frac{5}{64\pi^2R^5}\int\int \frac{1}{|\mathbf{r}-\mathbf{r}'|}\{(\mathbf{r}-\mathbf{r}')\cdot d\mathbf{S}\}\,\{(\mathbf{r}-\mathbf{r}')\cdot d\mathbf{S}'\} \tag{2.149}$$

in a model with a sharp surface and by Eq (2.139) for a diffuse charge distribution. The volume energy is shape-independent along the fission path, including the scission point. This holds also for the neutron-excess term if one assumes that the charge density Z/A stays constant at scission, $Z/A = Z_1/A_1$, which implies $Z_1/A_1 = Z_2/A_2$ and $I = I_1 = I_2$.

The diffuseness correction to the Coulomb energy and the Coulomb exchange-energy are often simplified by retaining only the volume terms of their leptodermous expansions [37]. From Eq. (2.138) one obtains

$$\begin{aligned} E_{\rm diff} &= -\frac{\rho_p^2e^2}{2}\frac{4\pi}{3}R^3\int d^3r\left(\frac{1}{r}+\frac{1}{2a_{\rm den}}\right)e^{-r/a_{\rm den}} \\ &= -3\frac{e^2}{r_0}\left(\frac{a_{\rm den}}{r_0}\right)^2\frac{Z^2}{A} \end{aligned} \tag{2.150}$$

and for the Coulomb exchange-energy, $E_{\rm Coulex}$, Eq. (2.141). These terms are therefore shape-independent. Note that the charge diffuseness parameter d, used in Ref. [37], refers to the diffuseness parameter of the Fermi function (2.116), which is related to the Yukawa parameter a by $a^2 = (\pi^2/6)d^2$ [200].

So far we have only considered the first order effects of the Coulomb force on the binding energy. But one has to keep in mind that even if the free

nucleon-nucleon interaction V_{nn} is charge symmetric, the effective force may violate that symmetry since it is a nonlinear functional of $V_{nn} + V_{\rm Coul}$. One has therefore to expect a contribution to the nuclear symmetry energy which violates charge symmetry. In leading order this effect yields a term linear in I in the nuclear volume energy

$$E_a = c_a I A = c_a (N - Z)\,. \tag{2.151}$$

The next term in the leptodermous expansion is the curvature energy

$$E_{\rm curv} = a_{\rm curv}(1 - \kappa_{\rm curv} I^2) A^{1/3} B_{\rm curv} \tag{2.152}$$

with the curvature form-factor

$$B_{\rm curv} = \frac{1}{8\pi R_0} \int \kappa \, dS\,,$$

where the integral is to be extended over the equivalent sharp surface of the nucleus and the integrand is twice the mean local curvature. For axially symmetric shapes, given in cylindrical coordinates by $\rho(z)$, one obtains

$$\begin{aligned} B_{\rm curv} &= \frac{1}{4R_0} \int_{z_{\min}}^{z_{\max}} \left(1 - \frac{\rho\rho''}{1+\rho'^2}\right) dz \\ &= \frac{1}{4R_0} \int_{z_{\min}}^{z_{\max}} (1 + \rho' \arctan \rho') dz\,, \end{aligned} \tag{2.153}$$

where R_0 is the radius of the sphere with equal volume. Expressions for $B_{\rm curv}$ in other coordinate systems are given in the book by Hasse and Myers [200]. It is worth noting that the representation of the profile function $g(\mathbf{r})$ in terms of a folding product yields no odd surface moments. It is therefore compatible with the folding ansatz for the surface energy to add a curvature term.

Often a number of terms are included in mass formulae which do not follow from leptodermous expansions. Among these is the odd-even term [197]

$$E_{\rm oe} = \begin{cases} \overline{\Delta}_p + \overline{\Delta}_n - \delta_{np} & Z \text{ and } N \text{ odd} \\ \overline{\Delta}_p & Z \text{ odd } N \text{ even} \\ \overline{\Delta}_n & Z \text{ even } N \text{ odd} \\ 0 & Z \text{ and } N \text{ even} \end{cases} \tag{2.154}$$

with

$$\overline{\Delta}_n = \frac{r_m}{N^{1/3}}, \qquad \overline{\Delta}_p = \frac{r_m}{Z^{1/3}}, \qquad \delta_{np} = \frac{r'_m}{A^{2/3}}$$

and empirical parameters r_m, r'_m (see Table 2.2). An alternative form is

$$E_{\rm oe} = \begin{cases} \Delta - \delta/2 & Z \text{ and } N \text{ odd} \\ \delta/2 & Z \text{ or } N \text{ odd} \\ -\Delta + \delta/2 & Z \text{ and } N \text{ even} \end{cases} \tag{2.155}$$

with $\Delta = 12$ MeV$/A^{1/2}$ and $\delta = 20$ MeV$/A$ [208].

Plotting the difference between the experimental binding energies and the liquid-drop formula Eqs. (2.144), (2.127) plus some shell correction versus I, the relative neutron excess, one obtains a cusp at $N = Z$. This motivated Myers and Swiatecki [37] to add a term

$$E_{\text{Wigner}} = -t \exp(-\alpha_W |I|) \text{ MeV} \tag{2.156}$$

to the mass formula. It was named after Wigner who was the first to derive an expression for the symmetry energy which contained a term proportional to $|N - Z|$ [209]. Myers and Swiatecki gave parameters t=7 MeV, α_W=10 for the Wigner energy in Ref. [37]. In a later paper [210] they used t=10 MeV and α_W=4.2 . Möller and Nix [211] reported t=11.19 MeV and α_W=13. The form of the Wigner term was changed in Refs. [208] and [212] to

$$E_{\text{Wigner}} = W \begin{pmatrix} |I| + 1/A \\ 0 \end{pmatrix} \begin{matrix} N = Z, \text{ both odd} \\ \text{otherwise} \end{matrix} \tag{2.157}$$

and eventually renamed "congruence energy" [210].

Satula and Wyss [213] found that for $N = Z$ nuclei and their nearest neighbors the isosinglet pn-pairing might outweigh the usually dominant isotriplet pairing which leads to a cusp in the mass formula around $N = Z$. Since a priori little is known about the relative strength of the isosinglet to the isotriplet part of the effective interaction in the particle-particle channel, it is not quite decided yet whether the Wigner cusp is only due to isosinglet pairing [214]. Since the effect is restricted to $N = Z$ nuclei and their neighbors, it is at any rate not parametrized by either of the forms (2.156) or (2.157).

One may question whether it is reasonable to include terms (2.154) - (2.157) in the bulk part of the mass formula when microscopic shell and pairing corrections are later added anyway. In view of inherent uncertainties in the liquid-drop expansion one may also question whether one should include some other terms, which appear sometimes in mass formulae. There is for instance a correction term to account for the difference between charge and proton densities because of the finite size of the charge density of the proton, characterized by the range constant r_p of its electric form factor [215]

$$E_{\text{formfactor}} = f(k_f r_p) Z^2/A \,. \tag{2.158}$$

One can argue that this effect can be taken care of by the choice of the parameter a_{den} in the diffuseness correction to the Coulomb energy with sufficient accuracy.

Another term, sometimes included in the mass formula [215, 216], is a zero-point energy, supposedly connected with the fission degree of freedom

$$E_{\text{zp}} = (1/2)\hbar\omega_{\text{quadrupole}} \,. \tag{2.159}$$

However, the Thomas-Fermi binding energy, which the macroscopic mass formula is to represent, contains the zero-point energies of all $3A$ degrees of

freedom, as does the Hartree-Fock approach. One may rather wonder that it contains too much zero-point energy because of the spurious center-of-mass motion. In fact, no allowance is made in mass formulae to correct for any of the symmetry-breaking features of the mean-field theory.

A further term of doubtful origin is a constant, i.e. a term of order A^0

$$E_0 = a_0\,. \tag{2.160}$$

Being of the same order as the shell corrections, it may in fact correct deficiencies of shell-correction recipes.

It is a common feature of the contributions (2.154)-(2.160) to the mass formula that they do not have a natural shape dependence. They are either considered as shape-independent with the undesirable consequence that they double at scission, or they are given rather ad hoc a shape dependence, for example for $E_{\rm Wigner}$ and E_0 in Ref. [217] or, in terms of the shape function $B_{\rm surf}$, for the pairing energy $E_{\rm oe}$ by Madland and Nix [130].

Table 2.2. The liquid-drop parameters in the first line are fitted to ground-state masses from Ref. [218] and a selection of fission barriers, including some with neutron numbers around 40 and around 50. In the second line only ground-state masses (from Ref. [219]) were used in the fit. The numbers in the third line were taken from Ref. [197]. In the fourth line the parameters of the Wigner term (2.156) were taken from Ref. [210], the Coulomb radius and diffuseness parameters were obtained from the mass fit.

type	a_V[MeV]	κ_V	a_S[MeV]	κ_S	$a_{\rm curv}$[MeV]	$\kappa_{\rm curv}$	a_0[MeV]	c_a[MeV]
FRLDM	16.025	1.932	21.330	2.378	–	–	2.040	0.097
LDM	15.4920	1.8601	16.9707	2.2938	3.8602	-2.376	–	–

type	W[MeV]	r_m[MeV]	r'_m[MeV]	$a_{\rm den}$[fm]	a[fm]	r_o[fm]	r_p[fm]	
FRLDM	30	4.8	6.6	0.7	0.68	1.16	0.8	

type	t[MeV]	α_W	$r_{\rm den}$[fm]	$a_{\rm den}$[fm]				
LDM	10	4.2	1.21725	0.62049				

A term of marginal importance in the mass formula is the total binding energy of the electrons, which is always smaller than 1 MeV [212]. It accounts for the fact that mass formulae refer to the masses of neutral atoms, rather than bound neutrons and hydrogen atoms. Its form is based on a result by Foldy [220], which he obtained in the framework of the Hartree approximation for the electrons,

$$E_{\rm el} = 1.43 \cdot 10^{-5}\ Z^{2.39}\ \text{MeV}. \tag{2.161}$$

Numerous fits of the liquid-drop parameters have been reported [197, 203, 215, 224, 226–228]. They depend not only on the continuously increas-

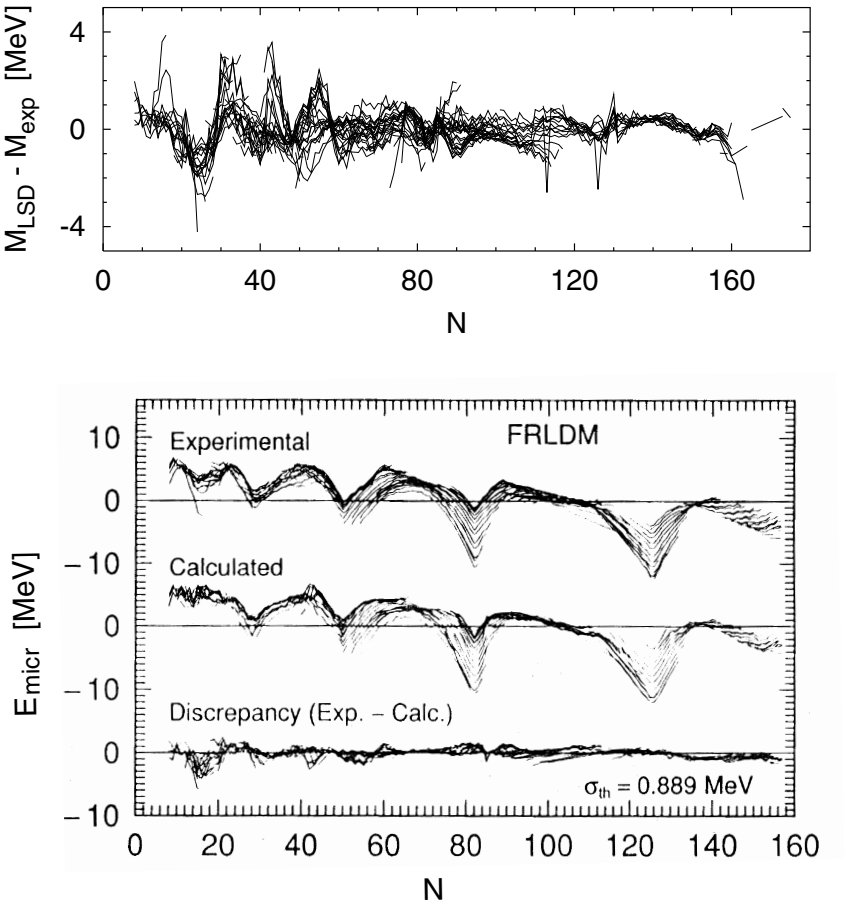

Fig. 2.6. Upper frame: Difference between calculated masses in the LDM with parameters from table 2.2 and measured masses for the 2766 nuclei from the tables of Antony [219]. Lines connect isotopes of the same element, from Ref. [221]. Lower frame: In the upper part the same for the FRLDM and experimental data for 1654 nuclides from Audi's midstream evaluation [218] (with four corrections). The calculated graphs refer to Strutinsky shell and pairing correction-energies, from Ref. [222].

ing empirical data base of very accurately measured ground-state binding-energies [121, 174, 219, 223, 229] and fission barriers, but also on the weight with which fission-barrier information is used in the fit, besides ground-state masses. It also depends on the selection of terms beyond the leptodermous expansion, Eqs. (2.154) - (2.161), which are retained in the fit. And it finally depends on the particular choice of the recipe to calculate shell and pairing corrections. In Table 2.2 we list the liquid-drop parameters obtained in re-

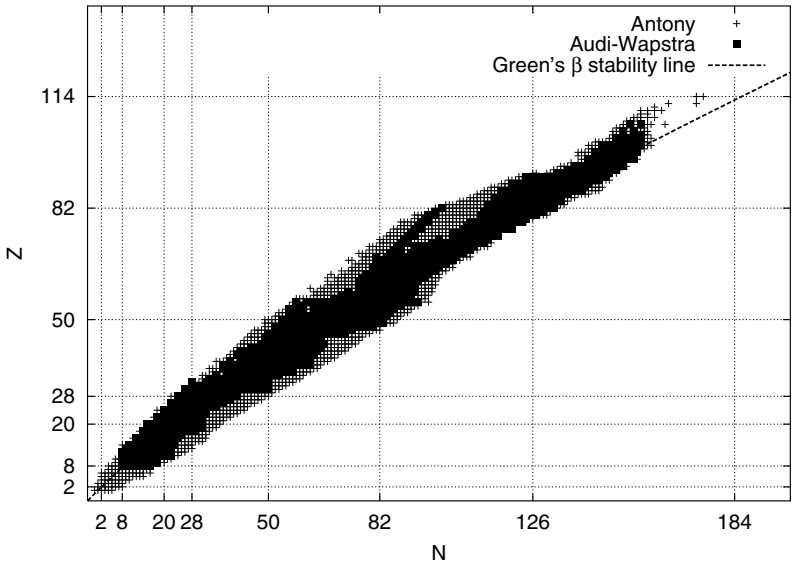

Fig. 2.7. The chart of isotopes for which the experimental binding energies are known. The crosses correspond to data from the compilation of Antony [219], while black squares to the data from Ref. [223] (from Ref. [228]).

cent fits. The finite-range liquid-drop model (FRLDM) was fitted by Möller Sierk, and Iwamoto [230] and the sharp-surface liquid-drop model (LDM) by Pomorski and Dudek [221, 228]. In both cases Strutinsky's shell and pairing corrections and ground-state deformation energies of Möller et al. [197] were taken into account. The Coulomb exchange-energy was expressed in the Slater approximation (2.141) in both fits. For the Coulomb surface-diffuseness correction in the LDM the expression (2.150) was used. The FRLDM fit includes a zero-point energy-term. Fig. 2.6 shows the deviation of experimental from calculated ground-state binding energies for the LDM fit of Ref. [221] and for the FRLDM fit of Ref. [222]. The quality of the fit is often characterized by the root-mean-square deviation σ of the fit. This would be an appropriate measure if the deviations had a random distribution. However, the figures show clearly systematic trends, presumably due to missing pieces of physics in the standard microscopic-macroscopic approach (to be discussed in the next section), which was used in both fits. The nuclides whose measured ground-state masses were used in some recent fits are shown in Fig. 2.7. Also indicated in the figure is Green's line of β stable nuclei [231]

$$Z = \frac{A}{2}\left(1 - \frac{0.4A}{A+200}\right) . \tag{2.162}$$

In Fig. 2.8 the fission barrier is plotted as function of the mass number A, calculated in various versions of the liquid-drop model (without shell and

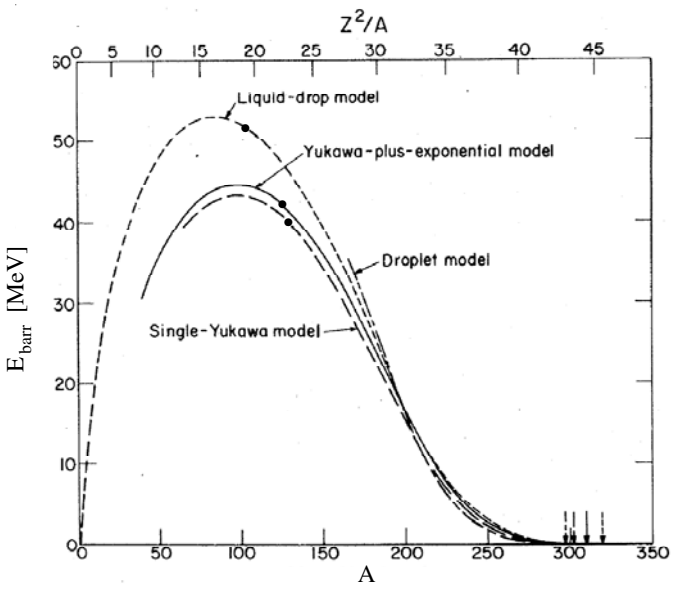

Fig. 2.8. Comparison of the fission barrier heights of β-stable nuclei obtained in four different macroscopic models. The parameter sets of the liquid-drop [224], droplet [208], single-Yukawa [225], and Yukawa-plus-exponential [203] are the same as in the original papers. The arrows indicate the vanishing of the macroscopic fission barrier in the four models. The thick black dots indicate the Businaro-Gallone point: to the left of these points the fission barrier is unstable with respect to left-right asymmetry. The four arrows indicate the $A_{\rm crit}$ at which the fission barrier disappears in the four models. The droplet model yields the smallest and the liquid-drop model the largest $A_{\rm crit}$, the two finite-range models give the two values in between (after Ref. [203]).

pairing corrections). For medium mass and light nuclei sharp-surface models give substantially higher barriers than diffuse-surface models. These nuclei have rather strongly necked-in saddle-point shapes. Therefore the proximity interaction between the nascent fragments becomes important. This interaction is automatically included in diffuse-surface liquid-drop models, but was not considered in the sharp-surface models shown in Fig. 2.8.

Instead of adding the contribution from crevices to the liquid-drop energy as proposed in Ref. [41], more recently the A^0 terms of the liquid-drop formula, i.e. the Wigner and the Gaussian curvature terms, have been used to mimic proximity effects. In Fig. 2.9 experimental and theoretical barrier heights are compared. Results of two calculations are shown: with the liquid-drop model of Ref. [221] and with a selfconsistent Thomas-Fermi approach using the Seyler-Blanchard interaction [181]. In both calculations shell corrections were neglected at the saddle point and a shape-independent Wigner term (2.157) was used. Assuming some smoothly interpolating shape dependence of the Wigner term, it is easy to lower the calculated barriers for the

four lightest systems in Fig. 2.9 [221]. These data points come from heavy-ion fusion-fission experiments [232, 233]. To extract from the measured data the symmetric, zero-temperature saddle-point of the non-rotating system, to which the diamonds in the Figure refer, quite a number of assumptions have to be made which are the source of systematic errors, not indicated in the figure. Besides, the macroscopic-microscopic approach used in Figs. 2.6 and 2.9 has its own sources of systematic errors: (a) too restricted choices of the deformation-parameter space for the ground and saddle-point states, and (b) ground state multiconfigurational mixing.

2.2.3 The droplet model

There are two rather small effects which were neglected in the leptodermous expansion, discussed above: First, nuclei are not completely incompressible with the consequence that large nuclei have a smaller central density than (neutral) bulk nuclear matter since they are dilated by the Coulomb repulsion of the protons. This effect is opposed by a compression effect due to the surface tension. The two effects roughly balance for medium-size nuclei, but for light nuclei a net increase of the central density results, compared to nuclear matter and a net decrease for heavy nuclei. A second deviation from the standard liquid-drop expansion is caused by the slightly smaller radius of the proton

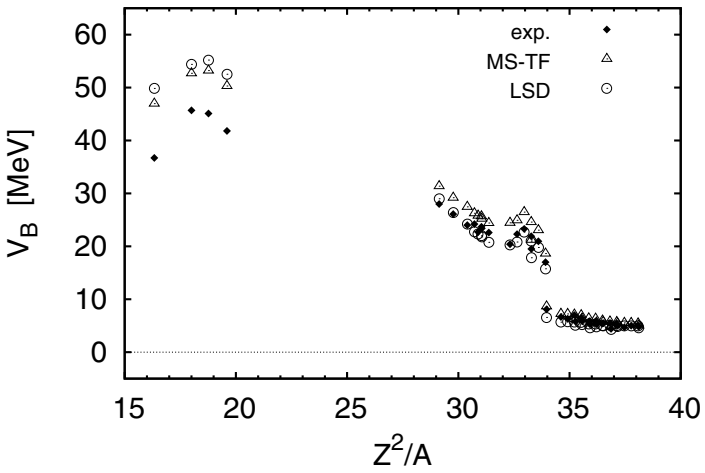

Fig. 2.9. The Myers and Swiatecki Thomas-Fermi (MS-TF, points) and the liquid-drop model [221] (LSD, circles) estimates of the fission barrier heights as functions of the parameter Z^2/A. The experimental data are denoted by diamonds. The Thomas-Fermi and the experimental values of the barrier heights are taken from Ref. [181].

density compared to the neutron density because of the excess of neutron numbers. The result is the development of a neutron skin.

Both effects lead to small changes in the liquid-drop formula. Myers and Swiatecki considered them in their droplet model [180] in a low-order power-series expansion. To simplify the discussion we restrict us in the following to spherical shapes. General shapes are treated in Ref. [182]. To define appropriate expansion parameters, Myers and Swiatecki define reference den-

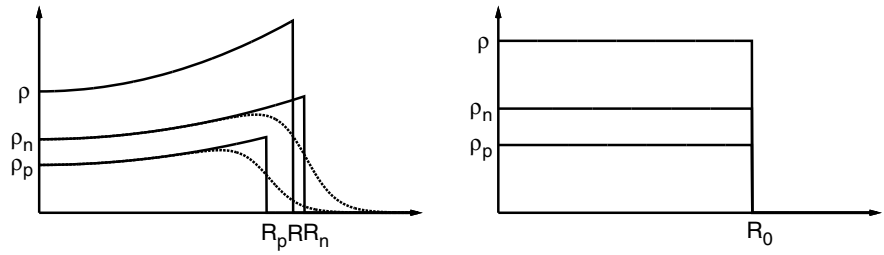

Fig. 2.10. Schematic plots of the droplet model densities as a functions of the nuclear radius are presented in the left figure. The solid lines show the bulk functions ρ_n , ρ_p, and ρ extrapolated out to the effective sharp neutron R_n, proton R_p, and liquid drop R radii. The dotted lines give the actual densities ρ_n^{actual} and ρ_p^{actual} with their realistic surface diffuseness. The corresponding plot for the generating densities $\rho_n^{(0)}$, $\rho_p^{(0)}$, and ρ_0 in the liquid drop model is shown in the right figure (after Ref. [180]).

sities for protons, neutrons, and for all nucleons with sharp surfaces. In the liquid drop model they are rectangular with a common radius $R^{(0)} = r_0 A^{1/3}$ and density $\rho_0 = 3/(4\pi r_0^3)$. They are shown in the right frame of Fig. 2.10. The actual distributions, given in the left frame by the dotted curves, have a central depression and proton and neutron densities have different radii. Besides the actual distributions, their sharp-surface generating functions $\rho_p(r)$, $\rho_n(r)$, and $\rho(r) = \rho_p(r) + \rho_n(r)$ are introduced. They are also shown schematically in Fig. 2.10. Myers and Swiatecki also defined two small, dimensionless functions of r

$$\epsilon(r) = \frac{\rho_0 - \rho(r)}{3\rho_0} \quad \text{and} \quad \delta(r) = \frac{\rho_n(r) - \rho_p(r)}{\rho(r)}, \qquad r \leq R. \tag{2.163}$$

They describe the deviation of the density ρ from its nuclear matter value ρ_0 and the local density asymmetry. In this definition the proton density $\rho_p(r)$ is assumed to be extrapolated smoothly from its bulk value $\rho_p(R_p)$) to the reference radius R to be defined below.

Using Eqs. (2.163) and keeping only linear terms in ϵ, one finds the following expressions for the total, the proton, and the neutron densities

$$\begin{aligned}\rho(r) &= \rho_0[1-3\epsilon(r)]\ ,\\ \rho_p(r) &= \frac{1}{2}\rho_0[1-3\epsilon(r)-\delta(r)],\\ \rho_n(r) &= \frac{1}{2}\rho_0[1-3\epsilon(r)+\delta(r)],\qquad\qquad r\le R.\end{aligned}\tag{2.164}$$

The reference radius R and the proton and neutron radii R_p and R_n, respectively, are defined by

$$\frac{4}{3}\pi R^3\bar{\rho}=A\ ,\qquad \frac{4}{3}\pi R_p^3\bar{\rho}_p=Z\ ,\qquad \frac{4}{3}\pi R_n^3\bar{\rho}_n=N\ .\tag{2.165}$$

in terms of average densities $\overline{\rho}$, where the average is taken over a sphere with radius R

$$\overline{\rho}=\frac{3}{R^3}\int_0^R\rho(r)r^2dr$$

and similarly for $\overline{\rho}_p$ and $\overline{\rho}_n$. Averaging in the same way Eqs. (2.164) yields, together with Eqs. (2.165) to linear order in $\bar{\epsilon}$ and $\bar{\delta}$,

$$\begin{aligned}R\ &= r_0A^{1/3}(1+\bar{\epsilon})\ ,\\ R_p &= r_0(2Z)^{1/3}(1+\bar{\epsilon}+\tfrac{1}{3}\bar{\delta})\ ,\\ R_n &= r_0(2N)^{1/3}(1+\bar{\epsilon}-\tfrac{1}{3}\bar{\delta})\ .\end{aligned}\tag{2.166}$$

The thickness parameter of the neutron skin τ is defined by

$$\tau=\frac{R_n-R_p}{r_0}.\tag{2.167}$$

To first order in small quantities one obtains

$$\tau\approx\frac{2}{3}(I-\bar{\delta})A^{1/3}\ ,\tag{2.168}$$

where $I=(N-Z)/A$ is the relative neutron excess.

The ansatz for the total energy of the nucleus

$$\begin{aligned}E &= E_{\rm vol}+E_{\rm surf}+E_{\rm curv}+E_{\rm Coul}+E_{\rm Coulex}\\ &= \bar{\rho}\int_R e(r)d^3r+\int_R\sigma(r)dS+\frac{a_{\rm curv}}{8\pi r_0}\int_R\kappa\,dS\\ &+\frac{e^2}{2}\int_{R_p}\frac{\rho_p(\mathbf{r})\rho_p(\mathbf{r}')}{|\mathbf{r}-\mathbf{r}'|}d^3r\,d^3r'-\frac{3e^2}{4}\left(\frac{3}{\pi}\right)^{1/3}\int_{R_p}\rho_p^{4/3}(r)d^3r\end{aligned}\tag{2.169}$$

shall be expressed as functional of ϵ and δ. In this equation the first integral is to be taken over a sphere of radius R, the second and third integral is over

the surface of the sphere with radius R, the fourth integral is in $\mathbf{r}$ and $\mathbf{r}'$ over spheres with radius $R_p(\bar{\epsilon}, \bar{\delta})$, and the last integral, the volume contribution to the Coulomb exchange term, extends over a sphere with radius R_p. To exhibit the dependence of the integrands on ϵ and δ the volume-energy density $e(r)$ is expanded in the droplet model in a Taylor series up to second powers of ϵ and δ^2

$$e = -a_V + J\delta^2 + \frac{1}{2}(K\epsilon^2 - 2L\epsilon\delta^2 + M\delta^4), \tag{2.170}$$

where a_V is the volume-energy constant of the liquid-drop model, K is the nuclear incompressibility, and J, L, and M are model parameters. Similarly the surface energy density is expanded in powers of $\delta(R)$ and τ up to second order

$$4\pi r_0^2\sigma = a_S + H\tau^2 + 2P\tau\delta(R) - G\delta^2(R), \tag{2.171}$$

where a_S is the surface-energy constant of the liquid-drop model and H, P, and G are further model parameters of the droplet model. In this expansion of the binding energy E, terms up to the order $A^{1/3}$, $I^2A^{2/3}$, and I^4A are kept in decreasing order of $A^{1/3}$ and increasing order of I^2.

Inserting the results (2.166), (2.168) and the expansions (2.170) and (2.171) into Eq. (2.169), yields E as functional of $\epsilon(r)$ and $\delta(r)$, besides its dependence on the liquid-drop parameters a_V, a_S, a_{curv}, and r_0. The functional is minimized with respect to ϵ and δ with the constraint that Eqs. (2.166) are satisfied for fixed A, Z, and N. After a lengthy calculation one obtains for the energy minimum [180, 182]

$$\begin{aligned} E = {} & (-a_V + J\bar{\delta}^2 - \frac{1}{2}K\bar{\epsilon}^2 + \frac{1}{2}M\bar{\delta}^4)A \\ & + \left(a_S + \frac{9}{4}\frac{J^2}{Q}\bar{\delta}^2\right)A^{2/3}B_{\mathrm{surf}} + a_{\mathrm{curv}}A^{1/3}B_{\mathrm{curv}} \\ & + c_1\frac{Z^2}{A^{1/3}}B_{\mathrm{Coul}} - c_2Z^2A^{1/3}B_r - c_5Z^2B_w - c_3\frac{Z^2}{A} - c_4\frac{Z^{4/3}}{A^{1/3}} \ . \end{aligned} \tag{2.172}$$

in terms of the minimum values of the parameters $\bar{\delta}$ and $\bar{\epsilon}$

$$\bar{\delta} = \left(I + \frac{3}{16}\frac{c_1}{Q}\frac{Z}{A^{2/3}}B_v\right) \Big/ \left(1 + \frac{9}{4}\frac{J}{Q}A^{-1/3}B_{\mathrm{surf}}\right) \ , \tag{2.173}$$

and

$$\bar{\epsilon} = \frac{1}{K}\left(-2a_SA^{-1/3}B_{\mathrm{surf}} + L\bar{\delta}^2 + c_1\frac{Z^2}{A^{4/3}}B_{\mathrm{Coul}}\right) \ , \tag{2.174}$$

where we report the result for the more general case of not necessarily spherical nuclei [182]. It is shown in Ref. [180] that the parameter G can be expressed in terms of parameters H, P, and J and the parameters H and P enter in the final result only in the combination $Q = H/[1 - (2/3)(P/J)]$.

The model has nine independent, adjustable parameters, whose values, as given by Myers [212], are

$$\begin{array}{llllll} a_V = 15.96 & \text{MeV}\,, & a_S = 20.69 & \text{MeV}\,, & a_{\rm curv} = 0 & \text{MeV}\,, \\ J = 36.8 & \text{MeV}\,, & Q = 17 & \text{MeV}\,, & K = 240 & \text{MeV}\,, \\ L = 100 & \text{MeV}\,, & M = 0 & \text{MeV}\,, & r_0 = 1.18 & \text{fm}\,, \end{array} \tag{2.175}$$

and five constants given in terms of them

$$c_1 = \frac{3}{5}\frac{e^2}{r_0}\,, \qquad c_2 = \frac{c_1^2}{336}\left(\frac{1}{J} + \frac{18}{K}\right)\,,$$

$$c_3 = \frac{5}{2}c_1\left(\frac{b}{r_0}\right)^2, \quad \text{where} \quad b = 0.99 \text{ fm}\,,$$

$$c_4 = \frac{5}{4}c_1\left(\frac{3}{3\pi}\right)^{2/3}, \qquad c_5 = \frac{c_1^2}{64Q}\,.$$

The shape functionals $B_{\rm surf}$, $B_{\rm Coul}$, $B_{\rm curv}$, B_r, B_v, and B_w describe the ratios of the surface, Coulomb, curvature, redistribution, and surface redistribution energies of the first and second kind to their corresponding values in the spherical case, respectively. They are given by the following integrals [182]

$$\begin{aligned} B_{\rm surf} &= \int\limits_S d\sigma/(4\pi R^2)\,, \\ B_{\rm Coul} &= \int\limits_V w(\boldsymbol{r})d\tau/(\tfrac{32}{15}\pi^2 R^5)\,, \\ B_{\rm curv} &= \int\limits_S \kappa d\sigma/(8\pi R)\,, \\ B_r &= \int\limits_V [\tilde{w}(\boldsymbol{r})]^2 d\tau/(\tfrac{64}{15\,7\,5}\pi^3 R^7)\,, \\ B_v &= -\int\limits_S \tilde{w}(\boldsymbol{r})d\sigma/(\tfrac{16}{15}\pi^2 R^4)\,, \\ B_w &= \int\limits_S [\tilde{w}(\boldsymbol{r})]^2 d\sigma/(\tfrac{64}{225}\pi^3 R^6)\,, \end{aligned} \tag{2.176}$$

where R is the equivalent sharp radius of a spherical nucleus, $\kappa = R_1^{-1} + R_2^{-1}$ is twice the surface curvature, defined by the two local principal radii of curvature R_1 and R_2, $w(\boldsymbol{r}) = \int_V |\boldsymbol{r} - \boldsymbol{r}\,'|^{-1} d\tau$ is proportional to the Coulomb potential, and $\tilde{w} = w(\boldsymbol{r}) - \bar{w}$ is its deviation from the average value $\bar{w} = \int_V w(\boldsymbol{r})d\tau/(\frac{4}{3}\pi R^3)$.

The droplet model for the macroscopic part of the nuclear binding energy is quite successful in representing ground-state masses and geometrical parameters like charge radii and density diffusenesses, but it rather fails in the description of fission barrier heights [226]. In present applications the droplet expression is used in combination with the Yukawa-plus-exponential (YPE) model [203]. In this hybrid model [197, 234]), which was named "finite-range droplet-model" (FRDM), the binding energy is given by

$$E = E_{\rm droplet} + E_a + E_{\rm formfactor} + E_{\rm zp} + E_0 + E_{\rm oe} + E_{\rm Wigner} + E_{\rm el}\,, \tag{2.177}$$

where the droplet-energy term $E_{\rm droplet}$ is slightly modified compared to Eq. (2.172)

$$E_{\rm droplet} = (-a_V + J\bar{\delta}^2 - (1/2)K\bar{\epsilon}^2)A + \left(a_S + \frac{9}{4}\frac{J^2}{Q}(\bar{\delta}\theta)^2\right)A^{2/3}B_{\rm surf}^{\rm fr} + a_{\rm curv}A^{1/3}B_{\rm curv} + c_1\frac{Z^2}{A^{1/3}}B_{\rm Coul}^{\rm fr} - c_2Z^2A^{1/3}B_r - c_5Z^2B_w\theta - c_4\frac{Z^{4/3}}{A^{1/3}}\,. \quad (2.178)$$

In this equation $B_{\rm surf}^{\rm fr}$ and $B_{\rm Coul}^{\rm fr}$ are the finite-range expressions (2.137) and (2.139). The latter includes also the diffuseness correction c_3Z^2/A. Also the ratio $\theta = B_{\rm surf}^{\rm fr}/B_{\rm surf}^{\rm sharp}$ between the surface shape-functions in the finite-range and the sharp-surface models appears in Eq. (2.178). The definitions of $\bar{\delta}$ and $\bar{\epsilon}$ are sightly modified, compared to Eqs. (2.173) and (2.174)

$$\bar{\delta} = \left(I + \frac{3}{16}\frac{c_1}{Q}\frac{Z}{A^{2/3}}B_v\theta\right)\Big/\left(1 + \frac{9}{4}\frac{J}{Q}A^{-1/3}B_{\rm surf}^{\rm fr}\theta\right) \quad (2.179)$$

and

$$\bar{\epsilon} = \frac{1}{K}\left(Ce^{-\gamma A^{1/3}} - 2a_SA^{-1/3}B_2 + L\bar{\delta}^2 + c_1\frac{Z^2}{A^{4/3}}B_4\right)\,, \quad (2.180)$$

with two additional shape functions

$$B_2 = \frac{1}{2x_0}\left.\frac{d\,(x^2B_{\rm surf}^{\rm fr})}{dx}\right|_{x=x_0}\,, \qquad B_4 = -y_0^2\left[\frac{d}{dy}\left(\frac{B_{\rm Coul}^{\rm fr}}{y}\right)\right]_{y=y_0}\,,$$

where $x = R/a$, $x_0 = (r_0/a)A^{1/3}$, $y = R/a_{\rm den}$, and $y_0 = (r_0/a_{\rm den})A^{1/3}$. In Ref. [235] it was felt to be useful to include a term $C\exp(-\gamma A^{1/3})$ in the expression (2.180) for $\bar{\epsilon}$. The term is nonanalytic in the expansion parameter $A^{-1/3}$ of the droplet model, where it can therefore not appear. But it does appear in the finite-range model for the sphere. No suggestion is made for its shape dependence. The remaining seven terms in Eq. (2.177) are given in Eqs. (2.151), (2.158) - (2.161), (2.154), and (2.157).

Of the many empirical parameters, which appear in the various terms of Eq. (2.177) the following constants were fitted to ground-state binding energies and binding-energy differences [197], all given in MeV

$a_V = 16.247$	volume-energy	$Q = 29.21$	surface stiffness
$a_S = 22.92$	surface energy	$C_a = 0.436$	charge asymmetry
$a_{\rm curv} = 0$	curvature energy	$a_0 = 0$	A^0-term
$J = 32.73$	symmetry energy	$C = 60$	C parameter in $\bar{\epsilon}$
$L = 0$	density symmetry	$W = 30$	Wigner term
$r_m = 4.8$	average pairing gap	$r'_m = 6.6$	n-p interaction

and the dimensionless constant $\gamma = 0.831$ in the exponent of the compressibility term of Eq. (2.180). Eq. (2.177) contains also a number of parameters

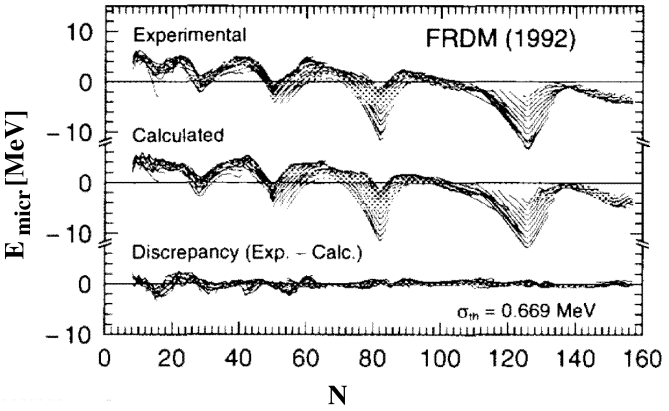

Fig. 2.11. Discrepancy between experimental and theoretical nuclear masses, calculated by adding shell and pairing corrections to the macroscopic energy. The latter was obtained from the FRDM of Ref. [222] (after Ref. [197]).

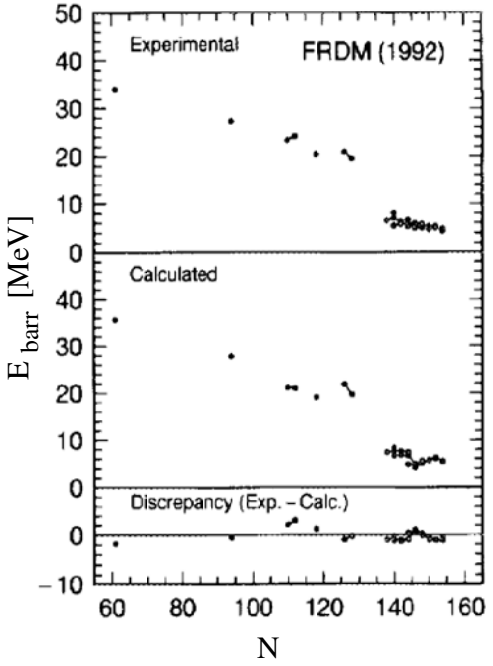

Fig. 2.12. Experimental and theoretical fission barriers, calculated by adding shell and pairing corrections to the FRDM of Ref. [222] (after Ref. [197]).

of the dimension of a length, which are either fitted to electron scattering or light-ion scattering data. All of them are given in fm in the following list

$r_0 = 1.16$ nuclear radius parameter, $a = 0.68$ Yukawa range in the surface energy,
$r_p = 0.80$ rms radius of the proton, $a_{\rm den} = 0.70$ Yukawa range in the Coulomb energy.

Finally, the nuclear incompressibility was assumed to be $K = 240$ MeV to account roughly for the position of the giant compression mode.

Adding Strutinsky shell and pairing corrections to the FRDM energy of Eq. (2.177) the remaining discrepancy with the 1654 experimental masses of Ref. [218] is shown in Fig. 2.11. A comparison of experimental barrier heights with calculated barriers is presented in Fig. 2.12.

2.3 Shell and pairing corrections to the macroscopic mass formula

It is desirable to have a scheme for calculating ground-state binding energies and energy surfaces which is numerically less expensive than selfconsistent HF+BCS or even HFB calculations. We have seen that the ETF expression for the binding energy admits the numerically very convenient liquid-drop expansion. One may therefore ask whether the difference between ETF and HF can also be calculated in a sufficiently convenient way. Strutinsky showed that this is indeed possible [99].

2.3.1 The Strutinsky shell-correction

Strutinsky observed that the deviation of the binding energy from the liquid-drop prediction was large for those nuclides with a smaller than average single-particle level-density above the Fermi surface. He therefore introduced an averaged reference level-density $\tilde{g}_q(\epsilon)$ for protons ($q = p$) and neutrons ($q = n$) by averaging the actual HF level density $g_q(\epsilon) = \sum_i \delta(\epsilon - \epsilon_i^q)$ by a folding procedure

$$\tilde{g}_q(\epsilon) = \frac{1}{\gamma} \int g_q(\epsilon') f\left(\frac{\epsilon - \epsilon'}{\gamma}\right) d\epsilon' = \frac{1}{\gamma} \sum_i f\left(\frac{\epsilon - \epsilon_i^q}{\gamma}\right) . \tag{2.181}$$

The folding function $f(\epsilon/\gamma)$ is required to have the range γ, of the order of the shell spacing $\hbar\omega \approx 41/A^{1/3}$ MeV and the folding operation (2.181) shall transform a smooth function, for example a polynomial Q_n of order $n \leq M$ into itself. Strutinsky proposed the ansatz $f(x) = w(x)P_M(x)$ with a weight function $w(x) > 0$ and a correction polynomial $P_M(x)$, which satisfies the equation

$$Q_n(x) = \int Q_n(x - x')P_M(x')w(x')dx' \tag{2.182}$$

for any polynomial Q_n with $n \leq M$.

An explicit representation of the polynomial P_M is obtained by expanding $Q_n(x - x')$ in Eq. (2.182) around x

$$Q_n(x) = \sum_{\mu=0}^{n} \frac{(-1)^\mu}{\mu!} \frac{d^\mu Q_n(x)}{dx^\mu} \int x'^\mu P_M(x')w(x')dx' \ ,$$

which implies the condition [236]

$$\int x'^\mu P_M(x')w(x')dx' = \delta_{\mu 0} \quad \text{for all} \quad \mu \leq M. \tag{2.183}$$

One can show [237] that from this equation follows that all odd powers of the polynomial P_M vanish because the odd moments $\int_{-\infty}^{\infty} x^{2n+1}w(x)dx$ are zero. In this case Eq. (2.183) is equivalent to the requirement that for any polynomial $\mathcal{Q}_n(x)$ of order $n \leq M$

$$\int \mathcal{Q}_n(x')P_M(x')w(x')dx' = \mathcal{Q}_n(0) \ . \tag{2.184}$$

For any weight function $w(x)$ there exists a set of orthonormal polynomials $p_n(x)$ with

$$\int p_n(x)p_m(x)w(x)dx = \delta_{nm}$$

(see e.g. Chap. 22 of Ref. [238]). In terms of these polynomials the ansatz

$$P_M(x) = \sum_{n=0}^{M} p_n(x)p_n(0) \tag{2.185}$$

is made. Expanding $\mathcal{Q}_n(x)$ in terms of the first n polynomials $p_n(x)$, the ansatz (2.185) is seen to satisfy the condition (2.184).

For the weight function Strutinsky chose a Gaussian $w(x) = \pi^{-1/2}e^{-x^2}$ and the integration interval $-\infty < x < \infty$ in order to make the average independent of the integration boundaries. The corresponding orthogonal polynomials are the Hermite polynomials $H_n(x)$ with normalization factor $[n!2^n]^{-1}$ [238]. Because the Gaussian is symmetric, we can restrict ourselves to the subset of Hermite polynomials with even index. Since $H_{2n}(0) = (-1)^n(2n)!/n!$, the correction polynomial becomes

$$P_M(x) = \sum_{n=0}^{M/2} (-1)^n \frac{H_{2n}(x)}{2^{2n}n!} = L_{M/2}^{1/2}(x^2) \ , \quad M \text{ even}, \tag{2.186}$$

where $L_{M/2}^{1/2}$ is a generalized Laguerre polynomial. The last equality of (2.186) can for instance be proved by induction using Eqs. 22.4.7, 22.7.30, and 22.5.40

of Ref. [238]. The functions $f(x) = \pi^{-1/2} L_{M/2}^{1/2} e^{-x^2}$ with $M = 0, 2, 4, 6, 8$ are given below

$$f(x) = \begin{cases} \frac{1}{\sqrt{\pi}} e^{-x^2} \\ \frac{1}{\sqrt{\pi}} e^{-x^2} (\frac{3}{2} - x^2) \\ \frac{1}{\sqrt{\pi}} e^{-x^2} (\frac{15}{8} - \frac{5}{2} x^2 + \frac{1}{2} x^4) \\ \frac{1}{\sqrt{\pi}} e^{-x^2} (\frac{35}{16} - \frac{35}{8} x^2 + \frac{7}{4} x^4 - \frac{1}{6} x^6) \\ \frac{1}{\sqrt{\pi}} e^{-x^2} (\frac{315}{128} - \frac{105}{16} x^2 + \frac{63}{16} x^4 - \frac{3}{4} x^6 + \frac{1}{24} x^8) \,. \end{cases}$$

Other weight functions $w(x)$ have been proposed [236, 239, 240]. However, the Gaussian weight has almost exclusively been used in actual calculations.

In the following we will drop the index q and derive the shell correction for neutrons. For protons analogous equations hold. In analogy with the relation

$$N = 2 \int_0^{\epsilon_f} \sum_i \delta(\epsilon_i - \epsilon) d\epsilon \,,$$

which defines the Fermi energy ϵ_f (the factor 2 accounts for the Kramers degeneracy of the single-particle levels), one introduces a chemical potential $\tilde{\lambda}$ by

$$N = 2 \int_0^{\tilde{\lambda}} \tilde{g}(\epsilon) d\epsilon \tag{2.187}$$

for the reference nucleus. Similarly its density matrix is defined in the HF basis (cf. Eq. (2.12) by

$$\tilde{n}_i = \frac{1}{\gamma} \int_{-\infty}^{\tilde{\lambda}} f\left(\frac{\epsilon - \epsilon_i}{\gamma}\right) d\epsilon \tag{2.188}$$

and in an arbitrary basis $\chi_l(\mathbf{r}, \sigma, \tau)$, using the unitary matrix U of Eq. (2.4), the density matrix becomes $\tilde{\rho}_{kl} = \sum_i U_{ki} \tilde{n}_i U_{il}^{-1}$. For the reference nucleus the Hartree-Fock energy, Eq. (2.7), is

$$\tilde{E}^{\mathrm{HF}} = \sum_{l_1 l_2} t_{l_1 l_2} \tilde{\rho}_{l_2 l_1} + 1/2 \sum_{l_1 l_1' l_2 l_2'} \tilde{\rho}_{l_1 l_1'} \overline{V}_{l_1' l_2' l_1 l_2} \tilde{\rho}_{l_2' l_2} \,. \tag{2.189}$$

In terms of the difference

$$\delta\rho_{l_2 l_1} = \rho_{l_2 l_1} - \tilde{\rho}_{l_2 l_1}$$

and using Eq. (2.10) the shell correction is, to linear order in $\delta\rho$

$$\delta E^{\mathrm{HF}} = E^{\mathrm{HF}} - \tilde{E}^{\mathrm{HF}} = \sum_{l_1 l_2} (t_{l_1 l_2} + \Gamma_{l_1 l_2}) \delta\rho_{l_2 l_1} + \mathcal{O}(\delta\rho^2) \,. \tag{2.190}$$

We now assume that a shell-model Hamiltonian $\hat{h}^{\mathrm{shell}}$ can be found with a local potential $V^{\mathrm{shell}}(\mathbf{r})$ having eigenvalues $\epsilon_i^{\mathrm{shell}}$ and eigenstates $\varphi_i^{\mathrm{shell}}$ which

approximate the eigenvalues ϵ_i and eigenstates φ_i of the HF Hamiltonian in the subspace $\mathcal{P}$ spanned by the states φ_i with eigenvalues ϵ_i in a vicinity of order γ on both sides of the Fermi energy ϵ_f

$$\sum_{l_1 l_2}(t_{l_1 l_2} + \Gamma_{l_1 l_2})\hat{a}^+_{l_1}\hat{a}_{l_2} \approx \hat{h}^{\rm shell} \qquad \text{in } \mathcal{P} \ .$$

Then the shell correction energy can be written

$$\delta E^{\rm HF} \approx \delta E^{\rm shell} = \sum_{i \le i_{\rm Fermi}} \epsilon_i^{\rm shell} - \int_{-\infty}^{\tilde{\lambda}} \epsilon\, \tilde{g}^{\rm shell}(\epsilon) d\epsilon \ . \tag{2.191}$$

To account for the effect of pairing correlations on the ground-state binding energy in the framework of the HF+BCS scheme, the pairing correction $\Delta P = \Delta E - \widetilde{\Delta E}$ from Eqs. (2.65) and (2.66) or (2.67) is added to the shell correction. If we assume that the smoothed HF energy $\tilde{E}^{\rm HF}$ admits a leptodermous expansion, we arrive at the basic formula of the macroscopic-microscopic approach of calculating binding energies

$$E^{\rm HF+BCS} = E_{\rm mac} + \sum_{q=n,p} (\delta E_q^{\rm shell} + \Delta P_q) \ . \tag{2.192}$$

In this formula the macroscopic energy, usually identified with the liquid-drop energy, depends smoothly on the proton and neutron numbers and accounts for most of the binding energy. The shell correction shows a rather oscillatory behavior as function of $N^{1/3}$ and $Z^{1/3}$, as will be shown below and contributes less than 10 MeV to the binding energy as seen in the upper frames of Fig. 2.11.

The Hamiltonian $\hat{h}^{\rm shell}(\mathbf{r})$, used to generate the shell correction, violates the translational invariance of the original N-body Hamiltonian. It may however be expected that the spurious energies connected with symmetry violations cancel in the average in the subtraction procedure (2.192).

Details of the potential $V^{\rm shell}$ far away from the Fermi energy do not influence the shell correction (2.191) at all. What matters is the size and shape of the surface, defined by $V^{\rm shell}(\mathbf{r}_{\rm surf}) = \epsilon_f$. The latter should approximately coincide with the shape of the equivalent sharp surface of the nucleus under consideration [241]. The size can be taken from the droplet model [196] or fitted to certain single-particle energies of odd nuclei, cf. Sec. 2.1.8 for results. Less sensitive is the shell correction to the slope of the potential at the Fermi surface $\boldsymbol{\nabla} V_{\rm cent} \cdot \hat{\mathbf{n}}|_{\mathbf{r}=\mathbf{r}_{\rm surf}}$, where $\hat{\mathbf{n}}$ is the unit vector in the direction of the normal on the equivalent sharp surface. Shell corrections have indeed been calculated successfully with Woods-Saxon as well as Nilsson potentials if their size and shape are properly chosen. For a quantitative investigation of the appropriate choice of the shell-model potential we refer to Refs. [242], [243] and [244].

Plotting the smooth energy $\tilde{E}^{\rm shell}(\gamma)$ for an harmonic oscillator potential versus the averaging width γ, one obtains a constant value when $\gamma \geq \hbar\omega$, provided the order of the correction polynomial is $M \geq 4$, since the smooth part of the oscillator spectrum is a polynomial of order 4 ("plateau behavior"). For other potentials this is not the case. The smooth part of their spectrum $\tilde{g}$ is therefore not exactly reproduced by the folding procedure of Eq. (2.184). To minimize the resulting error with respect to the choice of γ, one uses the plateau condition

$$\partial \tilde{E}^{\rm shell}/\partial\gamma = 0\,. \tag{2.193}$$

The resulting optimal γ depends on M. Brack and Pauli [239] showed that the plateau condition (2.193) implies the equality

$$\int_{-\infty}^{\tilde{\lambda}} \epsilon\tilde{g}(\epsilon)d\epsilon = \sum_i \epsilon_i \tilde{n}_i\,, \tag{2.194}$$

which can be used in Eq. (2.191).

The integration interval from $-\infty$ to $+\infty$, connected with the Gaussian weight function, causes problems for light nuclei because the Fermi energy may not be much more than by the width γ away from the lowest level, where the spectrum ends. Also in finite potentials the Fermi energy may not be much more than by γ away from the continuum limit, where the discrete spectrum also ends abruptly. In both cases the folding procedure leads to spurious edge effects because it reproduces polynomials, but not polynomials cut at two ends. Various recipes have been proposed to overcome this problem. Concerning the continuum limit, it is common practice to diagonalize the shell-model Hamiltonian in an oscillator basis, in which case one generates (spurious) discrete eigenstates $\epsilon_i > 0$, i.e. in the continuum. However, since they conveniently continue the sequence of the real (negative) eigenvalues smoothly, they dampen out the upper edge effect. The price to be paid is an uncontrollable effect on the smoothed properties of the reference nucleus, which becomes the more serious the smaller the distance of the Fermi energy (in units of γ) $|\epsilon_f|/\gamma$ is from the continuum limit. Moreover often the stationarity condition (2.193) cannot be satisfied. For neutron-rich nuclei this can become a serious problem. Another proposal is to mirror the spectrum at its lower and upper edges. A similar decrease of the reliability of the shell correction with decreasing $|\epsilon_f|/\gamma$ is again the drawback also of this procedure. Attempts to modify the averaging prescription by restricting it to a finite energy interval [240] were not satisfactory either since the resulting shell correction depends too strongly on the choice of the integration limits. Another recipe to cope with the edge effect was proposed by Tondeur [245]. He introduced energy-dependent coefficients in the polynomial $P_M(x)$ of Eq. (2.185) to improve the plateau condition (2.193) for sufficiently large γ.

In a series of papers Ivanyuk and Strutinsky [246–248] developed an alternative averaging procedure, which requires the knowledge of single-particle

levels only up to the level $i = N_2$. In this approach the smooth background energy $\tilde{E}^{\rm shell}(N)$ is obtained for a given potential by averaging the shell-model energy

$$E^{\rm shell}(N) = \sum_{i \le i_{\rm Fermi}} \epsilon_i(N)$$

with respect to N between N_1 and N_2. $\tilde{E}^{\rm shell}(N)$ is defined as a polynomial of order M in $N^{1/3}$ which minimizes the mean-square deviation $\sum_{N=N_1}^{N_2} [E^{\rm shell}(N) - \tilde{E}^{\rm shell}(N)]^2$ with respect to the coefficients of the polynomial (note: $M \ll N_2 - N_1$). To decrease the dependence of $\tilde{E}^{\rm shell}(N)$ on N_1 and N_2 a Gaussian weight function was later introduced in Ref. [247] and the averaged energy can then be written

$$\tilde{E}^{\rm shell}(N) = \sum_{N'=N_1}^{N_2} K\big(x(N), x(N')\big) e^{-x^2(N')} E^{\rm shell}(N')$$

with $x(N) = (N^{1/3} - N_0^{1/3})/\Delta N$ and the "curvature correction" $K(x, x') = \sum_{k=1}^{M} p_k(x) p_k(x')$, where $p_k(x)$ are the normalized orthogonal polynomials for the Gaussian weight function in the discrete interval $N_1 \le N \le N_2$, see Ref. [238], Sec. 22.17, and $N_0 \approx N$, $\Delta N \approx 3/4$. The difference $\delta U(N) = E^{\rm shell}(N) - \tilde{E}^{\rm shell}(N)$ turns out to have systematically a larger absolute value than the shell correction $\delta E^{\rm shell}(N)$ of Eq. (2.191). It was shown in Ref. [248] that

$$\delta E^{\rm shell}(N) = \delta U(N) + \frac{1}{2}\, \tilde{g}(\mu_N) \langle (\delta \mu_N)^2 \rangle \,, \tag{2.195}$$

where $\tilde{g}(\mu_N)$ is the mean level density at the Fermi energy and $\langle (\delta \mu_N)^2 \rangle$ is the variance of the Fermi energy. Ivanyuk investigated the use of Eq. (2.195) to calculate $\delta E^{\rm shell}$ when the Fermi energy is too close to the continuum limit to use the standard Strutinsky averaging safely [249].

The macroscopic-microscopic approach, Eq. (2.192), can easily be extended to shape-constraint HF energies. The single-particle energy-spectra in the corresponding deformed shell-model potentials show a remarkable level bunching for axially and reflection symmetric shapes when the axis ratio is close to 1:2, and, somewhat lesser, when it is 1:3. This is analogous to the even stronger level bunching in spherical potentials, giving rise to the magic numbers. The situation is shown in Fig. 2.13 for the deformed oscillator potential (without spin-orbit coupling). The Fourier components of the oscillating part of the level density have been related to the classical closed orbits in the shell-model potential [114]. The orbits with the smallest action along the trajectory give rise to the largest Fourier amplitudes. It turns out that for axis ratios expressed by small integers especially short (in units of the action) closed orbits exist which lead to a level bunching and corresponding large shell corrections. For a detailed discussion of the relation between shell corrections and closed classical orbits we refer to Strutinsky's review article [251] and to Chaps. 4 and 6 of Ref. [114].

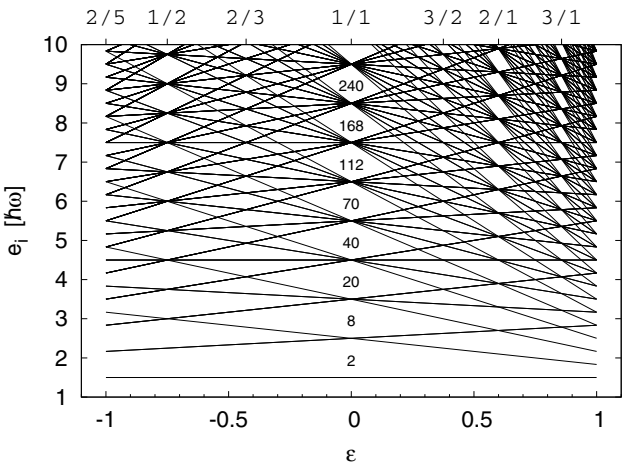

Fig. 2.13. Energy levels of an axially symmetric, harmonic oscillator potential as function of the spheroidal deformation parameter ϵ (after Ref. [250]).

Shell corrections are particularly large and negative when there is a large gap above the last occupied level. If the liquid-drop barrier has an extremum close to a maximum of the shell correction, the latter has a particularly strong effect on the topography of the total energy surface of such a nucleus: It can stabilize an unstable or almost unstable ground state of the liquid-drop model and convert a liquid-drop saddle-point into a local secondary minimum, corresponding to a fission-isomeric state.

2.3.2 Microscopic justification of the Strutinsky shell-correction

It remains to be shown that the smoothed HF energy $\tilde{E}^{\mathrm{HF}}$ can be identified with the ETF energy and therefore admits a leptodermous expansion. Migdal and Krainov [252] showed already that the energy of the atomic many-electron system in Hartree approximation becomes the Thomas-Fermi energy when sums over single-particle states are replaced by integrals over a smooth level density and the single-particle wave-functions are replaced by their WKB approximations. And in fact, Gross [253], Bhaduri and Ross [254], and Jennings [255] showed that the ETF energy approximates the Strutinsky-averaged HF energy.

The central tool in the prove of Refs. [254] and [255] is the single-particle partition-function

$$Z_{\mathrm{HF}}(\beta) = \sum_i e^{-\beta\epsilon_i} = \int_0^\infty g(\epsilon) e^{-\beta\epsilon} d\epsilon \,, \tag{2.196}$$

where the ϵ_i are the Hartree-Fock eigenstates, and the ETF analogue of Z_{HF} is

$$Z_{\rm ETF}(\beta) = Z_{\rm TF}(1 + \hbar\chi_1(\beta) \ldots + \hbar^4\chi_4(\beta))\,. \tag{2.197}$$

This expression is the result of a Wigner-Kirkwood expansion of $Z_{\rm HF}$ [114] and is often misleadingly called an expansion in "powers of $\hbar$". It is in fact an asymptotic expansion in inverse powers of the single-particle action, measured in units of $\hbar$. The Thomas-Fermi partition function $Z_{\rm TF}(\beta)$ in Eq. (2.197) is given by

$$Z_{\rm TF} = \frac{2}{h^3}\int e^{-\beta h^{\rm shell}(\mathbf{p},\mathbf{r})} d^3p d^3r\ ,$$

where $h^{\rm shell}(\mathbf{p},\mathbf{r})$ is the classical single-particle Hamiltonian and the factor 2 accounts for the spin degree of freedom. For the harmonic oscillator $Z_{\rm TF} = 2/(\beta\hbar\omega)^3$. The expansion (2.197) is divergent for $\beta \to \infty$. It is to be treated as a semiconvergent series and should be truncated with the term $\hbar^4\chi_4$. One can show [114] that for small β one has for the harmonic oscillator

$$Z_{\rm ETF}(\beta) \approx Z_{\rm HF}(\beta) \qquad \text{if } \beta\hbar\omega \ll 1 \tag{2.198}$$

(high-temperature limit). For more general potentials $\hbar\omega$ has to be replaced in this formula by the average distance between main shells.

The single-particle level density $g_{\rm HF}(\epsilon) = \sum_i \delta(\epsilon - \epsilon_i)$ is the inverse Laplace transform of the partition function

$$g_{\rm HF}(\epsilon) = \mathcal{L}^{-1}_{\beta\to\epsilon}[Z_{\rm HF}(\beta)] \equiv \frac{1}{2\pi i}\int_{c-i\infty}^{c+i\infty} Z_{\rm HF}(\beta)e^{\epsilon\beta}d\epsilon\,, \tag{2.199}$$

which follows immediately by inserting the definition (2.196). Analogously the ETF level density is defined by

$$g_{\rm ETF}(\epsilon) = \mathcal{L}^{-1}_{\beta\to\epsilon}[Z_{\rm ETF}(\beta)]\,.$$

According to Eq. (2.181) the averaged HF level density is a folding product $g_{\rm HF} * f(\epsilon/\gamma)/\gamma$. Using the folding theorem of Laplace transformations and the fact that the two-sided Laplace transform of $f(x)$ is

$$\int_{-\infty}^{\infty} e^{-\beta\epsilon} f(\epsilon\gamma)d\epsilon/\gamma = e^{(\gamma\beta/2)^2}\mathcal{P}_M(\beta\gamma)\,, \tag{2.200}$$

with some polynomial $\mathcal{P}_M$ of order M [255], the averaged HF level density can be written in terms of the partition function $Z_{\rm HF}$

$$\begin{aligned}\tilde{g}_{\rm HF}(\epsilon) &= \mathcal{L}^{-1}_{\beta\to\epsilon}[Z_{\rm HF}(\beta)e^{(\gamma\beta/2)^2}\mathcal{P}_M(\gamma\beta)] \\ &= \frac{1}{2\pi i}\int_{c-i\infty}^{c+i\infty} Z_{\rm HF}(\beta)e^{(\gamma\beta/2)^2}\mathcal{P}_M(\gamma\beta)e^{\epsilon\beta}d\beta\,.\end{aligned}$$

In the limit $c \to +0$ and introducing the new integration variable $x = -i\beta$, one obtains

$$\tilde{g}_{\mathrm{HF}}(\epsilon) = \frac{1}{2\pi} \int_{-\infty}^{\infty} Z_{\mathrm{HF}}(ix) e^{-(\gamma x/2)^2} \mathcal{P}_M(i\gamma x) e^{i\epsilon x} dx \,.$$

Because of the Gaussian in the integrand the most appreciable contributions to the integral come from $x < 1/\gamma$. The averaging width γ is of the order $\hbar\omega$. The partition function Z_{HF} is therefore only needed for $\beta\hbar\omega < 1$, where it can be replaced by its semiclassical approximation Z_{ETF}. We therefore conclude that $\tilde{g}_{\mathrm{HF}} \approx \tilde{g}_{\mathrm{ETF}}(\epsilon)$.

To complete the proof that the difference between the HF and ETF energies is well approximated by the Strutinsky shell-correction, we have to show that

$$N = \int_0^{\mu} g_{\mathrm{ETF}}(\epsilon) d\epsilon = \int_{-\infty}^{\mu} \tilde{g}_{\mathrm{ETF}}(\epsilon) d\epsilon$$

and (2.201)

$$E = \int_0^{\mu} g_{\mathrm{ETF}}(\epsilon) \epsilon d\epsilon = \int_{-\infty}^{\mu} \tilde{g}_{\mathrm{ETF}}(\epsilon) \epsilon d\epsilon$$

holds for the same value of μ. It is plausible that $g_{\mathrm{ETF}}(\beta)$ is a smooth function of β and may therefore be well represented by a polynomial. Since polynomials (of low order) are reproduced by the folding procedure, Eq. (2.182), one expects $\tilde{g}_{\mathrm{ETF}}(\epsilon) = g_{\mathrm{ETF}}(\epsilon)$, which implies the relations (2.201). A more formal proof is given in Ref. [255].

2.3.3 The extended Thomas-Fermi-plus-Strutinsky integral method

In order to overcome a certain ambiguity in the choice of the shell-model potential corresponding to a given liquid-drop-type macroscopic energy, Chu, Jennings, and Brack proposed the following procedure, halfway between self-consistent HF and the standard macroscopic-microscopic approach [187]. For a given Skyrme potential they solve the ETF equations for spherical nuclei self-consistently, using the generalized Fermi function (2.118) for a convenient representation of the proton and neutron densities. They obtain the total energy E_{ETF}, the densities $\rho^{(q)}_{\mathrm{ETF}}(r)$ and the kinetic energies $\tau^{(q)}_{\mathrm{ETF}}$ as functions of the density and of its gradients up to fourth order. With $\rho^{(q)}_{\mathrm{ETF}}(r)$ and $\tau^{(q)}_{\mathrm{ETF}}(r)$ the quantities $\tilde{V}_q(\mathbf{r})$, $\tilde{f}_q(\mathbf{r})$, and $\tilde{\boldsymbol{W}}_q(\mathbf{r})$ are calculated according to Eqs. (2.109), (2.112), and (2.113). For the single-particle Hamiltonian

$$\tilde{h}_q = -\frac{\hbar^2}{2M_{\mathrm{nucl}}} \boldsymbol{\nabla} \tilde{f}_q(\mathbf{r}) \boldsymbol{\nabla} + \tilde{V}_q(\mathbf{r}) - i\tilde{\boldsymbol{W}}_q(\mathbf{r}) \cdot (\boldsymbol{\nabla} \times \boldsymbol{\sigma})$$

the Schrödinger equation

$$\tilde{h}_q \phi^{(q)}_j = \varepsilon^{(q)}_j \phi^{(q)}_j \,,$$

is solved to get the eigenvalues $\varepsilon_i^{(q)}$. In terms of them the Strutinsky theorem can be written in the form

$$E_{\mathrm{HF}} = E_{\mathrm{ETF}} + \sum_q \left(\sum_{i \le i_{\mathrm{Fermi}}} \varepsilon_i^{(q)} - \mathrm{tr}\ \tilde{h}_{\mathrm{ETF}}^{(q)} \tilde{\rho}_q \right) + \mathcal{O}(\delta\rho^2) \tag{2.202}$$

with $\delta\rho = \rho_{\mathrm{HF}} - \tilde{\rho}$. Since it is less time-consuming to calculate self-consistent solutions in the ETF frame than in HF, this approach allows to calculate binding energies faster than in HF, but not so fast as with the standard macroscopic-microscopic approach.

It is the main advantage of this way of introducing shell corrections that no averaging over the single-particle level-density is needed. It can therefore be used up to the drip lines of the chart of nuclides (if, in addition, the pairing corrections are calculated appropriately). It may also appear to be an advantage that the smooth part of the binding energy, E_{ETF}, and the shell correction are derived from the same microscopic source, namely the underlying Skyrme potential. On the other hand, any errors caused by too narrow restrictions in the specific ansatz for the density $\rho(\mathbf{r})$ in the self-consistent solution of the ETF equations cannot be compensated as in the standard version of the macroscopic-microscopic approach, where the smooth part of the energy is fitted to the liquid drop or droplet model.

The method was called "Extended Thomas-Fermi plus Strutinsky Integral", ETFSI, by Dutta et al. [256–260] because the trace on the right-hand-side of Eq. (2.202) becomes an integral over $\mathbf{r}$ in space representation. These authors used the method in a version which was simplified for reasons of numerical convenience in two essential points: Skyrme potentials were restricted to those for which $M^*_{\mathrm{nucl}} = M_{\mathrm{nucl}}$ and the density $\rho(\mathbf{r})$ was restricted to a Fermi function. Presumably because of the latter restriction the authors found an intolerably large difference between the left and the right-hand-side of Eq. (2.202) when both sides were calculated independently with the same Skyrme potential. The authors then felt obliged to use different Skyrme parameters for HF and for ETFSI calculations.

2.4 Energy surfaces

There are two ways to construct energy surfaces: one may either solve a constrained HF or HFB problem, introducing appropriate constraining single-particle operators to control the shape of the resulting self-consistent density distribution or one adopts a priori a shape class, characterized by a number of shape parameters, for which the liquid-drop model yields the smooth part of the deformation energy to which shell and pairing corrections are added. These approaches will be discussed in the next two subsections. We will finally focus on the stationary points of the multidimensional energy surfaces and their dependence on the proton and neutron numbers of the corresponding nuclides.

2.4.1 Calculations with shape constraints

In this approach one looks for the lowest energy eigenvalue of the Schrödinger equation

$$(\hat{H}' - E)|\mathrm{HF}\rangle = 0 \tag{2.203}$$

in the set of N-particle HF states, where the Routhian $\hat{H}' = \hat{H} - \sum_{i=1}^{n} \lambda_i \hat{q}_i$ is defined in terms of n operators $\hat{q}_1 \dots \hat{q}_n$ constraining the shape of the density distribution and corresponding Lagrange multipliers $\lambda_1 \dots \lambda_n$. We restrict the discussion here to HF solutions, for HFB states analogous arguments hold. The solution of Eq. (2.203) yields a state $|\mathrm{HF}(\lambda_1 \dots \lambda_n)\rangle$ depending on the Lagrange multipliers λ_i. One introduces the expectation values $\overline{q}_i$ by the equations

$$\overline{q}_i(\lambda_1 \dots \lambda_n) = \langle \mathrm{HF}(\lambda_1 \dots \lambda_n)|\hat{q}_i|\mathrm{HF}(\lambda_1 \dots \lambda_n)\rangle, \qquad i = 1, \dots n, \tag{2.204}$$

which one may invert to obtain

$$\lambda_i = \lambda_i(\overline{q}_1 \dots \overline{q}_n), \qquad i = 1, \dots n. \tag{2.205}$$

We will assume that this inversion exists and is unique in a certain area of the n-dimensional space of deformation parameters $\overline{q}_i$, where $\det(\partial_{\lambda_i} \overline{q}_j) \neq 0$. Inserting this result into the energy expectation-value

$$E(\lambda_1 \dots \lambda_n) = \langle \mathrm{HF}(\lambda_1 \dots \lambda_n)|\hat{H}|\mathrm{HF}(\lambda_1 \dots \lambda_n)\rangle\,,$$

one obtains the energy $E(\overline{q}_1 \dots \overline{q}_n)$ as function of the deformation parameters, which is referred to as the potential-energy surface. For a detailed discussion how these steps can be numerically implemented for HFB wave functions we refer to the work of Younes and Gogny [261].

There is a naive interpretation of the Lagrange multipliers in Eq. (2.203) that they are the components of the generalized force, needed to keep the system in equilibrium at the deformation $\overline{q}_1 \dots \overline{q}_n$. In the context of a dynamical equation of motion in the collective variables $\overline{q}_i$ the force would be identified with the inertial force according to d'Alembert's principle. However, for a microsystem like a nucleus, one has to keep in mind that the variances $\langle \mathrm{HF}|(\hat{q}_i - \overline{q}_i)^2|\mathrm{HF}\rangle$ are in general not zero and cannot be neglected. The way in which the states $|\mathrm{HF}(\lambda_1 \dots \lambda_n)\rangle$ and the function $E(\overline{q}_1 \dots \overline{q}_n)$ enter into equations of motion is therefore a more subtle subject, to which we will return in Chapter 5. Here we are interested in stationary points only, local minima and saddle points, for which all Lagrange multipliers vanish so that they are independent of constraining conditions.

Often used constraining operators are $\hat{Q}_{20} = r^2 Y_{20}(\theta, \phi)$ to control the elongation along the z-axis, $\hat{Q}_{22} + \hat{Q}_{2-2}$ to control ellipsoidal nonaxiality, $\hat{Q}_{30}$ to control deviations from reflection symmetry, and $\hat{Q}_{40}$ to influence neck-formation [263]. To manipulate the scission shape, the constraint $\hat{Q}_N = \exp(-[z/a]^2)$ was used for necked-in configurations [264] with some length parameter $a \approx 1$ fm.

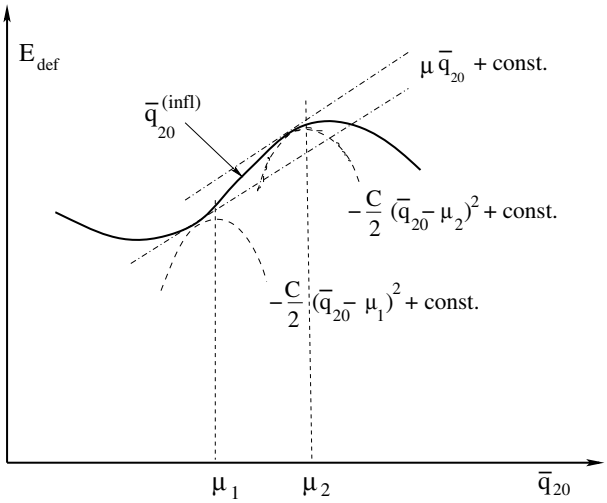

Fig. 2.14. Schematic plot of $E_{\rm def}(\overline{q}_{20})$, thick line. Linear and quadratic constraints are shown with dash-dotted and dashed lines, respectively, at a point on the left and on the right side of the inflection point $\overline{q}_{20}^{(\rm infl)}$. The geometrical meaning of the parameter μ is also indicated (after Ref. [262]).

It might appear that one can obtain all minima and saddle points along the fission path by introducing only one elongation parameter, for instance $\overline{q}_{20}$. However, already for the energy surface of the liquid-drop model there are two different $\overline{q}_{20}$ values for the same λ as can be seen in Fig. 2.14, since $\partial_\lambda \overline{q}_{20} = 0$ for the inflection point $\overline{q}_{20}^{(\rm infl)}$. Sometimes a quadratic constraint $-(C/2)(\overline{q}_{20}-\mu)^2$ was introduced to overcome this problem [265]. The meaning of the parameter μ is shown in Fig. 2.14. The value of C is rather arbitrary, if $C > |\, d^2E/d\,\overline{q}_{20}^2|$. This constraint leads to an effective Lagrange parameter $\lambda_{\rm eff} = C(\mu-\overline{q}_{20})$. For alternative methods to handle the multivalued functions (2.205) we refer to Sec. 7.6 of Ref. [108].

To calculate the energy surface around a saddle point with an unstable direction perpendicular to the elongation direction, a similar nonlinear constraint in that direction should be used. For instance, for a fissility x below the Businaro-Gallone point the fission saddle of the liquid-drop model is unstable with respect to reflection asymmetry. Therefore a quadratic constraint in $\overline{q}_{30}$ is required in this case. In order not to miss an extremum which has lower symmetry than the initial state of the iterative solution procedure of Eq. (2.203), it is necessary to include constraints in H' which have the same lower symmetry. It also happens that there are several solutions for the same $\overline{q}_{20}$. An example is given in Fig. 2.16. In such case an additional constraint is required – in the example a neck-size parameter – to distinguish between solutions. We refer to a discussion of this point by Berger, Girod, and Gogny [263] and to examples given in Ref. [261].

For the classical liquid-drop model with sharp-surface Coulomb, surface, and curvature energies Strutinsky [266] and Strutinsky, Lyashchenko, and Popov [267] proposed to look for a constrained, selfconsistent solution of the variational problem

$$\frac{\delta}{\delta\rho}[E_{\rm l.d.}\{\rho(z)\} - \lambda_1 {\rm vol}\{\rho(z)\} - \lambda_2 D\{\rho(z)\}] = 0\,, \tag{2.206}$$

where the function $\rho(z)$ gives the shape of the nucleus in cylindrical coordinates (axial symmetry is assumed) and $E_{\rm l.d.}\{\rho,\rho'\}$ is the liquid-drop energy, considered as functional of the shape function $\rho(z)$. The constraint $\lambda_1 {\rm vol}\{\rho\}$ shall guaranty volume conservation during shape variation, and $D\{\rho\}$ is the distance between the centers of mass of the left and the right part of the figure. From Eqs. (2.148) and (2.153) follow the variational derivatives

$$\frac{\delta E_{\rm surf}}{\delta\rho} = E^{(0)}_{\rm surf}\frac{\delta B_{\rm surf}}{\delta\rho} = \frac{E^{(0)}_{\rm surf}}{2R_0^2}\frac{1+\rho'^2-\rho\rho''}{(1+\rho'^2)^{3/2}} \tag{2.207}$$

$$\frac{\delta E_{\rm curv}}{\delta\rho} = E^{(0)}_{\rm curv}\frac{\delta B_{\rm curv}}{\delta\rho} = -\frac{E_{\rm curv}}{2R_0}\frac{\rho''}{(1+\rho'^2)^2}\,. \tag{2.208}$$

The variation of the Coulomb energy when ρ changes by $\delta\rho$ in the interval dz, is

$$\delta E_{\rm Coul} = \frac{3eZ}{4\pi R_0^3} 2\pi\rho\;\delta\rho dz\;\Phi(\rho,z)\,,$$

where $\Phi(\rho,z)$ is the Coulomb potential on the surface at the point ρ,z. Measuring Φ in units of eZ/R_0, this yields the functional derivative

$$\frac{\delta E_{\rm Coul}}{\delta\rho} = \frac{3}{2}\left(\frac{eZ}{R_0^2}\right)^2\rho\,\Phi\,. \tag{2.209}$$

Inserting the results (2.207)-(2.209) into Eq. (2.206) and dividing the equation by $E^{(0)}_{\rm surf}/(2R_0^2)$ one obtains the Euler equation of the variational problem (2.206)

$$\frac{\rho\rho''-1-\rho'^2}{(1+\rho'^2)^{3/2}} + \frac{E^{(0)}_{\rm curv}}{E^{(0)}_{\rm surf}}R_0\frac{\rho''}{(1+\rho'^2)^2} + 10x\frac{\rho}{R_0}\Phi - \lambda_1\frac{\rho}{R_0} - \lambda_2\frac{\rho|z|}{R_0^2} = 0\,. \tag{2.210}$$

In this equation x is the fissility and the potential Φ is given by

$$\Phi(z,\rho) = \frac{3}{4\pi R_0^2}\int_{\rm vol}\frac{d^3r'}{|\mathbf{r}(\rho,z)-\mathbf{r}'|} = -\frac{3}{8\pi R_0^2}\int_{\rm surf}\frac{(\mathbf{r}(\rho,z)-\mathbf{r}')\cdot d\mathbf{S}'}{|\mathbf{r}(\rho,z)-\mathbf{r}'|}\,,$$

where the identity

$${\rm div}_{r'}\frac{\mathbf{r}-\mathbf{r}'}{|\mathbf{r}-\mathbf{r}'|} = -\frac{2}{|\mathbf{r}-\mathbf{r}'|}$$

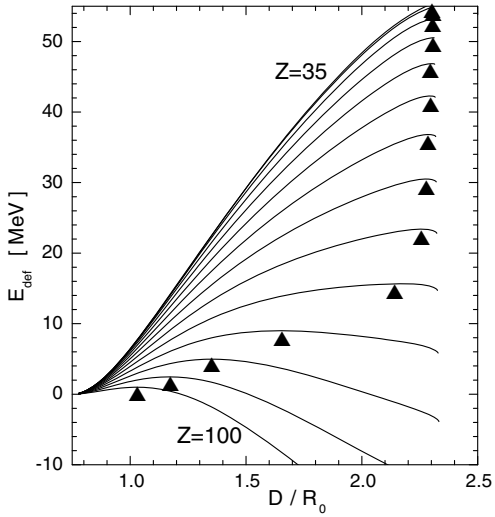

Fig. 2.15. Deformation energy along the fission valley as function of the distance D between the centers of mass of the two halves of the (reflection symmetric) shape for nuclei with $35 \leq Z \leq 100$. The neutron excess was taken to be $I = 0.26$. Liquid-drop parameters from Ref. [228]. The fission saddle points were indicated by black triangles (after Ref. [268]).

was used. In cylindrical coordinates one obtains

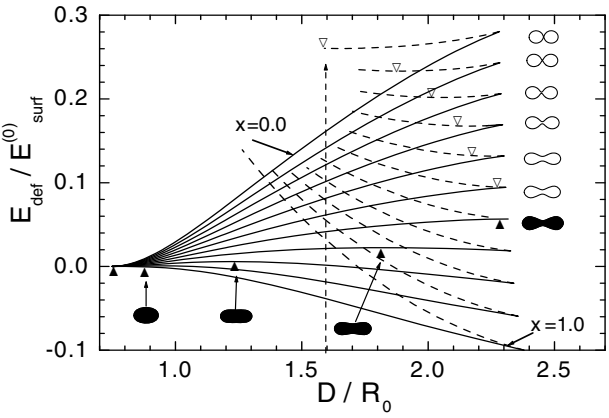

Fig. 2.16. Deformation energy along the fission valley as function of the distance D between the centers of mass of the two halves of the shape for nuclei with fissility $0 \leq x \leq 1$. Liquid-drop parameters of Ref. [228]. The fission saddle points with an unstable direction perpendicular to the elongation direction were indicated by open triangles (after Ref. [269]).

$$\Phi(\rho,z) = -\frac{3}{8\pi R_0^2}\int_0^{2\pi} d\phi' \int_{z_{\min}}^{z_{\max}} dz'$$
$$\times \frac{\rho(z)\rho(z')\cos(\phi-\phi') - \rho^2(z') - \rho(z)\rho'(z')(z-z')}{[\rho^2(z)+\rho^2(z')-2\rho(z)\rho(z')\cos(\phi-\phi')+(z-z')^2]^{1/2}} \,.$$

The nonlinear integro-differential equation (2.210) has to be solved with boundary conditions $\rho(z_{\min}) = \rho(z_{\max}) = 0$ and $\rho'(z_{\min}) = \infty$, $\rho'(z_{\max}) = -\infty$. The original iterative solution strategy converged only in certain areas of the (x, D) plane [267]. An improved relaxation procedure allowed Ivanyuk [270] to map the bottom of the fission valley from the spherical ground state to the end of the mountain ridge, separating the fission from the fusion valley, where the system becomes unstable against scission at fixed distance D. In Fig. 2.15 the energy along the fission valley is shown as function of the distance D for various fissilities x. The maximum of these curves corresponds to the fission barrier in the liquid-drop model. In Fig. 2.16 also dashed lines are added, which correspond to maxima of the constrained stationary-value problem. These lines map the mountain ridge separating fission and fusion valleys. The minima of these lines, indicated by open triangles, correspond to saddle points for transitions between these valleys at fixed distance D. Unfortunately, the bottom of the fusion valley has not yet been mapped by this method.

2.4.2 Calculations based on shape parametrizations

By far most often energy surfaces have been calculated by the macroscopic-microscopic method. In this approach one has first to fix a class of shapes, which one expects to contain the actual fission pass. For shapes close to the ground-state shape an expansion in multipoles is a natural choice since any smooth, compact shape can be represented in this way. However, for strongly necked-in shapes not all points on the surface can be "seen" from the origin (the origin is no longer a star point). Close to scission the multipole expansion therefore fails. Moreover, it turns out that it takes more than 14 multipoles to achieve convergence even for the very compact saddle point of the lighter actinides in the liquid-drop model [180]. It was therefore also a question of economy to find shape parametrizations, better adapted to what one believes to be the fission path.

A first one-parameter family of shapes was introduced by Hill and Wheeler [87]. They considered the sequence of saddle-point shapes in the liquid-drop model, shown in Fig. 1.1 as function of the fissility x, or rather of the "deformation" parameter $y = 1-x$. The shape class was therefore called y-family of shapes. For more detailed information on the y-family we refer to the monograph by Hasse and Myers [200].

Various other shape classes have been proposed for the same purpose. Their appropriateness has often been judged on their ability to describe fission

saddle-points with a few deformation parameters only. However, one has to keep in mind that the fission path is very much influenced by mass and friction parameters and must not necessarily pass over the fission barrier, as will be shown in Chapter 5. In particular, beyond the saddle point, down to scission, there are no reasonable criteria for the choice of a restricted shape class, based on the statics of the energy surface alone.

Since there is no one-to-one mapping of one of these shape classes onto another, even dynamically calculated fission paths in one shape class cannot easily be compared with results obtained in another class. Unfortunately, one often finds plots of the first two "important" shape parameters versus those two parameters of another shape class, giving the erroneous impression that such mapping is possible in more than very limited areas of the shape variables. With this cautioning in mind we shall discuss some of the more frequently used shape classes and refer for a more comprehensive discussion to Hasse and Myers' book [200].

Nilsson's ε_n parametrization

In connection with deformed, axially symmetric oscillator potentials Nilsson [92] introduced stretched, dimensionless cylindrical coordinates ρ_t, z_t, related to normal cylindrical coordinates ρ, z by

$$\begin{aligned} \rho_t &= c\,\omega_\perp^{1/2}\rho, \qquad & z_t &= c\,\omega_z^{1/2} z, \\ \cos\theta_t &= z_t/\rho_t, & r_t^2 &= z_t^2 + \rho_t^2 \end{aligned} \tag{2.211}$$

with $c^2 = M_{\rm nucl}/\hbar$ and

$$\omega_\perp = \omega(\varepsilon)(1{+}\varepsilon/3), \quad \omega_z = \omega(\varepsilon)(1{-}2\varepsilon/3), \quad \omega(\varepsilon)/\omega_0 = (1{-}\varepsilon^2/3{-}2\varepsilon^3/27)^{-1/3}$$

in terms of the spheroidal deformation parameter ε and a scaling factor ω_0. The oscillator potential becomes in the stretched coordinates

$$V_{\rm osci}(\rho_t, z_t; \varepsilon; \omega_0) = \frac{1}{2}\hbar\omega(\varepsilon) r_t^2 \left[1 - \frac{2}{3}\varepsilon P_2(\cos\theta_t)\right]. \tag{2.212}$$

The nuclear shape is identified with the equipotential surface

$$V_{\rm osci} = \epsilon_{\rm Fermi}\,. \tag{2.213}$$

Inserting Eqs. (2.211) into Eq. (2.212), one obtains from Eq. (2.213) an implicit equation for ρ as function of z and ε. Nilsson's shape parametrization was later generalized to an expansion around the spheroidal shape, involving additional shape parameters $\varepsilon_3, \ldots \varepsilon_N$ [93].

The Lawrence shape-class and its extensions

Lawrence proposed the quartic shapes

$$\rho^2 = az^4 + bz^2 + c\,, \tag{2.214}$$

where one of the three parameters a, b, c is determined by the requirement of volume conservation [271]. Hasse extended the ansatz to allow for mirror asymmetric shapes

$$\rho^2 = R_0^3\lambda[z_0^2 - (z+z_s)^2][z_2|z_2| + (z+z_s-z_1)^2]\,, \tag{2.215}$$

where λ is determined as function of the other parameters to ensure volume conservation and z_s serves to bring the center of mass to the origin [272]. There are three deformation parameters: z_0 and z_1 controlling the elongation and the asymmetry, respectively and z_2, connected with constriction.

A further extension of the shape class (2.214) was introduced by Trentalange, Koonin, and Sierk [273]

$$\rho^2 = R_0^2 \sum_{n=0} a_n P_n(z/z_0) \tag{2.216}$$

in terms of Legendre polynomials $P_n(z/z_0)$. The sum was restricted to even multipoles in Ref. [273]. The length of the nuclear shape is $2z_0 = (4R_0)/(3a_0)$ and volume conservation yields $a_0 = -\sum_{n=2} a_n$. Further restrictions of the deformation-parameter space are required to ensure geometrically sensible values of ρ^2. To describe shapes without axial symmetry, Sierk extended the class (2.216) by the ansatz [274]

$$\rho(z,\phi) = \rho^{(0)}(z)\;\eta(\phi)/\lambda \tag{2.217}$$

with $\eta(\phi) = 1+\alpha_1 P_2(\cos\phi)+\alpha_2 P_4(\cos\phi)$ and $\lambda = 1+\alpha_1/4+9\alpha_2/64$ in terms of two additional deformation parameters α_1 and α_2.

Pomorski and Bartel [275] included also odd Legendre polynomials in the sum (2.216) to describe shapes without mirror symmetry

$$\rho^2(z) = R_0^2 \sum_{n=0}^{n_{\max}} \alpha_n P_n\left(\frac{z-z_s}{z_0}\right)\,. \tag{2.218}$$

The first two α parameters should satisfy the relations

$$\alpha_0 = -\sum_{n=2,4,} \alpha_n\,, \qquad \alpha_1 = -\sum_{n=3,5,} \alpha_n$$

to yield reasonable shapes. Volume conservation requires $z_0 = 2R_0/(3\alpha_0)$ and $z_s = -2\alpha_1 R_0/(9\alpha_0^2)$ serves to keep the center of mass at the origin.

A modification of the shape class (2.215) was introduced by Brack et al. [103] to improve the description of deformed ground-state shapes

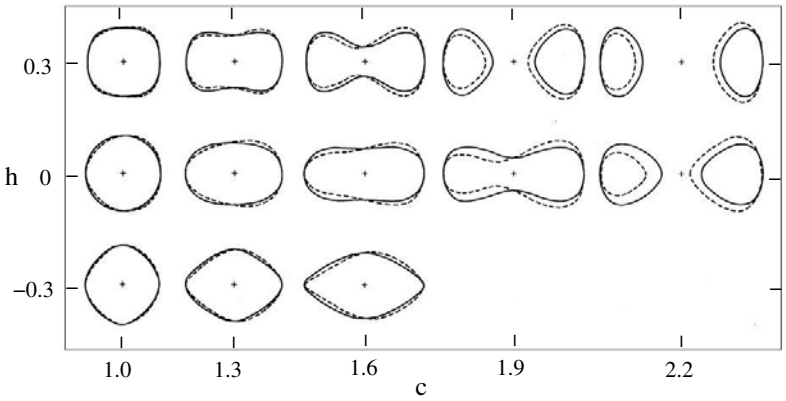

Fig. 2.17. Some shapes in the c, h, α parametrization. Full lines correspond to $\alpha = 0$, dotted ones to $\alpha = 0.2$ (after Ref. [103]).

$$\rho^2(z) = \begin{cases} (C^2 - z^2)[A + B(z/C)^2 + \alpha(z/C)] & \text{for} \quad B \geq 0 \\ (C^2 - z^2)[A + \alpha(z/C)]e^{BCz^2/R_0^3} & \text{for} \quad B < 0. \end{cases} \tag{2.219}$$

Volume conservation implies one functional relation between A, B, α, and C/R_0. After elimination of A by this relation two independent, dimensionless deformation parameters

$$\begin{aligned} c &= C/R_0 \\ h &= B/2 - (C/R_0 - 1)/4 \end{aligned}$$

are introduced besides the asymmetry variable α. The shape class (2.219) is shown in Fig. 2.17.

Still another modification of the class (2.215) is the so-called "Modified Funny-Hills" parametrization of Pomorski and Bartel [275] which allows to describe nonaxial shapes with an ellipsoidal cross section perpendicular to the z axis with eccentricity $\epsilon = \sqrt{2\eta/(1+\eta)}$ – independent of z – in terms of one extra nonaxiality deformation-parameter η. In cylindrical coordinates (ρ, z, ϕ)

$$\rho^2(z, \phi) = \tilde{\rho}^2(z) \frac{\sqrt{1-\eta^2}}{1 + \eta \cos 2\phi} \tag{2.220}$$

with

$$\tilde{\rho}^2(z) = \frac{R_0^2}{c\, f(a, B)} (1-u)(1 + \alpha u - Be^{-a^2u^2}), \tag{2.221}$$

where the function

$$f(a, B) = 1 - \frac{3B}{4a^2} \left[e^{-a^2} + \sqrt{\pi} \left(a - \frac{1}{2a} \right) \mathrm{Erf}(a) \right]$$

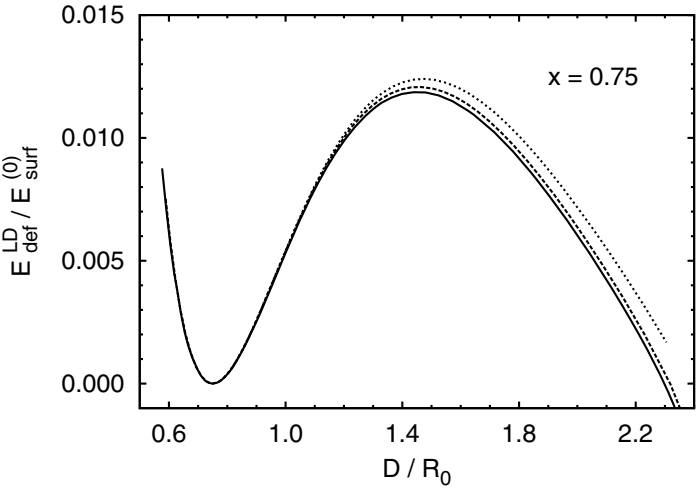

Fig. 2.18. Deformation energy along the fission valley as function of the distance D between the centers of mass of the two halves of the (reflection symmetric) shape for a nucleus with fissility $x = 0.75$, the region of lighter actinides. Liquid-drop parameters from Ref. [228]. The full line is the result of a variational calculation with Eq. (2.210). The dashed line was calculated within the shape class (2.220), where the parameter B was minimized out at fixed D (from Ref. [276]). The dotted line corresponds to the fission valley in the shape class (2.219), also with B being minimized out.

serves to keep the volume constant and $u = (z - z_s)/(cR_0)$. To fix the center of mass at the origin the shift $z_s = -4\alpha c R_0/[15 f(a, B)]$ is introduced. The parameter a is taken to be 1 and instead of B the parameter $h = B - c + 1$ is introduced. This leaves four independent, dimensionless deformation parameters: c, h, α, and η. Fig. 2.18 shows that the liquid-drop deformation energy along the fission valley is very well reproduced for lighter actinides in this shape class.

The shape class of Cassinian ovaloids and its extension

Stavinsky, Rabotnov, and Seregin introduced the shape class of Cassinian ovaloids [277]

$$\rho^2(z) = \sqrt{a^4 + 4c^2 z^2} - (c^2 + z^2) \ . \tag{2.222}$$

The volume-conservation condition allows to express the parameter a by $R_0 = r_0 A^{1/3}$ so that a one-parameter family of shapes results. Fig. 2.19 shows this shape family as function of the dimensionless deformation parameter $u = c/a$. It yields a fairly good description of the fission valley in the liquid-drop model

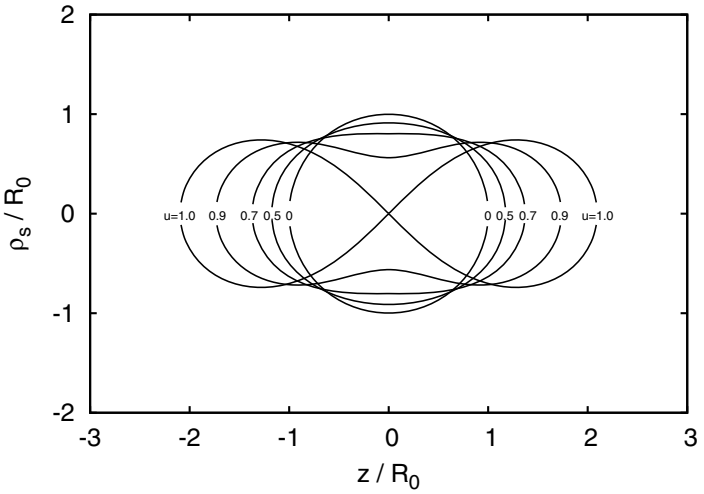

Fig. 2.19. The shape class of Cassinian ovaloids of constant volume (after Ref. [200]).

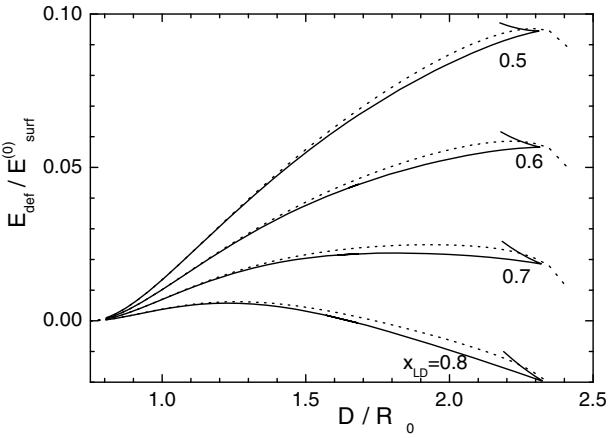

Fig. 2.20. Deformation energy along the fission valley as function of the distance D between the centers of mass of the two halves of the shape for nuclei with fissility $0.5 \leq x \leq 0.8$. Liquid-drop parameters of Ref. [228]. The full lines are calculated with the variational ansatz (2.206), (2.210), the dashed lines show the deformation energy in the shape class (2.222) (after Ref. [270]).

when compared with the constrained, self-consistent calculation using Eq. (2.210) as shown in Fig. 2.20.

An extension of the shape class (2.222) was proposed by Pashkevich [278]. He considers Cassinian oval coordinates [279], a system of orthogonal, curvi-

linear coordinates (R, x) in the plane, in terms of which cylinder coordinates (ρ, z) are given by [278]

$$\rho(R,x) = \frac{1}{\sqrt{2}}\{[R^4 + 2c^2R^2(2x^2-1) + c^4]^{1/2} - R^2(2x^2-1) - c^2\}^{1/2} \tag{2.223}$$

$$z(R,x) = \frac{\mathrm{sign}(x)}{\sqrt{2}}\{[R^4 + 2c^2R^2(2x^2-1) + c^4]^{1/2} + R^2(2x^2-1) + c^2\}^{1/2}.$$

For $R = a = \mathrm{const}$, elimination of x between these equations yields the shape class (2.222). Pashkevich extended the class by putting

$$R = R(x) = R_0\left(1 + \sum_l \alpha_l P_l(x)\right) \tag{2.224}$$

with Legendre polynomials $P_l(x)$, and additional deformation parameters α_l. The expression (2.224) is to be inserted into Eqs. (2.223). Besides the α_l Pashkevich introduced instead of u a deformation parameter α, defined implicitly by the equation

$$u^2 = \frac{\alpha-1}{4}\left\{\left(1+\sum_l \alpha_l\right)^2 + \left(1+\sum_l (-1)^l\alpha_l\right)^2\right\} + \frac{\alpha+1}{2}\left\{1+\sum_l (-1)^l \frac{(2l-1)!!}{2^l l!}\alpha_{2l}\right\}^2. \tag{2.225}$$

With this definition of α, α equals u^2 if all α_l vanish, and for any values of the α_l the neck radius vanishes if $\alpha = 1$. In Refs. [280–282] α is called ϵ. Since α and α_2 have a similar effect on the shape, these authors set α_2 equal to zero.

The class of three smoothly joined quadratic surfaces

In an attempt to interpolate smoothly between an initial sphere or spheroid and two coaxial spheroids in the exit channel of fission, Nix introduced the shape class of three smoothly joined surfaces of revolution [283]

$$\rho^2(z) = \begin{cases} a_1^2 - (a_1/c_1)^2(z-l_1)^2, & l_1 - c_1 \le z \le z_1 \\ a_2^2 - (a_2/c_2)^2(z-l_2)^2, & z_2 \le z \le l_2 + c_2 \\ a_3^2 + (a_3/c_3)^2(z-l_3)^2, & z_1 \le z \le z_2 \end{cases} \tag{2.226}$$

The meaning of the eleven parameters z_1, z_2, and a_i, c_i, l_i, $i = 1, 2, 3$ is described in Fig. 2.21 There are four relations between these parameters to ensure the smooth matching at z_1 and z_2, one relation to ensure volume conservation, and a sixth one to fix the center of mass at the origin. This leaves 5 independent deformation parameters, three of which are related with symmetric shapes. For ground-state shapes this parametrization is nevertheless

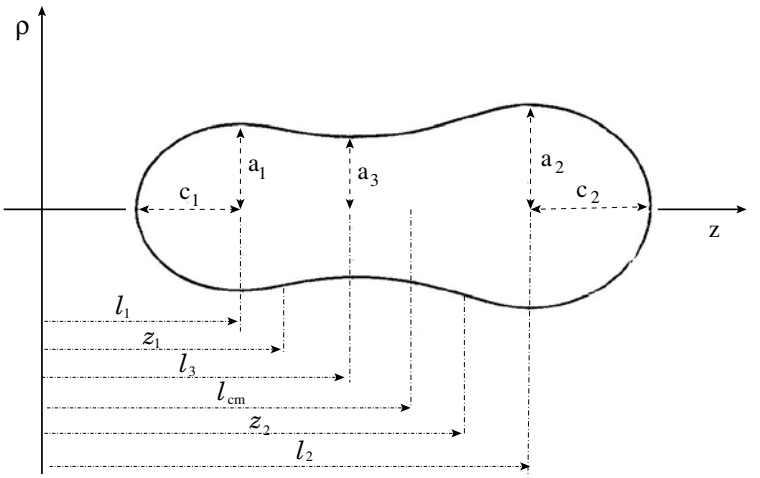

Fig. 2.21. The parameters of the three, smoothly joined quadratic surfaces (after Ref. [283]).

of inferior flexibility compared to a multipole expansion with the first three even multipoles. On the other hand none of the previously discussed shape classes contains two spheroids at given tip-to-tip distance, a configuration one expects in the fusion valley. Advantages of the shape class of three quadratic surfaces are therefore expected around and beyond scission. The shape class may be generalized to shapes with elliptic cross section perpendicular to the fission direction using the transformation (2.220).

In connection with dynamical calculations one is forced to restrict the dynamical variables to what are considered to be "essential" variables: elongation, constriction, and asymmetry. The shape class of three quadratic surfaces is for instance reduced by allowing only spheres for the two outer surfaces with radii R_1 and R_2. Błocki et al. [284–287] introduced the ρ, λ, Δ parametrization with

$$\rho = \frac{l_2 - l_1}{R_1 + R_2}, \quad \lambda = \frac{(z_1 - l_1) - (z_2 - l_2)}{R_1 + R - 2}, \quad \Delta = \frac{R_1 - R_2}{R_1 + R_2}\,. \tag{2.227}$$

Other parametrizations of the same restricted shape class can also be found in the literature [288].

2.4.3 Survey of the geometry of stationary points

We have seen that in constrained selfconsistent calculations stationary points of the energy surface are in principle independent of the choice of the constraining operator with the caveat mentioned in Sec. 2.4.1. This is in general not true for such topographical features as valleys and mountain ridges. They

are even more dependent on the choice of deformation parameters for energy surfaces calculated in a given shape class. As already stressed by Wilets [30] even a transformation of coordinates within one shape class may convert a valley into a mountain ridge. In Fig. 2.22 the function $f(x, y) = y^2 - x^2$ is represented in the left frame by its contour lines. The function has a saddle point at the origin where two valleys start along the positive and negative y-axis, separated by mountain ridges along the x-axis. In new coordinates x', y', related to x, y by

$$\begin{aligned} x &= x' \\ y^2 &= y'^3 - 3x'^2 y' + x'^2 \end{aligned} \tag{2.228}$$

the function $f(x', y')$ is given by the contour lines of the right frame of

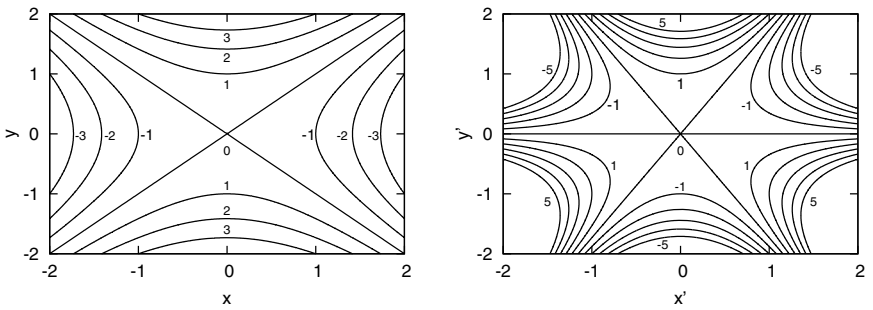

Fig. 2.22. Effect of the coordinate transformation (2.228) on the function f(x,y).

Fig. 2.22. The transformation leaves the saddle at the origin and the y-axis ($x = 0$) becomes the y'-axis ($x' = 0$). On the positive y'-axis is now a mountain ridge, instead of a valley. One should therefore not attach too much physical significance to valleys and ridge lines. In particular, one should not assume that in the fission process the fission valley is initially filled from the saddle with a rather sharp probability distribution in the phase space of the collective coordinates and that this probability distribution is subsequently running down the valley like honey. Note that only the equations of motion are covariant under coordinate transformations, but not topographical properties of the energy surface.

It is nevertheless useful to employ concepts like fission and fusion valleys to visualize the topological relation between various stationary points of the energy surface.

The energy surface in the liquid-drop model

The liquid-drop energy surface has one minimum which is the spherical ground state for nonrotating systems. For nuclei with finite angular momentum systematic investigations of the macroscopic energy surface are usually based on

the assumption of a rigid rotation, irrespective of how that can be realized microscopically. We presented in the Introduction the result obtained by Cohen, Plasil, and Swiatecki, Ref. [44], for the pure liquid-drop model, consisting of a volume, a sharp-surface, and a Coulomb term. It is summarized in Figs. 1.3. and 1.4: below line y_I of the phase diagram of Fig. 1.3 the ground state is axially symmetric, oblate, and rotates around the symmetry axis, between

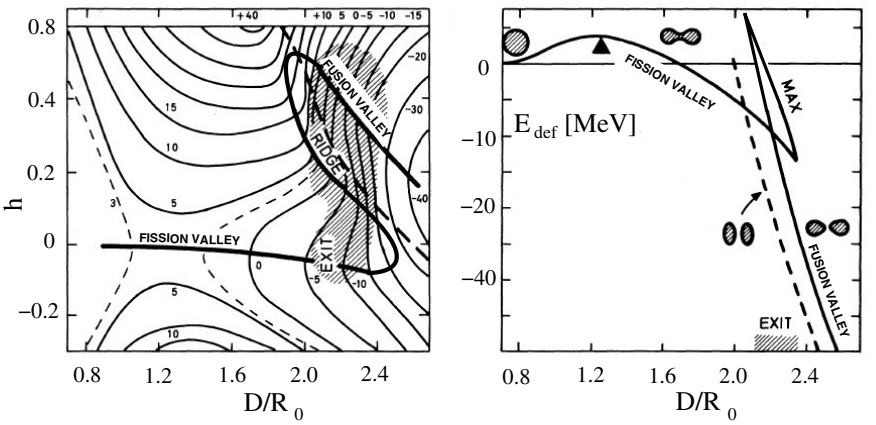

Fig. 2.23. Contour plot of the potential-energy surface of the liquid-drop model, calculated in the parametrization (2.219) and plotted vs. h and the centers-of-mass distance D for $\alpha = 0$. The fission and fusion valleys are indicated by thick lines, separated by a mountain ridge. Also shown by the thick, dashed line is the bottom of the fusion valley in a parametrization of two equal, coaxial spheroids. The right frame shows the energy of the valleys and the ridge line as function of D/R_0 (after Ref. [103]).

lines y_I and y_{II} the ground state is triaxial, rotating around the smallest axis, and beyond the line y_{II} there exists no minimum. The saddle-point shapes become increasingly more compact for increasing y at given fissility x. They are reflection symmetric between lines y_{II} and y_{III} and loose stability against mass-asymmetric distortions below line y_{III}, which is the continuation of the Businaro-Gallone point at $y = 0$ into the x, y plane.

A complete energy surface in the liquid-drop model for a nonrotating nucleus with $x = 0.8$ is shown in the left frame of Fig. 2.23. It was calculated in the shape class (2.219) and presented as function of the distance D between the centers-of-mass of the two nascent fragments and the neck parameter h. One sees the fission valley passing the saddle point in the lower half of the figure and the fusion valley leading upwards in the upper right corner of the figure. The two valleys are separated by a mountain ridge stretching from the upper end of the fusion valley at $D/R_0 \approx 1.9$ to the lower end of the fission valley at $D/R_0 \approx 2.6$. The shaded area was assumed by the authors

of Ref. [103] to be the area where the neck rupture occurs. This can actually only be determined by a dynamical calculation.

Since the c, h, α parametrization is not very suitable to describe the fusion valley, the energy of two coaxial oblate spheroids is shown by a dashed line in Fig. 2.23. It leads to substantially lower energies for the same distance D than the shape class (2.219). With decreasing fissility x the mountain ridge becomes shorter and eventually the fission and the fusion valleys coalesce. In Fig. 2.24 we show as an example the fusion energy-surface for the system ^{40}Ca+^{40}Ca. The shape class (2.226) of three quadratic surfaces was used, better suited for the fusion valley. An early version of a finite-range liquid-drop model is employed to account for the proximity potential in the fusion entrance-channel. As shown in Fig. 2.15, independent of any parametrization, selfconsistent liquid-drop model (LDM) calculations for symmetric shapes yield the end point of the fission valley at $D_{\rm crit}/R_0 \approx 2.23$, for all $x \leq 0.9$.

In the finite-range liquid-drop model (FRLDM) one can no longer absorb all model parameters in the dimensionless parameters x and y and collect all shape dependencies in the dimensionless functions $B_{\rm surf}$, $B_{\rm Coul}$, and $B_{\rm rot}$ of the shape parameters since there are additional independent lengths involved to characterize the diffusenesses of the nuclear energy density, of the charge density and the mass density, the latter entering the evaluation of the moments of inertia. Binding and deformation energies have therefore to be given as functions of A, Z, and the collective angular momentum L, besides the shape parameters, and are specific for each set of potential parameters. Results will

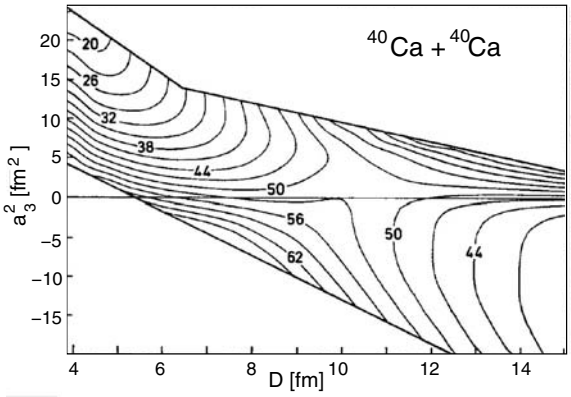

Fig. 2.24. Contour diagram of the potential energy for the system ^{40}Ca+^{40}Ca as function of the centers-of-mass distance D and the neck cross-section parameter a_3^2. The line $a_3 = 0$ is the scission line. The spherical compound state is in the upper left corner. The energy is minimized at each point with respect to the eccentricity of the outer spheroids. Potential parameters are taken from Ref. [225]. Energies on the contour lines are in MeV, counted from the configuration where the fragments are at infinite distance D (after Ref. [289]).

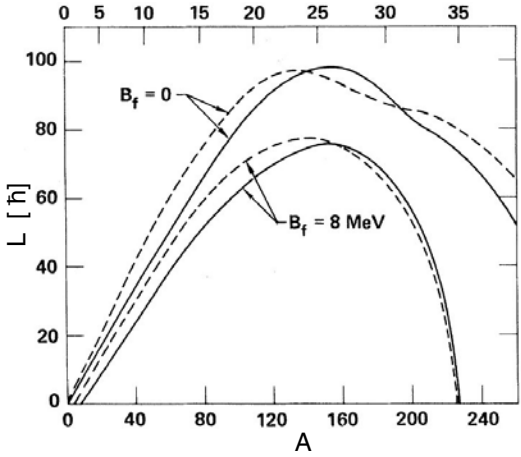

Fig. 2.25. Phase diagram of rotating nuclei in the L, A plane. The full lines are calculated in the FRLDM, the dashed lines in the LDM. The upper two lines are calculated for vanishing fission barrier, the two lower lines for a barrier height of 8 MeV (after Ref. [290])
.

be presented in the following for β stable nuclei, i.e. Z is given by Eq. (2.162) as function of A. It is not necessarily integer.

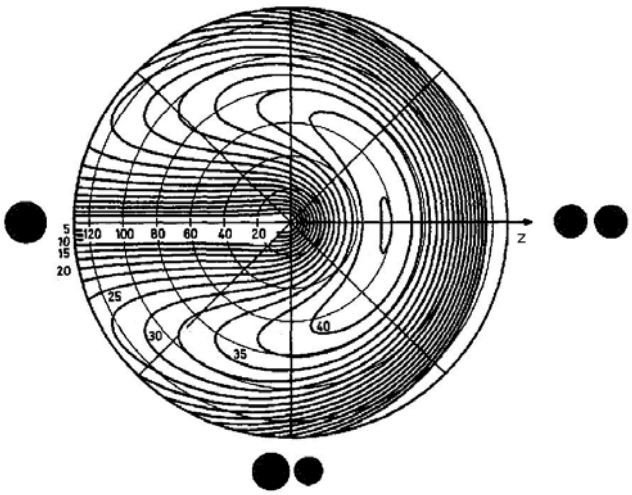

Fig. 2.26. Potential energy of the scission configuration of touching spheres in the FRLDM of Ref. [225]. The angular variable is the asymmetry ϕ, the radial variable is the charge number Z of the compound system. The compound nucleus, for $\phi = 180^o$, is taken as the energy zero-point for each Z (after Ref. [289]).

For zero angular momentum the saddle-point shapes in the FRLDM have a little larger necks compared to the same nuclei in the pure LDM [274]. The main difference, however, is the barrier height, shown in Fig. 2.8. For strongly necked-in saddle-point shapes the LDM does not account for the proximity potential between juxtaposed surface areas of the nascent fragments, which is included automatically in the FRLDM and leads to a substantial lowering of the fission barrier.

For finite (collective) angular momentum L the phase-space diagram of the LDM, shown in Fig. 1.3, remains qualitatively the same in the FRLDM [274, 290]. In Fig. 2.25 the dashed lines correspond to the lines y_I and y_{II}, the full lines are calculated by Mustafa, Baisden, and Chandra [290] in the FRLDM.

There is no systematic investigation of the saddle points with an unstable direction in the neck degree of freedom, indicated in Fig. 2.16 by the open triangles, under rotation or in the FRLDM.

Sometimes the mass asymmetry is plotted as an angular variable [291], e.g. $\phi = \pi(a_1^3 - a_2^3)/(a_1^3 + a_2^3)$ in the shape class (2.226) [289]. In Fig. 2.26 we show as an example the potential energy in the fusion valley for touching spheres. The radial variable is the charge number of the compound state. The N/Z ratio is assumed to have equilibrated between the reacting nuclei and is further assumed in this figure to follow Green's formula for β-stable nuclei, Eq. (2.162). Changes in the mass asymmetry at fixed total mass (or Z) proceed in Fig. 2.26 on a circle. For instance for $Z = 100$ the driving force is seen to lead to fusion if $\pi \geq \phi > \phi_{\rm crit}(Z)$, where $\phi_{\rm crit}(100) \approx 2\pi/3$, "the larger eats the smaller". For $\phi < \phi_{\rm crit}$ the driving force is in the direction of making the size of the reacting nuclei equal. With decreasing Z the critical angle $\phi_{\rm crit}(Z)$ decreases and for $Z < 60$ the driving force is always in the direction of fusion. Note that shell effects are not considered in this picture. For collectively rotating systems the range of initial asymmetries favoring fusion is shrinking [289].

The energy surface including shell and pairing corrections (in the macroscopic-microscopic approach)

Microscopic corrections to the liquid-drop energy surface are largest for spherical nuclei and second largest when the ratio of the axes of the nuclear shape is roughly 1:2. Fig. 2.27 shows a cut through the energy surface for axial and reflection symmetric shapes of some actinides as function of the elongation parameter y within the y-family of shapes, (explained in Sec. 2.4.2). The dashed lines represent the liquid-drop energy, the full lines include shell-plus-pairing corrections. The first minimum corresponds to the ground state, the second minimum represents an isomeric state, and the two outer maxima are saddle points. Clearly it takes a representation of the energy in more dimensions and a more flexible shape parametrization to establish the character of these extrema.

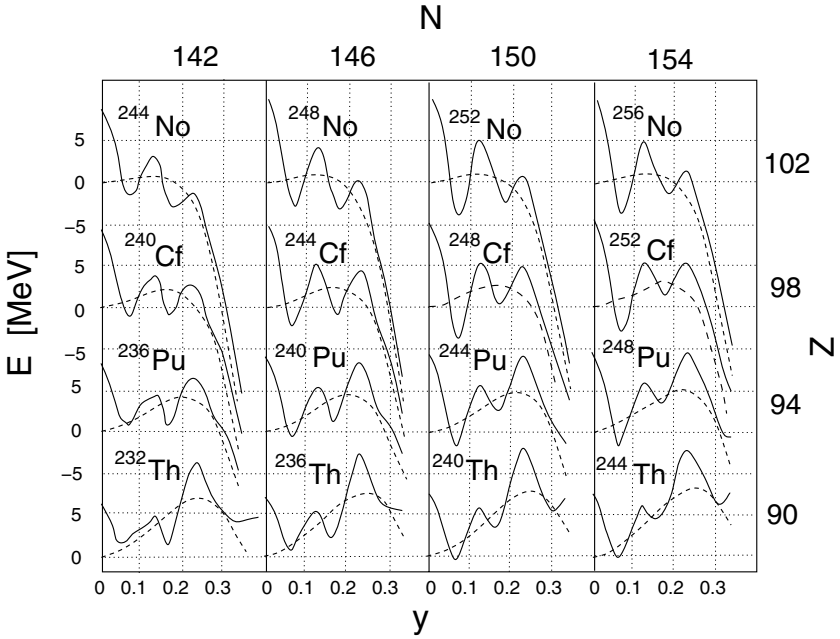

Fig. 2.27. Potential energy for some actinides within the y-family of shapes. The dashed lines are liquid-drop energies, the full lines include the microscopic corrections (after Ref. [96])

.

There are however two features which can be learned from this crude picture. The ground states of all nuclides of Fig. 2.27 are deformed. The reason is the following: All nuclei shown in the figure are mid-shell nuclei with respect to their protons as well as to their neutrons. In a spherical mean-field potential both types of nucleons would fill some of a bunch of levels lying closely together. By breaking the spherical symmetry of the potential some of these levels would go down, some would go up. Occupying mostly downsloping levels leads therefore to a lower Hartree-Fock ground-state energy. This lowering of the energy because of a spontaneous symmetry breaking of the mean field is called Jahn-Teller effect. It causes the shell correction for actinides to be positive for the spherical shape and to decrease with increasing elongation y, thus shifting the ground state to a finite deformation. The situation is opposite for the double magic nucleus ^{208}Pb and nuclides in its neighborhood where the shell correction is large and negative for the spherical ground state because no energy is gained by breaking the spherical symmetry. The Jahn-Teller effect is partly diminished by the pairing correction since the pairing correlation energy increases with increasing level density at the Fermi energy.

The other interesting feature in Fig. 2.27 is the position of the second minimum. It lies always at the same elongation of $y \approx 0.18$, corresponding roughly

to an axes ratio of 1:2. The liquid-drop barrier on the other hand, does not only decrease with increasing charge number Z, but moves to smaller elongations. For uranium the liquid-drop barrier appears at about the same elongation as the second minimum of the shell correction, for the heavier actinides this minimum is beyond the liquid-drop barrier, for the lighter actinides it lies at smaller deformations. As a consequence the outer barrier is lower than the inner barrier for the heavier actinides and disappears for superheavy nuclei. For the lighter actinides the situation is just the opposite. For thorium the liquid-drop barrier lies at so large deformation that even a third, somewhat

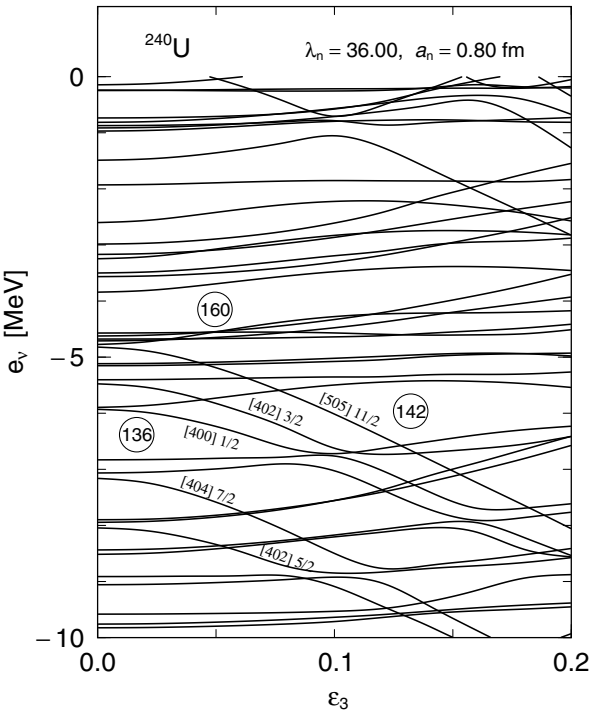

Fig. 2.28. Neutron single-particle levels in the folded Yukawa potential with fixed symmetric deformation parameters $\epsilon = 0.85$, $\epsilon_4 = 0.12$ as function of the octupole deformation parameter ϵ_3 with ϵ_5 being minimized out for fixed values of the other ϵ_n. Relevant couplings are between reflection-symmetric states [404 7/2], [402 5/2], [402 3/2], [400 1/2] and odd states [514 7/2], [512 5/2], [512 3/2], [510 1/2] (not labelled in the figure), respectively, (after Ref. [292]).

smaller, shell-correction minimum at axis ratio 1:3 has a chance to produce a further shallow, hyperdeformed minimum in the energy surface [293].

The latter and some other details are not visible in Fig. 2.27, but a more flexible shape parametrization than the y-family leads to a lowering of minima and saddle points. The most important modification is again due to a Jahn-Teller effect: Gustafsson, Möller, and Nilsson [294] first noticed that adding a parity-violating term $\sim \rho^2 P_3$ to the standard Nilsson potential leads to a strong coupling between positive-parity Nilsson levels with asymptotic quantum numbers $[40\Lambda\Omega]$ and negative-parity states $[51\Lambda\Omega]$ when the elongation corresponds to that of the second barrier. Some of the eigenstates in the octupole-deformed Nilsson potential are bending downwards and some go up

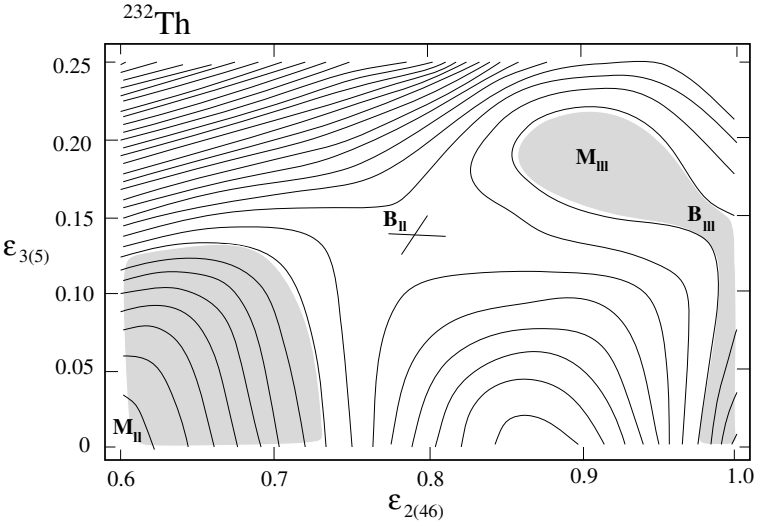

Fig. 2.29. Potential-energy surface for ^{232}Th in the region of the third minimum ($\mathrm{M_{III}}$) on the $(\varepsilon_2, \varepsilon_3)$ plane. The distance between contour lines is 0.5 MeV. The shaded area corresponds to lower energies (after [295]).

with increasing octupole deformation ϵ_3 as shown in Fig. 2.28. For actinides with neutron numbers between 132 and 160 the Nilsson states originating from reflection-symmetric $[40\Lambda\Omega]$ states are occupied, the levels coming from $[51\Lambda\Omega]$ states are unoccupied. In a simple single-particle picture such nuclei can therefore reduce their energy by breaking the mirror symmetry. Qualitatively the same situation as in the Nilsson potential occurs in finite-depth single-particle potentials.

In the region of the second minimum a similar energy gain is observed due to a breaking of the axial symmetry. This time it is a term $\sim \rho^2(Y_{22} + Y_{2-2})$, added to the standard Nilsson potential, which couples states $[Nn_z\Lambda\Omega]$ with states $[Nn_z\Lambda \pm 2\Omega \pm 2]$ as pointed out by Larsson, Möller, and Nilsson [296].

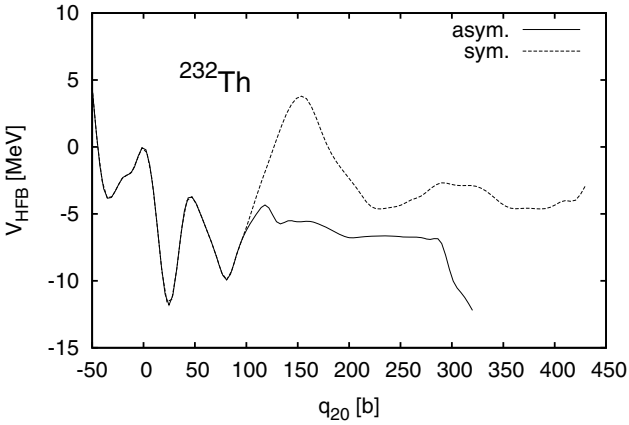

Fig. 2.30. The fission barrier of ^{232}Th evaluated in Ref. [304] within the HFB theory with the Gogny force as function of the quadrupole moment. The barrier evaluated without and with conserving of the reflection symmetry are marked by the solid and dashed lines, respectively.

For a discussion of the experimental determination of various saddle points and local minima of fissile nuclei we refer to review articles by Lynn [297] and Weigmann [298]. The latter contains also a list of experimentally determined barrier heights and energies of fission isomers. Stationary points of the energy hypersurfaces of fissile nuclei, calculated in various selfconsistent and macroscopic-microscopic schemes are compared in Refs. [299, 300].

There have been extensive experimental and theoretical studies of hyperdeformed minima. The existence of such hyperdeformed states was experimentally inferred from fission-fragment angular distributions together with an analysis of the microstructure in the excitation functions of the reactions ^{230,231,232}Th(n,f) [301] and of the (d,pf) reactions ^{229,230,231,232}Th(d,pf) [301], ^{233}U(d,pf) [302], and ^{231}Pa(d,pf) [303], measured with high energy resolution.

As an example for a calculated potential-energy surface in the region of the third minimum we show in Fig. 2.29 a two-dimensional plot for ^{232}Th. The energy is obtained in the macroscopic-microscopic model with a Nilsson single-particle potential [295].

Also selfconsistent calculations have predicted hyperdeformed shape isomers in nuclei close to ^{232}Th. The fission barrier of ^{232}Th, evaluated within the constrained HFB model with the Gogny force D1S, [304] is shown in Fig. 2.30. The barrier is plotted as function of the quadrupole moment. The solid line represents the energy, obtained with constraints on the quadrupole, hexadecapole, and octupole moments. The dashed line is calculated using only the constraining operators $\hat{q}_{20}$ and $\hat{q}_{40}$ and restricting the calculation to reflection-symmetric shapes. There is a sequence of an oblate, a prolate, a super-deformed, and a hyperdeformed minimum in the energy. The second

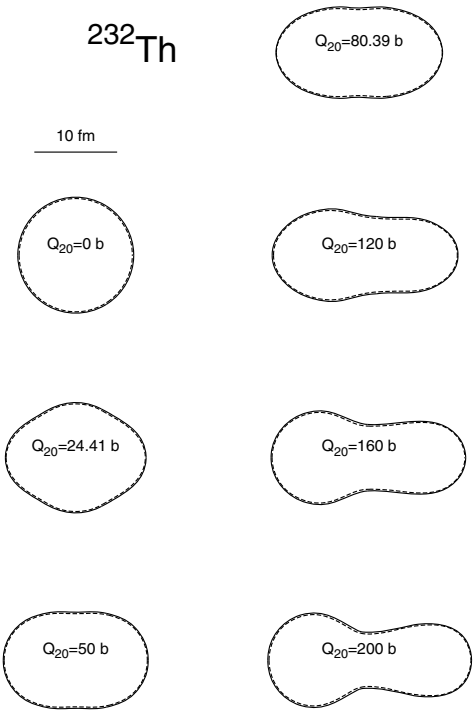

Fig. 2.31. The half-density contours of ^{232}Th for a spherical configuration, for the ground-state, at the top of the first barrier, in the second minimum, on top of the second symmetric and asymmetric barriers, as well as in the hyper-deformed minimum of the energy presented in Fig. 2.30. The neutron and proton shapes are marked by the solid and the dashed lines, respectively.

minimum at about 80 b is well developed. The height of the inner and outer barriers are of the order of 5 MeV, while the third super-deformed minimum is rather shallow with an outer barrier of only 0.5 MeV. Half-density shapes of ^{232}Th in the stationary points corresponding to subsequent extrema along the static fission path are presented in Fig. 2.31. The solid and dashed lines represent neutron and proton shapes, respectively. One can see that in the hyperdeformed minimum, which is located around q_{20}=200 b, the fission fragments are already well formed. The heavier fragment is almost spherical, while the lighter one has a significant prolate deformation. More detailed studies of the density distributions in both fragments reveal [305] that the heavier one corresponds to the isotope ^{132}Sn, while the light fragment is very close to ^{92}Zr. The remaining neutrons are mainly located in the neck region.

Fission isomers

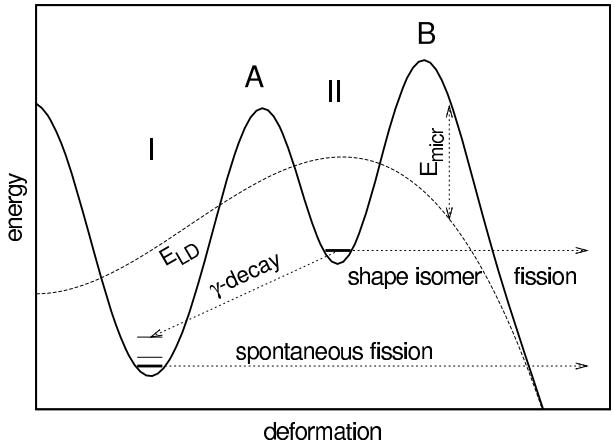

Fig. 2.32. Schematic plot of the double-humped fission barrier as function of the elongation. The ground state (I), first barrier (A), second minimum (II), and the second barrier (B) are marked. The dashed line corresponds to the macroscopic (LD-type) energy, while the solid line represents the whole energy. The difference between the both energies is equal to the microscopic, shell+pairing correction-energy.

If the potential pocket, corresponding to the secondary minimum, is deeper than about 1 MeV, the nucleus may be caught there. Traditionally states in the ground-state minimum are called class I states, those in the second minimum class II states. Decay modes of shape-isomeric states are shown schematically in Fig. 2.32. These states undergo either fission by tunneling through the outer barrier or decay by γ transitions into class I states [306]. Lifetimes for fission decay of shape-isomers are typically many orders of magnitude shorter than for spontaneous fission from the ground state because of the considerably larger barrier for the latter decay. At present around 40 shape-isomers between ^{232m}Th and ^{245m}Bk are found. Their fission half-lives lie between 14 ms and 6 ps.

Specht, Weber, Konecny, and Heunemann reported 1972 the first measurement of a rotational band in ^{240m}Pu by conversion-electron spectroscopy [307]. The moment of inertia corresponding to this band was more than two times larger than its value in the ground-state band. This was an indirect indication of the large deformation of fission isomers. Calculations of the moment of inertia by Sobiczewski, Bjørnholm, and Pomorski [308] in the framework of the cranking model with pairing confirmed this interpretation. In several uranium and plutonium isotopes rotational bands above the shape-isomeric state have been observed since by γ and by conversion-electron spectroscopy [302, 309].

Quadrupole deformations of shape isomeric states have been determined with optical spectroscopy and life-time measurements of the transitions in the rotational bands [309, 310]. They are in good agreement with calculations by Nerlo-Pomorska using the macroscopic-microscopic approach [311].

2.4.4 Effect of an odd-particle on the fission barrier

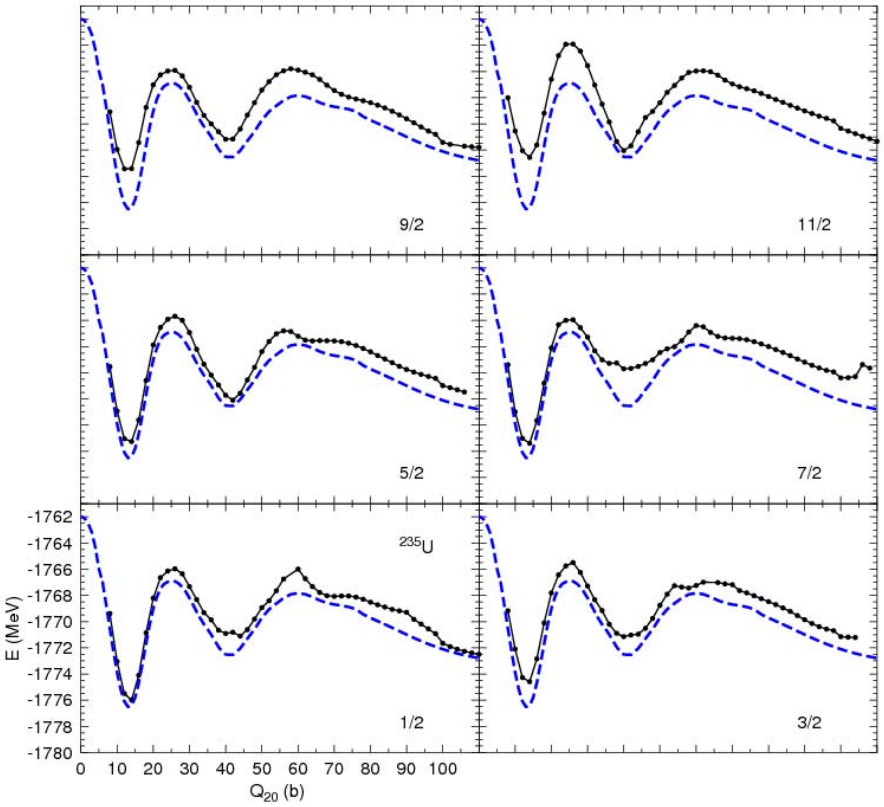

Fig. 2.33. The fission barriers for ^{235}U evaluated for different values of Ω (solid lines with points) in comparison with the corresponding barrier (dashed line) of an even-even system. The values of Ω of the odd particle are shown in the lower-right corners (private communication by L. M. Robledo).

The projection Ω of the angular momentum on the fission axis of the odd particle in an odd nucleus is a constant of motion along the fission path if the single-particle potential remains axially symmetric during fission. Since the quantum number Ω of the ground-state orbital of the odd particle is in

general not the same as in the lowest single-particle state above the fission barriers of the neighboring even nuclei, the latter are typically lower than the barrier of the odd nucleus. This extra barrier energy of odd nuclei is called specialization energy [313]. A similar argument holds for the conservation of the parity of the odd particle as long as the nuclear shape is reflection-symmetric. However, since violations of the axial or reflection symmetry occur often along the fission path, a reduction of the actual specialization energy must be expected, compared to the case of a fully symmetric path. In addition, the blocking effect of the odd nucleon reduces the pairing energy compared to neighboring even nuclei.

The effect of an odd neutron on the fission barrier of ^{235}U is shown in Fig. 2.33 for various assumed quantum numbers Ω (the actual ground-state spin of ^{235}Pu is 1/2). The energy was evaluated in the HFB frame [312] using the D1S Gogny interaction. For comparison the mean HFB energy of the neighboring even nuclei is also shown. The difference between both curves is the specialization energy, which corresponds roughly to the quasiparticle energy of the odd particle. It is seen that the specialization energy is different for different orbitals occupied by the odd neutron and varies significantly with deformation. The influence of this effect on the spontaneous fission probability will be discussed in Sec. 5.1.4.

Notice that the effect of an odd particle is not additive. In odd-odd nuclei only the sum of the angular momenta of the two odd nucleons and the product of their parities are conserved

$$\Omega = \Omega_p + \Omega_n \quad , \qquad \pi = \pi_p \cdot \pi_n \tag{2.229}$$

This constraint is weaker than conserving angular momentum and parity of each particle separately. Therefore the modification of the fission barrier is in this case comparable to that of a single odd particle.

2.5 Effect of rotation on the fission barriers

It was already shown in the 1970's (cf. e.g. Ref. [314]) that shell effects do not disappear with growing angular momentum of a rotating nucleus. In fact, at high spin even new shells can appear. In order to obtain the potential energy of the rotating nucleus in mean-field approximation one has to satisfy the constraint

$$\langle \Psi | \hat{J}_x | \Psi \rangle = \sqrt{I(I+1)}\,. \tag{2.230}$$

In this equation the wave function $|\Psi\rangle$ is either $|\mathrm{HF}\rangle$ or $|\mathrm{HFB}\rangle$ and $\hat{J}_x$ is the sum over the x components of the single-particle angular-momentum operators. It is assumed that the collective rotation is around the x-axis, for which the moment of inertia shall be the largest and I is the total spin. Therefore an additional Lagrange term $-\omega \hat{J}_x$ has to be added in the energy-minimization conditions, Eqs. (2.9) or (2.26) in the HF or HFB scheme, respectively.

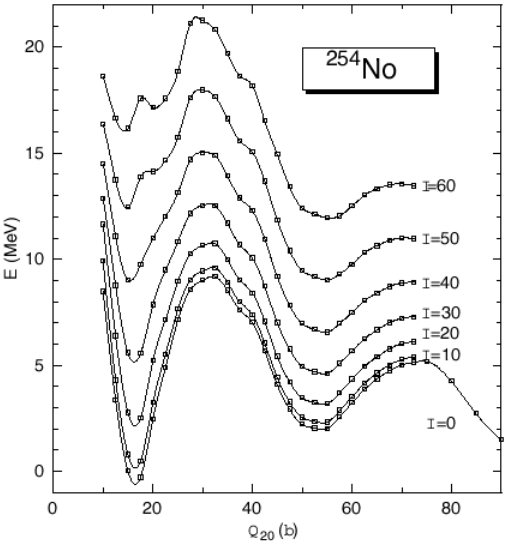

Fig. 2.34. Self-consistent fission barriers of ^{254}No, evaluated for various angular momenta using the Gogny potential D1S (from Ref. [315]).

An example of fission barriers evaluated selfconsistently for ^{254}No for a sequence of angular momenta is presented in Fig. 2.34 as function of the mass quadrupole moment Q_{20}. The curves were obtained by Egido and Robledo [315], using the Gogny potential D1S in a constrained HFB calculation. (No energy corrections for symmetry-violating HFB wave-functions are considered in Fig. 2.34.) It is seen that the double-humped barrier survives up to high angular momenta.

To formulate the macroscopic-microscopic approach for rotating nuclei [316], we consider the single-particle Schrödinger equation with the cranked shell-model Hamiltonian $\hat{h}' = \hat{h}^{\rm shell} - \omega \hat{j}_x$

$$(\hat{h}^{\rm shell} - \omega\, \hat{j}_x)|i\rangle = e_i^{\omega}\, |i\rangle \ , \tag{2.231}$$

where e_i^{ω} and $|i\rangle$ are the eigenvalues and eigenstates in the rotating frame.

The shell-model energy of a rotating nucleus becomes

$$E(I_x) = \sum_i n_i^{\omega}\, e_i^{\omega} + \omega\, I_x \ , \tag{2.232}$$

where the summation goes over all single-particle states and the angular momentum I_x is equal to

$$I_x = \sum_i n_i^{\omega} \langle i|\hat{j}_x|i\rangle \ . \tag{2.233}$$

The occupation numbers n_i^ω in formulae (2.232) and (2.233) are 1 for the states with the Z (or N) lowest eigenvalues e_i^ω and zero else. The shell-model moment of inertia $\mathcal{J}_{\rm SM}$ is defined in analogy to classical mechanics by

$$\mathcal{J}_{\rm SM} = \frac{I_x}{\omega} \ . \tag{2.234}$$

To obtain the parameters of the reference nucleus in the Strutinsky procedure, one introduces averaged occupation numbers $\tilde{n}_i^{\tilde{\omega}}$ by Eq. (2.188) using ϵ_i^ω instead of ϵ_i. The two Lagrange parameters $\tilde{\lambda}$ and $\tilde{\omega}$ are determined implicitly by the two constraints

$$\sum_i \tilde{n}_i^{\tilde{\omega}} = Z(\text{ or } N) \quad \text{ and } \quad \sum_i \tilde{n}_i^{\tilde{\omega}} \langle i|\hat{j}_x|i\rangle = I_x \ . \tag{2.235}$$

The energy of the reference nucleus is then

$$\widetilde{E}(I_x) = \sum_i \tilde{n}_i^{\tilde{\omega}} \, e_i^{\tilde{\omega}} + \tilde{\omega} \, I_x \ . \tag{2.236}$$

The smoothed moment of inertia is defined in analogy to Eq. (2.234) as

$$\widetilde{\mathcal{J}}_{\rm SM} = \frac{I_x}{\tilde{\omega}} \ . \tag{2.237}$$

One can show that for a realistic single-particle potential the smoothed moment of inertia is close to the moment of inertia of a rigid body [314] which is given by

$$\mathcal{J}_{\rm rig} = \frac{3AM_{\rm nucl}}{4\pi R_0^3} \int\limits_V \left(y^2 + z^2\right) \, d^3r = \mathcal{J}_{\rm sph} \cdot B_{\rm rot}({\rm def}) \, , \tag{2.238}$$

where

$$\mathcal{J}_{\rm sph} = \frac{2}{5} AM_{\rm nucl} R_0^2 = \frac{2}{5} M_{\rm nucl} r_0^2 A^{5/3}$$

is the rigid-body moment of inertia of a spherical nucleus and $B_{\rm rot}$ is a geometrical factor which depends on the deformation of the nucleus.

The shell-correction energy of a rotating nucleus is defined as

$$\delta E_{\rm shell}(I) = E(I) - \widetilde{E}(I) \tag{2.239}$$

and the total energy becomes in the macroscopic-microscopic approach

$$E_{\rm tot}(I, {\rm def}) = \left\{ E_{\rm mac}({\rm def}) + \frac{I(I+1)}{2\mathcal{J}_{\rm rig}({\rm def})} \right\} + \delta E_{\rm shell}(I, {\rm def}) \, . \tag{2.240}$$

As an example for the potential-energy surface of a rotating nucleus we show in Fig. 2.35 the energy of the superheavy nucleus $^{298}114$. The liquid-drop model with parameters from Ref. [317] was used for the macroscopic part

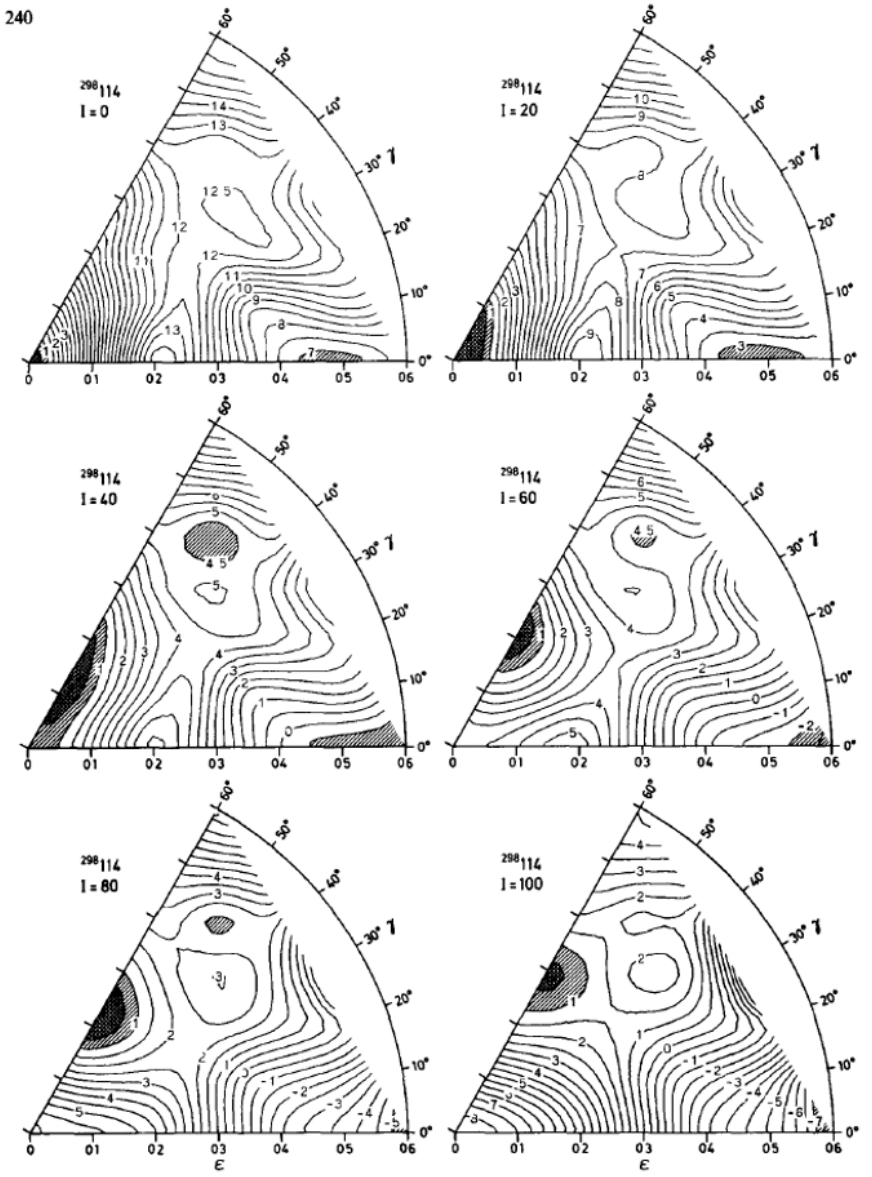

Fig. 2.35. The potential energy surfaces of the $^{298}114$ nucleus, projected on the (ε, γ) plane. The plots are made for I=0, 20, 40, 60, 80, and 100 in units of $\hbar$ (from Ref. [314]).

and in the Strutinsky shell-correction the Nilsson potential with deformation parameters ε and γ was employed. For their definition we refer to Eqs. (2.211) and (1.11), respectively. Fig. 2.35 shows that also a superheavy nucleus follows

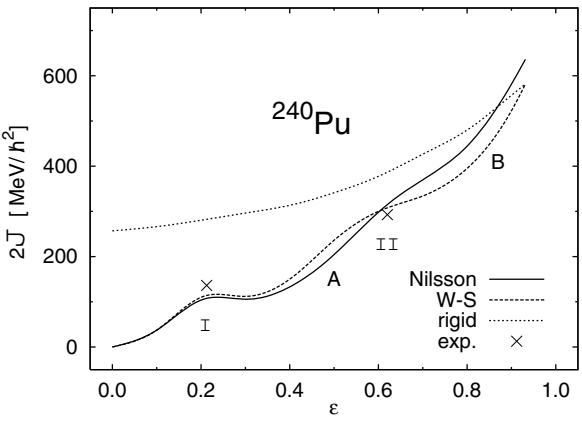

Fig. 2.36. The moment of inertia of ^{240}Pu along the fission path as a function of the quadrupole deformation ε. The microscopic moments (2.243) obtained with the Nilsson (solid line) and Woods-Saxon (dashed lines) potentials are compared with the rigid body moment of inertia (dotted line) and the experimental data (crosses) in the first (I) and the second minimum (II). The positions of the first and second saddle points are marked by A and B respectively (after Ref. [295]).

the general rule of Ref. [44] that with increasing angular momentum a nucleus becomes increasingly deformed in the oblate direction ($\gamma = 60^0$). Even a superheavy nucleus, whose fission barrier comes from shell effects only, is seen to be rather stable with respect to collective rotation.

For small angular velocities ω the eigenvalue problem of the single-particle Hamiltonian in a rotating frame (2.240) can be solved in second order perturbation theory. The result is Inglis' cranking formula [318]

$$E(\omega) = \sum_i n_i \, e_i + \frac{1}{2} \mathcal{J}_{\rm crank} \, \omega^2 \ , \tag{2.241}$$

where

$$\mathcal{J}_{\rm crank} = 2\hbar^2 \sum_{j>i_{\rm Fermi}} \sum_{i\leq i_{\rm Fermi}} \frac{|\langle i|\hat{j}_x|j\rangle|^2}{e_j - e_i} \tag{2.242}$$

is the moment of inertia. In the framework of the BCS theory the cranking formula becomes [97]

$$\mathcal{J}_{\rm crank} = 2\hbar^2 \sum_{i,j>0} \frac{|\langle i|\hat{j}_x|j\rangle|^2}{E_j + E_i} (u_j v_i - u_i v_j)^2 \ , \tag{2.243}$$

where E_j and E_i are the quasiparticles energies (2.51), u_j and v_i the BCS occupation coefficients (2.46). The cranking moment of inertia, evaluated along the fission path, for ^{240}Pu with Nilsson and with Woods-Saxon potentials is compared in Fig. 2.36 with the rigid moment of inertia (2.238). It is seen that for

large elongation, corresponding to the second saddle (B), both macroscopic-microscopic calculations yield results close to the rigid-body moment of inertia.

http://www.springer.com/978-3-642-23514-6

Theory of Nuclear Fission
A Textbook
Krappe, H.J.; Pomorski, K.
2012, IX, 320 p. 101 illus., Softcover
ISBN: 978-3-642-23514-6